# Poly-*N*-isopropylacrylamide-based Thermoresponsive Hydrogels for Retinal Pigment Epithelial Cell Delivery

# Poly-N-isopropylacrylamide-based Thermoresponsive Hydrogels for Retinal Pigment Epithelial Cell Delivery

Nicole Amaral, HBSc
McMaster University, amaralnm@mcmaster.ca

A Thesis Submitted to the School of Graduate Studies in Partial Fulfillment of the Requirements for the Degree of Master of Applied Science

Master of Applied Science (2021)

Chemical Engineering

McMaster University

Hamilton, Ontario

Canada

TITLE: Poly-N-isopropylacrylamide-based Thermoresponsive Hydrogels for Retinal Pigment Epithelial Cell Delivery

AUTHOR: Nicole Amaral, HBSc (McMaster University)

SUPERVISOR: Dr. Heather Sheardown

NUMBER of PAGES: xxiii, 100

# ABSTRACT

Despite being the most prevalent presentation of Age-Related Macular Degeneration (AMD), dry AMD (dAMD) lacks a therapeutic treatment. Retinal pigment epithelium (RPE) dysfunction preceding the onset of dAMD has inspired interest in regenerative medicine approaches seeking to replenish the RPE and preserve visual acuity. Cell delivery to the subretinal space however has been met with challenges surrounding ease of access and invasive surgical implantation. Two-dimensional scaffolds have made use of natural and polymeric materials to act as carriers for RPE cells and various progenitor lines. These substrates mitigate issues surrounding the handling of delicate cell sheets harvested for transplant. As well, they are often successful in preserving RPE phenotype, supporting growth, and can be fine tuned to possess morphologies comparable to native extracellular matrix (ECM). Despite aiming to act as replacement Bruch's membrane on which RPE resides, two-dimensional substrates are often notably bulky and require traumatic surgery for implantation.

As a result, the use of injectable methods of cell delivery has gained appeal. Bolus injections, despite improved methods of administration, are correlated with issues of inadequate cell localization. In response, three-dimensional hydrogel carriers for retinal applications aim to encapsulate cells, allowing for better cell distribution as these materials spread throughout the subretinal space. Increased viscosity of hydrogels as compared to saline injections, is hypothesized to improve cell loss and reduce aggregation. Of particular interest are *in situ* gelling systems, which undergo physical changes upon injection. Gelation upon delivery works to further assist in maintaining the cells within their target site.

Purity and reproducibility concerns associated with the use of natural materials in the development of hydrogel cell carriers, have inspired the use of synthetic thermoresponsive poly-N-isopropylacrylamide (pNIPAAm). pNIPAAm undergoes a liquid to gel transition at a lower critical solution temperature (LCST) of 32°C. Copolymerization with various hydrophobic and hydrophilic groups can be used to adjust gel properties such as increasing or decreasing LCST, allowing for degradation, and improving water retention.

In the work described herein, two NIPAAm-based thermoresponsive hydrogels intended for use as subretinal cell carriers are proposed. Poly-NIPAAm-*co*-NAS-*co*-PEGMEMA$_{1070}$-*co*-DBA (pNNPD) and Poly-NIPAAm-*co*-NAS-*co*-PEGMEMA$_{510}$-*co*-DBA-*co*-TRIS (pNNP5DT) possess LCSTs below physiological. However, intramolecular hydrophobic and hydrophilic polymer-polymer interactions appear to modulate complete phase transition which occurs above LCST for both materials. The Tgel, defining the complete transition from the viscous phase to the elastic phase, lies below physiological for pNNP5DT but above physiological for pNNPD. pNNPD however is able to better retain optical transparency and water content at 37°C as compared to pNNP5DT, making it preferential for back of the eye administration. Modification with adhesion peptides YIGSR and RGDS was explored to improve biocompatibility and ECM mimicry. When cultured with

immortalized ARPE-19 cells, pNNP5DT-RGDS gels were associated with robust cell lifting as compared to pNNPD. However, cells treated with pNNPD materials showed higher viability (>80%) than those cultured with pNNP5DT (<70%) after 24 and 48 h. The results suggested that RGDS may be better suited for RPE delivery as compared to YIGSR, likely due to the role RGDS plays in RPE cell migration. A material which is able to leverage the benefits of both pNNPD and pNNP5DT may offer more benefits to cell delivery than either material alone. These results provide valuable insight for further optimization of these formulations and their associated bioconjugation, as well as for comparable pNIPAAm biomaterials.

# ACKNOWLEDGMENTS

I am a product of the hard work and sacrifice of those who came before me, the faith of others to provide the opportunities I have been warranted, and the love and support of too many to name. Still, I will try my best to summarize my immense gratitude. This work would not have been made possible without the relentless patience and kindness of Dr. Heather Sheardown. In moments of doubt, she has continually reminded me to persist, to trust myself, and to not take it all too seriously. I am continually grateful for her understanding, her generosity, and inspired by her seemingly superhuman ability to cycle hundreds of kilometers at a time. I would also like to thank Dr. Mike Brook for introducing me to the world of research and for continuing to act as a mentor and friend since. It is his expertise, honesty, and lessons in perseverance which have fostered a deep sense of resilience and motivation. I thank Dr. Boyang Zhang for reigniting my interest in biomedical devices through his teaching. It was an honour to be a student of his first class at McMaster, his lessons always engaging and his humility unwavering. I thank Dr. Mike Brook and Dr. Boyang Zhang for serving as members of my committee and for helping me see through various parts of my Masters experience.

I would like to thank my colleagues in the Sheardown Lab. To Lina Liu for being the leader and innovator that she is. Our go-to in moments of equipment failure and lab maintenance, Lina always finds a solution and is always willing to help. Dr. Talena Rambarran for her expertise in polymer synthesis and generosity. Talena's open-door support and mentorship have been a rock throughout this work. She always made time for the graduate students and would go through protocols and spectra step-by-step to ensure we felt confident in anything we were tackling. Talena's friendship and warmth has carried me through the unexpected and has provided hope. Dr. Aftab Taiyab for his mastery of cell culture and countless life chats. I could always count on Aftab for motivation and to ask me a question he already knew the answer to. It is these pop quizzes that have allowed me to continually ask "Why?", to think critically about every step of an assay, and inspire further inquiry. Dr. Vida Rahmani for being a friend throughout despite our time in the lab overlapping ever so slightly, for all the encouragement, and chocolate. Dr. Karim Soliman for the meals he has shared and his engaging presentations which have contextualized the work we do. Dr. Ben Muirhead and Dr. Fran Lasowski for all the heckles and the laughs. For the roles they each play, at times behind the scenes, to ensure we are well supported and taken care of.

Eva Chang, Ridhdhi Daves, Jennifer Tian, Emily-Anne Hicks, and Payal Lahoti thank you for the dog memes, face masks, board games, Jelly Kings, plant love, movie/series recommendations, and caring check-ins. Taylor Goosetry, thank you for always being down to talk through data analysis, for surviving below freezing in a tent not recommended for below freezing temperatures, for Caribou Lou, and Crocodile Rock (RIP). Finally, thank you Mitchell Ross for being my ride or die for a large part of this work. For answering the silly questions, sharing pints,

and making my introduction to graduate studies more than I ever could have hoped. I am terribly lucky to have been a member of this lab alongside those mentioned, to share the memories we have within the walls of JHE 257A, 257B, 367 and beyond.

We would like to acknowledge and give a special thank you to the Natural Sciences and Engineering Research Council as well as the C20/20 Ontario Research Fund for providing the financial support which funded this project.

To our dream team, Kristina Trollip, Michelle Whalen, and Linda Ellis for everything they do for the Chemical Engineering department. For all her help in planning PolyMac, thank you Kristina. I will miss you three and the banter which accompanied popping into the office. Dr. Marta Princz and Heera Marway for all their assistance and expertise surrounding the plate reader/inverted scope and DHR/DSC respectively. You are the hearts behind pretty images and graphs across departments. To the ChE 3L02 family, Doug Keller, Dr. Li Xi, Timothy Stephens, and all those I was able to TA alongside, thank you for teaching a biology major the fundamentals of mass and heat transfer.

A very special thank you to Jon Dorogin, Ali Affar, Matt Campea, Doren Singh, Robert Bui, Cody Gale, Nate Dowdall, Luis Portillo, Taylor Stimpson, Devan Wagner, Daniel Osorio, Madeline Simpson, Eva Mueller, Sophie Emerson, and Alex D'Souza for all their love and friendship. Ali Babar for being a call away, for hallway tears, NFR, Watermelon Sugar, and for that one time you came to my birthday. Christian Bellissimo thank you for being the kind of researcher I aspire to be, for always making the time, and for being the Katya to my Trixie (and/or vice versa, still to be determined). To those behind the scenes, Timothy Swampillai, Justin McConnell, Leah McComb, Alexis Gallant, Yinan Zhang, Bahar Aarabi, Jessica Kanowitz, David Czaplinski, Karisa Tyler, and Preethi Anbalagan thank you for believing in me, for being my anchors and light always. I don't think I will ever be able to adequately express how much you each mean to me. To Michael Kiriakou, this past year would not have been nearly as manageable if it weren't for all you do. Thank you for all the early morning drives to campus, for bringing me food between equipment bookings, and for reminding me that writing wasn't the opportune time to adopt another dog and maybe also a cat. For being the unexpected in this journey, my buddy, my pal, and an unreal pandemic roommate.

Finally, thank you to my family. To my parents, Helen and Carlos, and my brother Paul for everything and all of it. To Cookie, the most stubborn dog I have ever met because her persistence is truly inspiring. To my grandparents, Pappou, Yiayia, and Avo, who risked everything to give me a chance at something like this. This milestone is not mine alone, it belongs to them.

# TABLE OF CONTENTS

# TABLE OF FIGURES

# TABLE OF TABLES

# LIST OF ABBREVIATIONS

| | |
|---|---|
| $^{1}$H NMR | Proton nuclear magnetic resonance spectroscopy |
| A2E | N-retinylidiene-N-retinylethanoamine |
| ACRYL-PEG-RGDS | (acrylate)-(polyethylene glycol)-(arginine-glycine-aspartate-serine) |
| AFM | Atomic force microscopy |
| AM | Amniotic membrane |
| AMD | Age-Related Macular Degeneration |
| ANOVA | Analysis of variance |
| AREDS | Age-Related Eye Disease Study |
| ARMS2 | Age-Related Maculopathy Susceptibility Protein 2 |
| ARMS2 A69S | Age-Related Maculopathy Susceptibility Protein 2 gene alanine to serine mutation at codon 69 |
| BDNF | Brain derived neurotrophic factor |
| BPO | Benzoyl peroxide |
| BRB | Blood retinal barrier |
| BrM | Bruch's Membrane |
| CFH | Complement Factor H |
| CFH Y402H | Complement Factor H gene tyrosine to histidine mutation at codon 402 |
| CNTF | Ciliary neurotrophic factor |
| $D_2O$ | Deuterated water |
| dAMD | Dry Age-Related Macular Degeneration |
| DBA | (R)-α-Acryloyloxy-β,β-dimethyl-γ-butyrolactone |
| DHR | Dynamic Hybrid Rheometer |

| | |
|---|---|
| DMAEMA | 2-(dimethylamino) ethyl methacrylate |
| DMEM/F12 | Dulbecco's Modified Eagle Medium/Nutrient Mixture F-12 |
| DMF | N,N-Dimethylformamide |
| DMSO | Dimethyl sulfoxide |
| DMSO-d6 | Deuterated dimethyl sulfoxide |
| DSC | Differential Scanning Calorimetry |
| EB | Embryoid body |
| ECM | Extracellular matrix |
| ESCs | Embryonic stem cells |
| FBS | Fetal bovine serum |
| FITC | Fluorescein isothiocyanate |
| G’ | Storage modulus |
| G’’ | Loss modulus |
| GFP | Green fluorescent protein |
| GPC | Gel permeation chromatography |
| GRGDSP | Glycine-Arginine-Glycine-Aspartate-Serine-Proline |
| Gtn-HPA | Gelatin-hydroxyphenyl propionic acid |
| HA | Hyaluronic acid |
| HCE-T | Human corneal epithelial cells |
| IGF-1 | Insulin-like growth factor 1 |
| iPSCs | Induced pluripotent stem cells |
| LCST | Lower Critical Solution Temperature |

| | |
|---|---|
| LiBr | Lithium Bromide |
| LPCB | London Project to Cure Blindness |
| MC | Methylcellulose |
| MPS | γ-methacryloxypropyltrimethoxysilane |
| MTT | Thiazolyl blue tetrazolium bromide |
| NAS | Acrylic acid N-hydroxysuccinimide |
| NHS | N-hydroxysuccinimide |
| NIPAAm | N-isopropylacrylamide |
| OCT | Optical coherence tomography |
| PBS | Phosphate Buffered Saline |
| PCL | Poly(ε-caprolactone) |
| PEDF | Pigment Epithelium Derived Factor |
| PEG | Polyethylene glycol |
| PEGDA | Poly(ethylene glycol) diacrylate |
| $PEGMEMA_{1070}$ | Polyethylene glycol methyl ether methacrylate (MW = 1070 g/mol) |
| $PEGMEMA_{510}$ | Polyethylene glycol methyl ether methacrylate (MW = 510 g/mol) |
| PEO-PPO-PEO | Poly(ethylene oxide)-b-poly(propylene oxide)-b-poly(ethylene oxide) |
| PLA | Polylactic acid |
| PLDLA | Poly(L-lactide-*co*-D-lactide) |
| PLGA | Poly(lactic-co-glycolic acid) |
| PlGF | Placenta Growth Factor |

| | |
|---|---|
| pNAPD | Poly-N-isopropylacrylamide -*co*-acrylic acid-*co*-polyethylene glycol methyl ether methacrylate (MW = 1100 g/mol)-*co*-(R)-α-Acryloyloxy-β,β-dimethyl-γ-butyrolactone |
| pNIPAAm | Poly-N-isopropylacrylamide |
| PNN-10 | 90:10 mol% poly-N-isopropylacrylamide-*co*-acrylic acid N-hydroxysuccinimide |
| pNNAD | Poly-N-isopropylacrylamide -*co*-acrylic acid N-hydroxysuccinimide-*co*-acrylic acid-*co*-(R)-α-Acryloyloxy-β,β-dimethyl-γ-butyrolactone |
| PNN-HA | 90:10 mol% poly-N-isopropylacrylamide -*co*-acrylic acid N-hydroxysuccinimide modified with hyaluronic acid |
| PNN-HA.RGDS | 90:10 mol% poly-N-isopropylacrylamide -*co*-acrylic acid N-hydroxysuccinimide modified with hyaluronic acid and Arginine-Glycine-Aspartate-Serine |
| pNNP5DT | Poly-N-isopropylacrylamide -*co*-acrylic acid N-hydroxysuccinimide-*co*-polyethylene glycol methyl ether methacrylate (MW = 510 g/mol)-*co*-(R)-α-Acryloyloxy-β,β-dimethyl-γ-butyrolactone -*co*-Methacryloxypropyltris(trimethylsiloxy)silane |
| pNNP5DT-RGDS$_{33}$ | pNNP5DT whereby 33% of acrylic acid N-hydroxysuccinimide is modified with Arginine-Glycine-Aspartate-Serine |
| pNNP5DT-RGDS$_{48}$ | pNNP5DT whereby 48% of acrylic acid N-hydroxysuccinimide is modified with Arginine-Glycine-Aspartate-Serine |
| pNNP5DT-YIGSR$_{27}$ | pNNP5DT whereby 27% of acrylic acid N-hydroxysuccinimide is modified with YIGSR |
| pNNPD | Poly-N-isopropylacrylamide -*co*-acrylic acid N-hydroxysuccinimide-*co*-polyethylene glycol methyl ether methacrylate (MW = 1070 g/mol)-*co*-(R)-α-Acryloyloxy-β,β-dimethyl-γ-butyrolactone |

| | |
|---|---|
| pNNPD-RGDS$_{117}$ | pNNPD whereby 117% of acrylic acid N-hydroxysuccinimide is modified with Arginine-Glycine-Aspartate-Serine |
| pNNPD-RGDS$_{28}$/YIGSR$_{18}$ | pNNPD whereby 28% of acrylic acid N-hydroxysuccinimide is modified with Arginine-Glycine-Aspartate-Serine and 18% with Tyrosine-Isoleucine-Glycine-Serine-Arginine |
| pNNPD-RGDS$_{31}$ | pNNPD whereby 31% of acrylic acid N-hydroxysuccinimide is modified with Arginine-Glycine-Aspartate-Serine |
| pNNPD-RGDS$_{37}$ | pNNPD whereby 37% of acrylic acid N-hydroxysuccinimide is modified with Arginine-Glycine-Aspartate-Serine |
| PNN-RGDS | 90:10 mol% poly-N-isopropylacrylamide-*co*-acrylic acid N-hydroxysuccinimide modified with Arginine-Glycine-Aspartate-Serine |
| qPCR | Qualitative polymerase chain reaction |
| RGD | Arginine-Glycine-Aspartate |
| RGDS | Arginine-Glycine-Aspartate-Serine |
| ROS | Reactive oxygen species |
| RPE | Retinal pigment epithelium |
| SEM | Scanning Electron Microscopy |
| SH3 | Src homology 3 |
| Sol-gel | Solution to gel |
| sVEGFR-1 | Soluble vascular endothelial growth factor receptor 1 |
| Tgel | Solution to gel transition temperature as defined by storage over loss modulus crossover |
| TGF | Transforming growth factor |
| THF | Tetrahydrofuran |

| | |
|---|---|
| TRCS | Thermoresponsive culture substrates |
| TRIS | Methacryloxypropyltris(trimethylsiloxy)silane |
| UCST | Upper Critical Solution Temperature |
| VEGF | Vascular Endothelial Growth Factor |
| wAMD | Wet Age-Related Macular Degeneration |
| YIGSR | Tyrosine-Isoleucine-Glycine-Serine-Arginine |
| ΔH | Change in enthalpy |
| ΔS | Change in entropy |

# DECLARATION OF ACHIEVEMENT

This thesis comprises original work conceived, conducted, analyzed, and written by the author of this contribution, under the supervision of Dr. Heather Sheardown who also provided editorial assistance. With the following exceptions:

The formulation of pNNPD was previously conceived by Scott Fitzpatrick as part of his doctoral thesis (2012). Similarly, the formulation for pNNP5DT was based upon a previous material lacking DBA and NAS conceived by Mitchell Ross, who also advised the recommended molar feed ratios used herein.

# Chapter 1: INTRODUCTION

## 1.1 ANATOMY OF THE EYE

"Who would believe that so small a space could contain the images of all the universe?" – Leonardo Da Vinci [1]. The human eye depicted in **Figure 1.1**, is a remarkable system capable of moderating intensity of external light, focussing this stimulus through a lens to form an image, and sending this image to the visual cortex through phototransduction via the optic nerve [2]. This delicate organ is protected by accessory structures including the eyebrows, eyelids and eyelashes, the conjunctiva, the lacrimal gland and nasolacrimal duct, as well as six extrinsic eye muscles. These features serve to protect the eye from external particulate, provide lubrication, and allow for motion.

Residing within the snug orbit of the skull, the globe of the eye is organized into three chambers. The anterior chamber (between the cornea and the iris) and the posterior chamber (between the iris and the lens), are filled with aqueous humour. Contrarily, the vitreous chamber is surrounded almost entirely by the retina and is filled with the more gelatinous vitreous humour. Both the aqueous and vitreous humour help maintain intraocular pressure allowing the eyeball to hold its shape while preserving the integrity and placement of its structures. Similarly, the eye wall is composed of three layers: an outer fibrous tunic, an intermediate vascular tunic, and an inner nervous tunic [1].

The fibrous tunic is made up of the sclera and the cornea, with the sclera acting in part as protective support as well as an attachment point for the extrinsic muscles. The sclera is composed of collagenous tissue and elastic fibers. The cornea is avascular, allowing for the permeation of oxygen from the external air. Transparency due to its high concentrations of proteoglycans and low water content, as well as reduced large collagen fibers as compared to the sclera, allows light passage into the eye. Next, the vascular tunic contains blood vessels derived from the short ciliary arteries of the ophthalmic artery, originating from the carotid. Short ciliary arteries penetrate the sclera to form the choroid, a 0.1 to 0.2 mm membrane. The vascular tunic of the anterior segment possesses the iris and ciliary body. The ciliary body functions to change the shape of the lens and produce aqueous humour, as such its associated muscles are often considered the intrinsic muscles of the eye. Contraction of the intrinsic muscles pulls on suspensory ligaments connected to the lens. This changes the shape of the lens allowing it to focus in response to stimuli. Similarly, the contractile processes of the iris regulate the amount of light entering the eye [1].

Finally, the nervous tunic or the retina is composed of a polarized monolayer of pigmented cuboidal epithelium and a neural layer housing approximately 120 million rods and 7 million cones along with their associated neural networks. Lying behind the ciliary body, the retina contains two unique features. First, the macula, a 4 mm yellow spot localized near the

centre of the posterior retina, and the optic disc. Within the macula a pit referred to as the fovea centralis (fovea) contains a high density of tightly packed cone cells. This area of the retina therefore has the highest visual acuity, important in central vision. The optic disc however, lacks photoreceptor cells in favour of the central retinal artery and vein, along with the neurons of the retina which unite here to exit the eye via the optic nerve. Because of this, the optic disc is incapable of responding to light and is nicknamed the blind spot [1]. These intricate structures work collectively to compile visual stimulus into an electrical signal which can be interpreted by the brain. With age, the functionality of these structures is subject to change, altering the way in which the world is pictured.

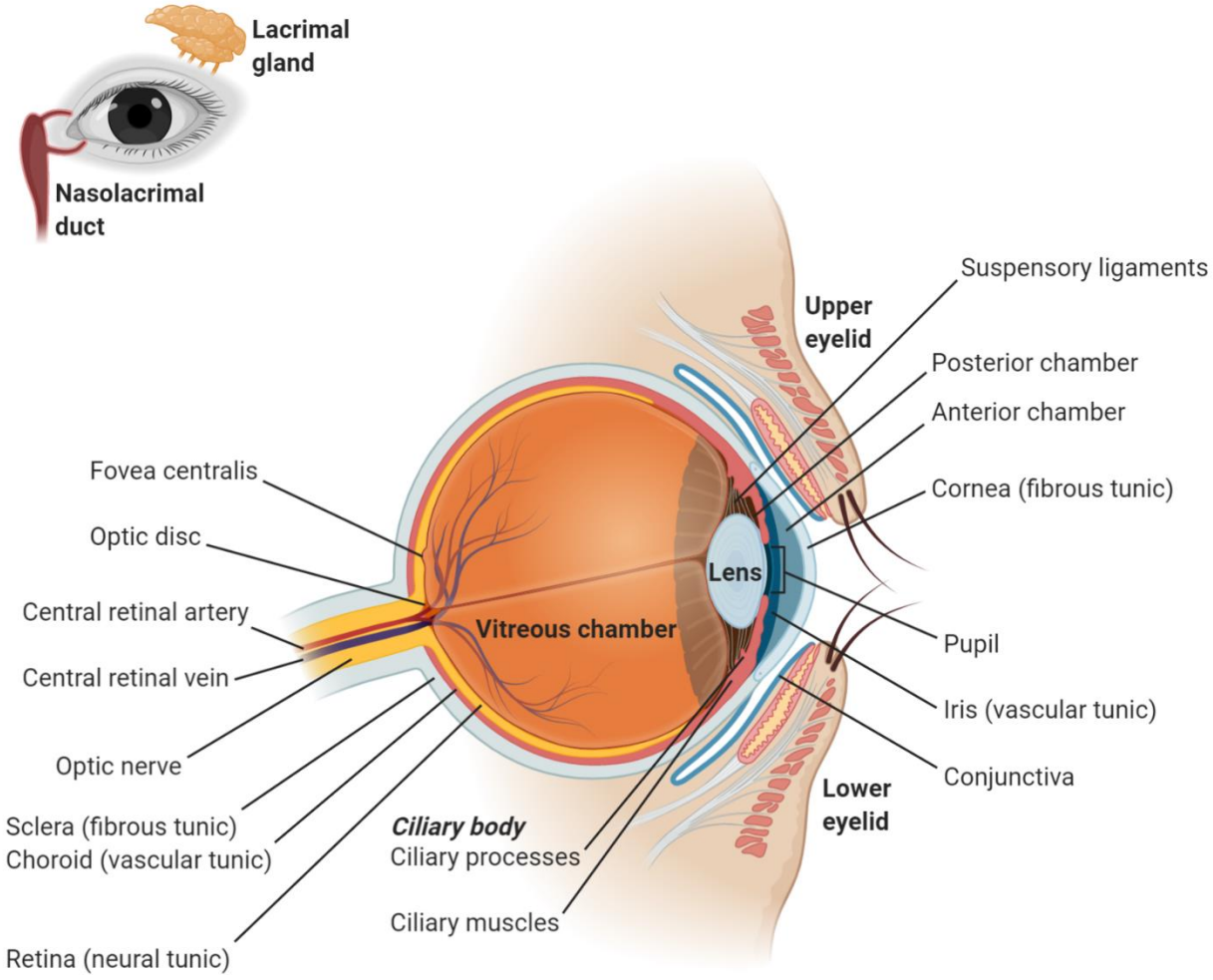


**Figure 1.1.** Front view of eye displaying lacrimal apparatus (top left). Sagittal section of the eye (center). Image created using BioRender.com.

## 1.2 AGE-RELATED MACULAR DEGENERATION

Age-related macular degeneration (AMD) is a leading cause of vision loss worldwide, predominantly affects those over 50 years of age. Characterized by the break down of the macula, AMD limits the ability to see fine details in the central line of sight [3]. To a patient, symptomatic AMD may begin as a blur in the direct visual axis. As portrayed in **Figure 1.2**, this can gradually worsen to distortion and a blank patch variable in size [4]. Visual loss can be monitored by means of an Amsler grid or through preferential hyperacuity perimetry (PHP), tests which are able to track presence of distortions and missing fields in sight [5-7]. Due to the redundancy of the human visual system, patients having two eyes may experience different symptoms of AMD in one eye as compared to the other. For this reason, AMD can persist without diagnosis in early stages as one eye will compensate for irregularities in the afflicted macula [8]. AMD exists on a spectrum and is multifactorial in nature. Slow progression from early and intermediate forms of AMD can lead to advanced forms defined by geographic atrophy (advanced dry AMD) or choroidal neovascularization (wet AMD). Vision loss in later stages of AMD is caused by photoreceptor damage in cases of geographic atrophy and/or hemorrhaging due to abnormal angiogenesis in the nervous tunic [9].

AMD has been associated with several hereditary components involved in stress and immune response, lipid transport, extracellular matrix (ECM) remodelling, DNA repair, angiogenesis and programmed cell death [10, 11]. Mutations in the age-related maculopathy susceptibility protein 2 (ARMS2) and complement factor H (CFH) genes are two of the major contributors to AMD [12]. The most common loci variants are nonsynonymous alanine to serine mutation at codon 69 in ARMS2 (ARMS2 A69S) and tyrosine to histidine mutation at codon 402 in CFH (CFH Y402H) [13]. However, genome wide analysis has defined at least 34 genetic loci having 52 variants with AMD onset [14]. Recently, an additional 12 novel loci were identified, through meta-analysis of genome-wide association studies, which are thought to be involved in AMD pathogenesis [11]. Individuals who are homozygous for both CFH Y402H and ARMS2 A69S are of the highest risk, being 50 times more likely than controls to develop AMD [15]. In addition, CFH mutations have been affiliated with development of geographic atrophy where ARMS2 has been more closely tied to neovascularization [16].

**Figure 1.2.** Simulation of AMD for a patient experiencing geographic atrophy. The image to the left depicts a fall landscape at Killarney Provincial Park in Ontario, Canada. In the image to the right, AMD is represented with distortion of figures (often described as wavy and/or blurry regions) in the central axis, along with dark blank areas (scotomas) caused by geographic atrophy. AMD presenting with choroidal neovascularization, leads to hemorrhaging which can result in more severe loss of sight. Image created using a Nikon D3100 and Adobe Photoshop.

Alongside genetic predisposition, advancing age has been hypothesized to increase the risk of developing AMD by 1.2 times every five years [17]. Age is the most prominent factor contributing to pathogenesis; however, research has tied AMD to other events. For example, cataract surgery has also been correlated, with those undergoing surgery being 3 times more likely to develop AMD than those who have not [18]. Along with cataracts, AMD has shown to be comorbid with myopia, glaucoma, and systemically with coronary heart disease, atherosclerosis, hypertension, hypercholesterolemia, coronary heart disease, chronic obstructive pulmonary disease, emphysema, and arthritis [19]. Patients with AMD are also at increased risk of developing anxiety and depression [20, 21]. Angiotensin-converting enzyme inhibitors, prescribed to lower blood pressure in diagnoses such as hypertension and diabetes, have been associated with an increased risk of developing AMD by 3.26 times [22]. Similarly, patients diagnosed with diabetes have been found to be 1.6 times more likely to develop AMD [18]. Many of these risk factors and comorbidities are unavoidable or hereditary. Modifiable areas which can minimize likelihood of developing AMD are diet and minimal tobacco use [10], with lifelong smokers being twice as likely to develop AMD as non-smokers [22].

### 1.2.1 Dry AMD

Dry AMD (dAMD) is often characterized as early stage or nonexudative AMD, however late-stage AMD with geographic atrophy is also encompassed by this diagnosis. Clinicians use the four-point Age-Related Eye Disease Study (AREDS) classification to diagnose AMD from ocular fundus photographs. AREDS classification categorizes patients as having either no AMD or normal aging, early AMD (having drusen >63 µm and ≤125 µm with no pigment changes), intermediate

AMD (drusen >125 µm, any pigment changes, geographic atrophy lacking fovea involvement), or advanced dry or wet AMD (geographic atrophy involving the fovea and/or neovascularization) [23, 24]. Geographic atrophy describes the localized degeneration of the photoreceptors, the retinal pigment epithelium (RPE), and choriocapillaris (the capillary layer of the choroid) in dAMD. Mitochondrial dysfunction of the RPE coincides with AMD onset and so RPE functionality has gained widespread acceptance as a key factor in nucleation of pathogenesis [25-27].

The RPE is mounted on the Bruch's membrane (BrM) and forms the blood-retinal barrier (BRB) between the choroid and the retina. As such, the RPE acts as a filter, regulating diffusion of oxygen and nutrients to the photoreceptor cells while simultaneously removing waste products through phagocytosis and directing waste back into the choriocapillaris [4]. It is the RPE which maintains both the photoreceptors and the BrM. Recent study has suggested that impaired mechanisms of autophagy and mitophagy in RPE contribute to accumulation of waste within retinal layers [26]. In addition, RPE is pigmented by granules called melanosomes which absorb light to protect the retina from UV radiation [28]. Hyperpigmentation in early dAMD has therefore been tied to RPE dysfunction, where hypopigmentation in late dAMD can be considered to be a cause of RPE loss and atrophy.

If the RPE is not maintained, photoreceptors are at risk of damage due to non-specific diffusion from the choroid, high exposure to UV rays, and waste accumulation. This often leads to mitochondrial defects and cell death [29]. In addition, rods and cones possess the highest oxygen consumption per gram of tissue than any cell type [30]. This increased oxygen uptake paired with the increase of light exposure due to aging has made the retina a susceptible site for reactive oxygen species (ROS) which accumulate in the RPE layer further contributing to atrophy [31, 32]. Lipofuscin, a fluorescent amalgamation of oxidized proteins, lipids, and sugars, is a by-product of the visual system which naturally accumulates with age. In dAMD, an abnormal concentration of lipofuscin is correlated with disease state. Lipofuscin's N-retinylidiene-N-retinylethanoamine (A2E) fluorophore has been shown to further disorder mitochondrial function, activate the complement cascade, inhibit lysosome transport, inhibit phagocytosis, and cause oxidative damage leading to compromised cell membranes and apoptosis when exposed to RPE *in vitro* [33]. At critical concentrations A2E prevents the degradation of phagolysosomes containing photoreceptor waste products in RPE [34]. By in large, A2E's influence on lysosome transport and phagocytosis has supported the belief that lipofuscin accumulation also leads to presence of drusen in AMD.

Drusen are aggregates composed of inflammatory debris as well as oxidized proteins and lipids. These remains derive from cells of the choroid, RPE, photoreceptors, and from within vasculature as the blood-retina barrier allows cholesterol passage from serum. Appearing as yellow deposits, drusen can be described as "hard" possessing distinct borders or "soft" with undefined margins. Although drusen accumulation is typical with age, over accumulation localized between BrM and the RPE inhibits oxygen and nutrient transfer affecting maintenance

of photoreceptors [35]. Drusen larger than 63 µm is indicative of early stage dAMD. As drusen increase in number, agglomerates may lead to detachment of the RPE and slow progression into geographic atrophy [36]. Drusen has been shown to possess activators of the complement system, contributing to increased complement activation correlated with chronic inflammation in AMD pathogenesis [37, 38]. Interestingly, drusen has also been shown to possess β-amyloid and amyloid fibrils sharing similarities with plaques present in atherosclerosis, elastosis, and Alzheimer's disease [39-42]. Despite the interconnectedness of chronic inflammation, RPE dysregulation, lipofuscin, and drusen build-up, no single target has been identified as the predominant initiator of dAMD; the most common presentation of AMD amongst patients.

### 1.2.2 Wet AMD

Wet AMD (wAMD) deviates from dAMD as it is characterized by choroidal neovascularization, or the growth of abnormal blood vessels which cross the BrM from the choroid and enter the macula. Loss of vision is heightened as these young leaky vessels cause hemorrhaging which obstructs sight and causes separation or misalignment of the BrM, the RPE, and the photoreceptors. For these reasons, wAMD is sometimes referred to as exudative or neovascular AMD [43, 44]. **Figure 1.3**, depicts ocular fundus presentations of both dAMD and wAMD forms as compared to a healthy macula. In order to ensure vasculature formation is controlled in the choroid, concentrations of pro-angiogenic and anti-angiogenic factors are highly balanced. When dysregulated, an increase in pro-angiogenic factors such as vascular endothelial growth factor (VEGF) and decrease in anti-angiogenic factors such as pigment epithelium derived factor (PEDF), proliferation of endothelial cells results in new vessel formation [43].

VEGF glycoproteins, are a platelet derived pro-angiogenic and pro-lymphangiogenic super family of factors. In mammals the VEGF family consists of five members: VEGF-A (often simply referred to as VEGF), VEGF-B, VEGF-C, VEGF-D, and placenta growth factor (PlGF). VEGF-A in particular has been shown to be heavily involved in initiating the proliferation and migration of endothelial cells in blood vessel formation [45]. During embryogenesis VEGF-A is critical. In heterozygous knockout studies using mouse models, whereby embryos lacked a single VEGF allele, production of immature blood vessels resulted in premature death [46, 47]. VEGF-A functions through binding to receptor kinases VEGFR-1 and VEGFR-2. VEGFR-1 (Flt-1) binds with high affinity but induces low tyrosine kinase activity as compared to VEGFR-2 [48]. The exact role of VEGFR-1 continues to be an area of study, however it has been shown to be upregulated during hypoxia [49]. Related, research has suggested that VEGFR-1 may act more like a decoy in mitogenesis, working to sequester VEGF-A from VEGFR-2 and lower proliferation of endothelial cells [50]. This work is further supported by studies involving homozygous Flt-1 knockout mice, whereby lack of both Flt-1 alleles resulted in embryonic death due to endothelial overgrowth and disorganized blood vessel formation [51].

Interestingly, a soluble form of VEGFR-1 known as sFlt-1, has been described as an endogenous VEGF inhibitor with work associating wAMD with its downregulation [52, 53]. This leads to an increase of VEGF-A in the retina related to abhorrent angiogenesis [53]. Although binding affinity of VEGF-A to VEGFR-2 receptors is 10 times lower than VEGF-1, VEGFR-2 is widely accepted as a key receptor in endothelial proliferation and angiogenesis [48, 54]. Genes associated with VEGF-A have confirmed involvement in AMD pathogenesis [12]. VEGF-A and its receptors play a significant role in choroidal neovascularization and are popular targets for wAMD treatment.

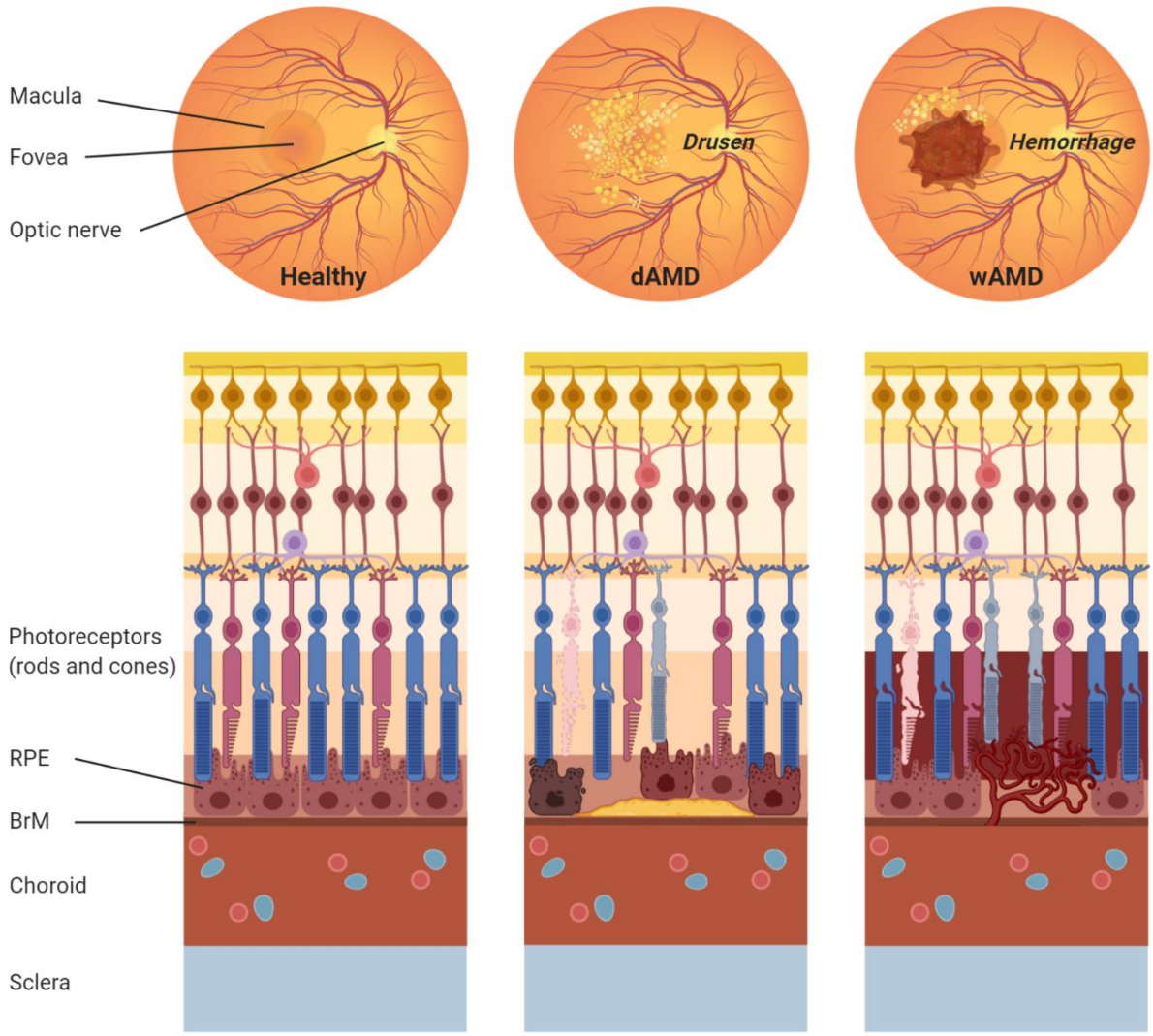


**Figure 1.3.** Illustration of possible presentations of dAMD (drusen accumulation in the subretinal space along with photoreceptor and RPE cell death associated with geographic atrophy) and wAMD (drusen accumulation, some photoreceptor atrophy, and abnormal angiogenesis from the choriocapillaris) as compared to a healthy macula. Ocular fundus images depict what clinicians may see during diagnosis. It is important to note that AMD exists on a spectrum, presentations of these symptoms vary from patient to patient as well as between eyes. Image created using BioRender.com.

### 1.2.3 Treatments in AMD

The secretion of VEGF-A has been shown to be upregulated in RPE under oxidative stress [55]. The abnormal angiogenesis which follows, produces young vessels inclined to leakage. Pressure associated with this hemorrhaging can also result in the separation of retinal layers leading to disordered and damaged photoreceptors. This can further develop into fibrotic scarring [56]. Hence, the key to prevention of progression in wAMD is early detection and inhibition of blood vessel formation. In the early 2000s, wAMD vessels were occluded by means of photodynamic therapy which involved the intravenous administration of QLT/Novartis' photosensitizer Visudyne (verteporfin). With a tendency to accumulate in the choroid, Visudyne in the presence of oxygen and non-thermal light, produces ROS which effectively cauterizes vessels. However, the high risk of collateral damage to healthy tissues has made this intervention less common [57]. Today, wAMD is primarily treated by reducing concentrations of VEGF-A.

Interest in angiogenic factors began over 80 years ago, when the existence of factors responsible for blood vessel formation was hypothesized in tumour growth [58]. It was later determined that tumours are dependent on a new supply of blood vessels which feed the mass directly [59]. This inspired research to define therapeutic targets for preventing angiogenesis. In 2004, US Food and Drug Administration (FDA) approval of Genentech/Roche's monoclonal anti-VEGF-A antibody, Avastin (bevacizumab), was supported by increased survival rates when co-administered with chemotherapeutics in metastatic colorectal cancer [60]. In December of that same year, Eyetech (now Valeant)/Pfizer's Macugen (pegaptanib), a pegylated aptamer capable of blocking the VEGF-A isoform $VEGF_{165}$, became the first FDA approved anti-VEGF treatment for ocular conditions [57, 61, 62].

Today, anti-VEGF therapeutics are current market leaders in wAMD treatment specifically: Regeneron/Bayer's Eylea (aflibercept – anti-VEGF-A and anti-VEGF-B) and Genentech/Roche/Novartis' Lucentis (ranibizumab – anti-VEGF-A). Despite being the first to obtain FDA approval in the US, Macugen has become an obsolete treatment for wAMD with lower efficacy than Eylea and Lucentis. Interestingly, Avastin is sometimes prescribed as a first line of defense in wAMD. Despite not being approved as an ophthalmic drug, Avastin is often used off label to treat wAMD due to its low cost and comparable efficacy. However, its prescription must follow patient informed consent and its use continues to vary amongst the seven major markets (United States, France, Germany, Italy, Spain, United Kingdom, and Japan). Because anti-VEGF therapeutics are delivered via intravitreal injection on a monthly/bimonthly timescale, patient compliance is one limiting factor in treatment success [57]. There is therefore a demand for treatments in AMD which require less frequent intervention and reap long term rewards.

In the retina, the complement cascade works alongside various retinal innate immune cells: microglia, perivascular macrophages, and a small number of dendritic cells to maintain homeostasis. Low-grade activation of the complement cascade, the para-inflammatory response,

is important for retinal remodelling and neuroprotection. However, in AMD this response is dysregulated, leading to chronic inflammation, accumulation of drusen in dAMD, and upregulation of VEGF-A leading to wAMD [63-68]. Given the role of complement in disease progression, anti-complement drugs have been developed as potential therapeutics. Amongst the most notable are Zimura (Ophthotech) and APL-2 (Apellis) which are currently in clinical trials [57, 69].

Still, there are currently no approved treatments for early to advanced forms of dAMD. As this diagnosis represents a majority of all AMD patients, there lies a large unmet need in the clinic. As dAMD also largely represents early symptoms of AMD, its progression can lead to vision loss through geographic atrophy and/or through neovascularization. Preventing progression in early stages can inhibit worsening symptoms and protect photoreceptors from further damage. The National Institutes of Health (NIH) has conducted Age-Related Eye Disease Studies which suggest that the risk of progression into late stage AMD from intermediate dAMD could be reduced by 25% through vitamin E, vitamin C, zinc, beta carotene, lutein/zeaxanthin, and omega-3 fatty acids (docosahexaenoic acid and eicosapentaenoic acid) supplementation [56, 70]. These vitamin and mineral recommendations remain the only clinical interventions for dAMD. Given complications with the RPE in early dAMD, as described above, cell-based therapies which may minimize repetitive treatment regimens and improve or restore visual acuity have been sought out.

## 1.3 THERMORESPONSIVE HYDROGEL BIOMATERIALS

Hydrogels are hydrophilic polymeric networks capable of swelling with water to a significant extent. The resulting three-dimensional structure is able to retain its shape due to physical or chemical crosslinking. Chemical crosslinks are driven by ionic or irreversible covalent bonds where physical crosslinks are a product of intermolecular forces resulting in conformational changes [71, 72]. The potential to tune water content as well as their porous structure resembling that of ECM make hydrogels suitable candidates for a variety of biomaterials applications [73]. Hydrogels also offer the potential for *in situ* gelation by means of chemical crosslinking, photopolymerization, or response to environmental stimuli such as pH or temperature [74]. Thermoresponsive hydrogels are of particular interest as an injectable. The ability to promote gelation through temperature alone offers an elegant system which can change properties from ambient to physiological temperature. This solution to gel (sol-gel) transition may occur at a lower critical solution temperature (LCST), whereby hydrogels move from a soluble to insoluble state above a defined temperature. Alternatively, thermoresponsive systems may have a sol-gel transition below an upper critical solution temperature (UCST) [75].

Various polymeric systems have been studied for their ability to respond to thermal stimuli. These systems include, but are not limited to, derivatives of natural polymers such as polysaccharides (chitosan, xyloglucan, and cellulose) and proteins (gelatin). In addition, synthetic

materials such as poly-N-isopropylacrylamide (pNIPAAm), poly(ethylene oxidel)-b-poly(propylene oxide)-b-poly(ethylene oxide) (PEO-PPO-PEO), polyethylene glycol (PEG) copolymers, poly(organophosphazenes), and 2-(dimethylamino) ethyl methacrylate (DMAEMA) [74, 76-78]. By far the most studied of synthetic thermoresponsive hydrogels, pNIPAAm-based polymers have a well-established history in biomedical research applications.

### 1.3.1 pNIPAAm-based thermoresponsive hydrogels

The acrylamide monomer was first synthesized in 1956 [79], later patented in its polymerized form as a rat repellant in 1957 [80]. pNIPAAm, depicted in **Figure 1.4**, went on to be extensively studied and in 1968 Heskins and Guillet provided a detailed report of macroscopic phase separation of pNIPAAm upon heating. This work indicated that water molecules will orient in a more ordered fashion around non-polar N-isopropyl groups while also having the ability to participate in hydrogen bonding with polar amide groups of the pNIPAAm chain. The interactions which dominate are dependent on the temperature of the solution as described by study of an endotherm at the LCST of pNIPAAm using Differential Scanning Calorimetry (DSC). DSC measurements of pNIPAAm correlate with the amount of energy required to break hydrogen water-polymer bonds [81]. Later research focused on characterizing the behaviour of pNIPAAm at its LCST as a coil to globule conformational change driven by the hydrophobic effect [82-84]. Below its LCST, polar groups of pNIPAAm are exposed and can of interact with surrounding water molecules, polymer chains are coiled and flexible. As pNIPAAm is heated, chains undergo a collapse and subsequent aggregation driven by an increase in entropy ($\Delta S$) that dominates the exothermic enthalpy ($\Delta H$) of the system [85-90]. Increase in intramolecular polymer-polymer interactions aim to limit surface area of non-polar groups exposed to water [91].

Homopolymers of pNIPAAm have an LCST of 32°C, are non-degradable, and respond to changes in pH [74, 92], making pNIPAAm an excellent candidate for thermoresponsive culture substrates (TRCS) intended for tissue engineering [93, 94]. pNIPAAm TRCS are formed through grafting (p)NIPAAm to culture substrates such as polystyrene via spin coating, free radical polymerization, atom transfer radical polymerization (ATRP), reversible addition fragmentation chain transfer (RAFT), electron beam polymerization, or plasma polymerization [95]. Cells cultured on TRCS are able to form monolayers atop globular hydrophobic pNIPAAm at 37°C. Once removed from incubation however, the temperature drop below 32°C induces a change in state in the pNIPAAm. Coiled hydrophilic pNIPAAm swells with culture media, simultaneously releasing the cell sheet [96]. TRCS have a high impact in tissue engineering, allowing for cell sheet harvest with preserved and intact ECM suited for transplant [97]. These systems have been used to harvest RPE sheets *in vitro* [98, 99].

Synthetically, the LCST of pNIPAAm can be adjusted through copolymerization with various hydrophobic or hydrophilic groups [85]. In biomaterials this is leveraged, whereby NIPAAm is often polymerized with hydrophilic monomers to increase LCST near physiological

temperature, creating potential for *in situ* injectable applications [100]. Incorporating monomers which will alter LCST over time can also act as a degradation mechanism for pNIPAAm-based biomaterials. Incorporation of enzymatically or hydrolytically labile groups, which increase LCST upon cleavage, allow for the formation of materials which initially possess LCSTs below physiological upon injection and above physiological over time [101-105]. These materials dissolute with increased LCST offering clearance potential from target sites. Given these opportunities for tunability, pNIPAAm-based materials have been heavily studied for drug delivery and tissue engineering [106].

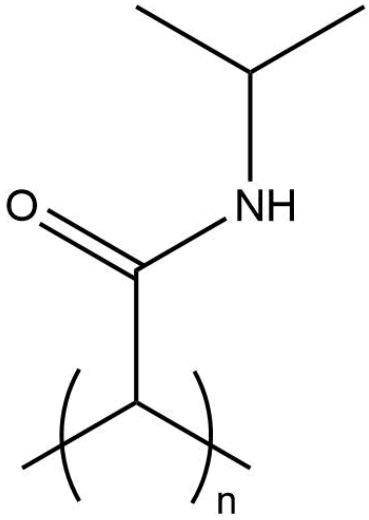


**Figure 1.4.** Molecular structure of pNIPAAm.

## 1.4 CELL DELIVERY TO THE BACK OF THE EYE

Access to the back of the eye remains a primary barrier in retinal cell transplantation. Nevertheless, regenerative therapies for retinal diseases remain a major focus in ophthalmic research, with an expansive array of autologous and allogeneic cell lines being tested. Cell lines of interest are often dependent on the disease application. In early stages of AMD, RPE dysfunction is closely tied to disease onset. Here an aim to protect photoreceptors and prevent further atrophy, may be fulfilled by replenishing the outer RPE alone. In later stages of AMD, damage to the Ruysch's complex (RPE, BrM, choriocapillaris) and neural inner retina may also require transplant of photoreceptor, pluripotent, or multipotent lines to restore vision [107]. As summarized in **Figure 1.5**, implantation of cell sheets, full and partial retinal transplants, cell suspensions, as well as two- and three-dimensional scaffolds have been explored within the subretinal space.

Retinal transplant was first described in 1959, when a fetal rat retina was transplanted into the anterior chamber of its parent [108]. This later inspired work focused on transplantation

of full thickness retinal tissue which pioneered delivery of free cell suspensions and cell aggregates [109-115]. Transplant of neural retinal lines as well as improved surgical intervention for full retina transplant [116-124], is attributed to the work of Silverman & Hughes who developed methods of isolating photoreceptor sheets from adult and postnatal retinas [125]. However, limited sourcing of complete retinal cell sheets has rendered these harvesting and transplant methods as more model-like than clinically accessible [126].

As such, translocation of autologous RPE sheets has also been explored for patients with choroidal neovascularization. In order for translocation to be successful though, the Ruysch's complex must be intact thereby excluding cases of AMD with geographic atrophy [127-129]. A small subset of RPE cells can be activated into stem-like mesenchymal progenitors [130]. These RPE stem cells have very recently been explored for monolayer transplant in non-human primates, showing appropriate differentiation into RPE and maintenance of photoreceptors [131]. Induced pluripotent stem cells (iPSCs) and embryonic stem cells (ESCs) have also been proposed as viable sources for RPE and neural retina regeneration [132-134]. iPSCs have been successfully differentiated into functional retinal cell lines with promising results both *in vitro* and *in vivo* [134-138]. With ESC sourcing remaining an ethical concern, self-sourced iPSCs have the potential to circumvent access to progenitor lines as well as reduce risk of immune rejection associated with donor tissue.

Research using photoreceptor progenitors suggests that committed cell types may have higher success after transplantation compared to pluripotent cells. This is marked by appropriate differentiation into rod progenitors, synapse formation, and improved vision *in vivo* in mouse models [139]. A major concern with stem cell delivery is off-target differentiation or teratoma formation. In order to prevent this from occurring, researchers must ensure that delivered cells are fully differentiated prior to transplant or will only differentiate into desired cell types [115]. In this way, multipotent progenitor delivery holds great potential compared to pluripotent lines. Retinal progenitor delivery has also proven to be effective in restoring vision in rat models [140]. Here, retinal progenitor cells are not only celebrated for their ability to replace functional elements, but also for their capacity to introduce trophic factors which contribute to cell differentiation and survival [140-142]. Mesenchymal stem cells, adipose-derived stem cells, and dental pulp stem cells have also been studied for their ability to provide neurotrophic growth factors to retinal ganglion [143]. Delivery of cell-free encapsulated ciliary neurotrophic factor (CNTF) has shown protective benefits in Phase I clinical trials and is currently being explored in Phase II as a therapy for geographic atrophy, retinitis pigmentosa, and macular telangiectasia type 2 [144-146].

Clinical trials involving delivery of iPSCs, ESCs, stem cell derived lines, and various other progenitors are underway [107, 147, 148]. Ocata Therapeutics has conducted a 4 year follow up of human ESC derived RPE (hESC-RPE) subretinal suspension delivery in dAMD and Stargardt disease. Of 18 subjects, 13 displayed increased pigmentation surrounding atrophic sites [149]. In

Japan, the RIKEN Center for Developmental Biology and the Center for iPS Cell Research and Application has described a case of iPSC-RPE sheet delivery in a 77-year-old patient with advanced wAMD and choroidal vasculopathy. The transplanted sheet remained intact and symptoms did not develop or worsen one year following transplantation [150]. The London Project to Cure Blindness (LPCB) used a similar method of transplantation as the RIKEN Center, involving excision of the choroidal neovascular membrane seen in wAMD subjects prior to insertion of an RPE sheet. Where the RIKEN Center did not explore a synthetic cell carrier, LPCB used a 6 mm by 3 mm polyester sheet for hESC-RPE cell delivery. Following one year of study, the two subjects tested were found to have improved visual acuity marked by letter gain, biomicroscopy, and optical coherence tomography (OCT) [151]. However, authors of the LPCB study note that even with a custom device to transplant the described cell sheet, surgical methods of subretinal implantation continue to be highly invasive limiting this type of therapy to advanced cases of AMD.

Janssen has explored a novel *ab externo* approach for less invasive subretinal injection of human umbilical derived cells. Stem cells were isolated from the stroma of donated umbilical tissue through enzymatic digestion prior to further selection ensuring absence of spontaneous differentiation. This CNTO-2476 (Palucorcel) line is believe to be of benefit for delivery of cells which can replenish the neural retina and RPE, as well as in delivery of neurotrophic factors such as thrombospondins, brain derived neurotrophic factor (BDNF), and soluble vascular endothelial growth factor receptor 1 (sVEGFR-1) [152]. Palucorcel's novelty is tied to its method of delivery which intends to improve cell distribution within the subretinal space. This method uses an iTRACK™ 275 microcatheter and endoscope to allow for near parallel subretinal cannulation through a 3 mm opening created by sclerotomy (9-12 mm from the corneal limbus) followed by choroidotomy. In Phase I/IIa clinical trials, Palucorcel delivered using this approach in patients with geographic atrophy improved visual acuity. However, this method was correlated with an increase in retinal detachments and perforations [153, 154].

As a response, Janssen underwent a Phase IIb trial using a suprachoroidal surgical approach. In this study, 21 participants with geographic atrophy received $3.0 \times 10^5$ cells in 50 µL via Palucorcel. As opposed to *ab externo* delivery, in Phase IIb access to the subretinal retinal space began through cannulation to the suprachoroidal space through sclerotomy, followed by microneedle advancement through the choroid, BrM, and RPE into the subretinal site of interest. Delivery was better visualized through direct microscopy as opposed to endoscopy. Despite no occurrences of retinal detachments or perforations, and adverse events such as conjunctival hemorrhage, vitreous floaters, and retinal hemorrhage being mainly mild resolving in one month, improved visual acuity was not reported in this follow up. In addition, reduction in area of geographic atrophy was not found [152, 155]. However, Janssen's Phase IIb Palucorcel study represents a landmark in improving surgical approaches in subretinal cell delivery. Beyond which cell types to employ and improved surgical interventions however, an immediate barrier to

subretinal delivery continues to be how cells are presented to the subretinal space. To improve clinical handling and integration with native tissue post transplant, cell carriers are recommended.

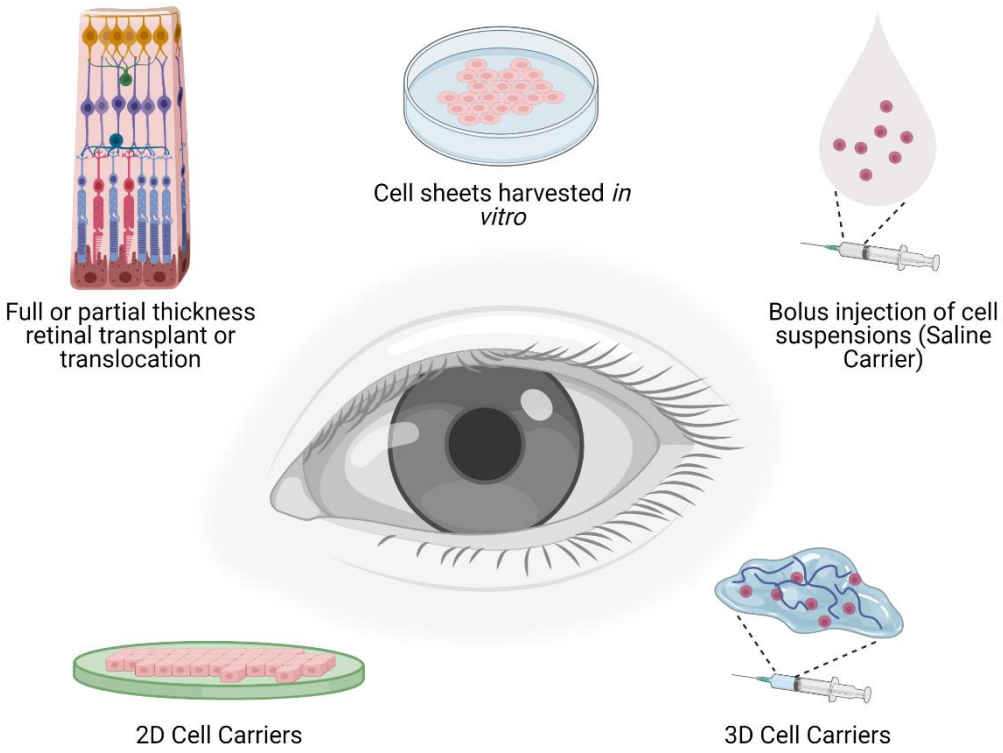


**Figure 1.5.** Summary of cell regenerative therapies for retinal disease. Image created using BioRender.com.

### 1.4.1 2D cell carriers for subretinal delivery

Cell carriers seek to improve delivery of cell suspensions or complete cell sheets. In particular, cell sheets lacking a substrate are delicate making transplantation difficult for clinicians. Two-dimensional substrates for subretinal delivery aim to replace and mimic BrM. Research has explored the use of porcine amniotic membrane (AM) [156-159]. Studies, conducted by la Cour and colleagues, looked at AM implantation into porcine models that had surgically induced choroidal neovascularization. Initially, with the intent of exploring histology changes in a porcine model of neovascularization compared to fluorescein angiography and fundus photography, AM was found to integrate well with tissue and support RPE migration [156]. The group went on to look at how injury influenced RPE regeneration and concluded that trophic factors in AM increased proliferation following debridement of the RPE layer [157]. AM was then shown to reduce neovascularization when placed directly over the site of hemorrhage

and could maintain RPE pigmentation. However, if placed incorrectly atypical angiogenesis into the basal surface of AM was reported [158]. Further study with larger sample sizes would be of interest in determining the potential of AM in the back of the eye.

Donated BrM has also been explored as a substitute. To improve RPE phagocytosis [160], proliferation, and reduce incidence of apoptosis [161]. BrM with an exposed inner collagen layer coated with the ECM proteins fibronectin, vitronectin, and laminin showed improved proliferation and survival of human adult and fetal RPE. Interestingly, analysis of 45 human donor maculas has revealed that drusen deposition favours regions of the BrM lacking underlying vascular lumen [162]. This is complemented by the work of Skottman et al. (2017), whereby co-culture of hESC-RPE and microvascular endothelial cells on either side of polyethylene terephthalate (PET) membranes, improved RPE barrier properties as measured by transepithelial electrical resistance [163]. Further, researchers have also attempted to determine which bioactives are necessary for RPE survival on aged BrM and BrM associated with dAMD. This was done by performing size exclusion filtration on conditioned medium derived from bovine corneal endothelial cells. It was found that components of the 3 kDa and 10-50 kDa filtrate contributed to fetal human RPE adhesion and, in the case of 10-50 kDa media, RPE survival. Mass spectrometry revealed 175 ECM associated proteins unique to the 10-50 kDa filtrate, where 29 proteins were found to be unique to the 3 kDa filtrate. Transforming growth factor (TGF)β-2 was determined to play a particularly important role [164]. Unfortunately, use of BrM and AM is limited by difficulty in sourcing, fear of immune rejection, and potential disease transmission in xeno- and allogeneic tissues [107].

Various other natural materials such as denuded retinal ECM [165], silk fibroin [166-169], acetylated bacterial cellulose [170, 171], fibrin [172], spider silk [173], gelatin [174], and soy protein [175] have also been investigated for subretinal cell delivery. Many of these materials are celebrated for their biocompatibility, safe degradation products, and ability to mimic ECM. Batch-to-batch variability of natural products as well as increased likelihood of allergy, has opened up interest in synthetic polymers for tissue engineering. Synthetic polymers rely more heavily on modification, with ECM proteins and/or growth factors, to mimic BrM than their natural counterparts. However, ease of reproducibility and improved sterility have made synthetic polymers a promising choice for cell delivery to the subretinal space [107].

Noting difficulty maintaining RPE phenotype and minimizing the inflammatory response, White et al. (2017) explored use of poly(ethylene glycol) diacrylate (PEGDA) with molecular weights ranging from 3.4 to 20 kDa. Scaffolds with molecular weights of 20 kDa and 5 kDa, possessing Young's modulus of 60 and 1200 kPa respectively, were modified with the adhesion peptide sequence Arginine-Glycine-Aspartate-Serine (RGDS). The authors reported uniform spreading of ARPE-19 cells cultured in DMEM/F12 (15% FBS) on high modulus scaffolds as compared to low modulus. Fluorescent imaging of all surfaces revealed cell aggregation and clumping on the low modulus substrates. Increase in metabolic activity, using a PrestoBlue

mitochondrial reduction assay on days 7 and 14 of culture, was found on high modulus scaffolds as compared to low modulus and tissue culture plate controls. However, inflammatory markers IL-6 and MCP-1 were upregulated on both high and low modulus substrates, with IL-8 and IL-6 expression being significantly higher in high modulus substrates compared to the low modulus substrates. In addition, the RPE marker CRALBP was downregulated on high and low modulus substrates compared to tissue culture plate controls while the de-differentiation marker SMAD3 showed a non-significant increase [176]. This study confirms that modulus plays a notable role in RPE attachment and viability, however scaffolds tested were much thicker than native BrM. *In vivo* analysis of the high modulus material is recommended to determine extent of inflammation as well as ability to maintain RPE phenotype post implantation. Inflammation is an important component in healing upon insertion of implants intended for cell delivery. However, excessive inflammation can lead to host rejection of the scaffold.

Comparing the fibrillar mesh morphology of the inner collagenous layer of native BrM, a strong likeness to electrospun materials can be noted. Warnke et al. (2013), highlighted this in their work with 85:15 mol% poly(lactic-co-glycolic acid) (PLGA) materials as well as materials fabricated from bovine Type I collagen. Collagen scaffolds were further chemically crosslinked after electrospinning, through application of a solution of 1:5 mol% N-hydroxysulfosuccinimide:1-ethyl-3-(3-dimethylaminopropyl)-carbodiimide in 95% ethanol. Fiber diameter of the PLGA and collagen materials were reported as approximately 331 nm and 299 nm respectively, where BrM was measured to have fibers around 60 nm. No comparison was made between the moduli of electrospun materials versus BrM. Material thickness was measured to be 14 µm where native BrM was reported to be near 2-4 µm. The authors reported comparable hexagonal morphology and RPE65 and ZO-1 expression on all substrates after 11 days, with electrospun materials allowing for microvilli formation comparable to that observed on BrM controls. Microvilli were limited on controls lacking fibrillar topology (glass cover slips and PLGA films) confirming that topology may be important in RPE transplantation [177]. Polylactic acid (PLA) and PLGA substrates have also been developed to support the growth of retinal progenitor [178] and retinal ganglion cells [179-181].

A recent study by Krishna et al. (2020), noted the importance of fiber diameter on cell function in electrospun poly(ε-caprolactone) (PCL) membranes. PCL membranes with nanofiber diameters of 500 and 1300 nm and comparable moduli (7.5 and 11.1 kPa respectively) were formed. Cell studies using ARPE-19 and human corneal epithelial cells (HCE-T) revealed a variable response which could be correlated with fiber diameter. On 500 nm PCL scaffolds, ARPE-19 cells secreted VEGF-A and displayed an increase in expression of pluripotent markers Oct ¾, Sox2, and Nanog as determined through qualitative polymerase chain reaction (qPCR). On the other hand, HCE-T displayed increased expression of markers of differentiation (as measured by mRNA expression of CK3 and CK12) and proliferation (as measured through fluorescence-activated cell sorting analysis of propidium iodide staining as well as increased Ki67-positivity, a marker of

active phases of the cell cycle). HCE-T cells also displayed a decrease in pro-apoptotic factor Bax and complimentary increase in anti-apoptotic factor BCL2 on 500 nm scaffolds. In contrast, 1300 nm mats were met with opposite trends, with an increase in proliferative markers and decrease in apoptosis in ARPE-19 cultures. ARPE-19 cells also displayed greater phagocytic activity as indicated by engulfment of fluorescein isothiocyanate (FITC) labelled latex beads. As well, pluripotent markers were upregulated in HCE-T culture on 1300 nm scaffolds. Although the findings described were not always significant, a notable trend was observed and corroborated across assays. Authors were thorough and included various experiments to confirm expression of markers of interest [182].

Furthermore, along with displaying moduli conducive to attachment and spreading, permeable scaffolds delivering RPE are desired for adequate oxygen, nutrient, and waste transport. Lu et al. (2012), explored a submicron parylene-C substrate with a 0.6 µm thick frame and 0.3 µm semipermeable "pores" forming a mesh micropattern which could be easily handled. The thickness of the semipermeable region was determined through comparison of FITC labelled dextran diffusion across parylene-C of varying thickness. From this, diffusion coefficients were determined which later could be used to extrapolate a theoretical size exclusion limit for the membranes. The results were compared to previously reported diffusion flux studies using donated human BrM of various ages. In these earlier studies, size exclusion limits of 200 kDa [183] and 500 kDa [184] were reported, leading Lu et al. to conclude the theoretical 1008 kDa exclusion limit of their 0.3 µm material was sufficient for nutrient transport [185].

Perfusion studies using ARPE-19 and H9-RPE (in DMEM/F12 with 10% FBS and serum-free X-VIVO 10 media respectively) were conducted to explore viability of cells receiving nutrients supplied from the opposite side of the parylene-C mesh on which they were seeded. This confirmed 0.3 µm thickness to be sufficient for nutrient transport supporting growth. These materials were coated with Matrigel to support adhesion. Further cell work using H9-RPE, showed adhesion and spreading after one day, confluence after one week, and some pigmentation after 4 weeks of culture on the 0.3 µm parlylene-C mesh. ZO-1 staining of tight junctions displayed hexagonal morphology and SEM images revealed RPE polarization [185]. However, it is unclear how many samples were included in each described cell study and statistical analysis was not performed. Parylene-C materials have since been shown to improve vision through delivery of intact monolayers in animal models [186-188]. Regenerative Patch Technologies (RPT) is currently exploring a parylene substrate for hESC-RPE cell delivery in dAMD. Preliminary data from the phase I/IIa clinical trial is indicative of slowed progression of visual loss and implant retention [189].

Permeability has also been controlled through pore size and distribution of 96:4 mol% poly(L-lactide-*co*-D-lactide) (PLDLA) films [190]. In this work, authors note the effect of humidity on pore size tunability, with 50, 65, and 80% humidity conditions yielding average pore diameters of 2.8, 3.8, and 5.0 µm respectively. These films had a characteristic honeycomb structure as

imaged with atomic force microscopy (AFM) and scanning electron microscopy (SEM). All films had thicknesses greater than native BrM at around 20 µm. Electrical resistance measurements as well as FITC labelled dextran flux studies were used to explore permeability, with 5.0 µm pores having a significant increase in permeability compared to the 2.8 and 3.8 µm films. In order to improve adhesion of hESC-RPE, scaffolds were dip-coated in type IV collagen. Dip-coating was reported to have no effect on permeability and after 3 weeks of culture all three scaffolds showed indications of cell adhesion, proliferation, polarization, pigmentation, and expression of RPE marker CRALBP as well as tight junction marker ZO-1. However, despite having synthesized elegant looking materials, this study severely lacked adequate cell controls and a reported sample size.

### 1.4.2 3D cell carriers for subretinal delivery

Unfortunately, 2D elastomeric matrices in the subretinal space continue to be limited by bulkiness and traumatic surgical intervention. Minimally invasive cell suspension delivery mitigates this. However, bolus saline injection of cells typically results in cell aggregation, cell death, limited control over cell fate, and poor localization to regions of interest [191]. To improve cell distribution following injection, hydrogel systems have garnered appeal. Hydrogels can be modified to encapsulate and hold delivered cell lines within target sites, allow for controlled release of biologics, and promote differentiation.

Shoichet and colleagues have contributed much to subretinal tissue engineering using a unique shear thinning hyaluronic acid and methylcellulose (HA/MC) gel [192]. HA/MC gels of varying HA and MC concentrations have been shown to support retinal progenitor stem cell proliferation *in vitro* as well as *in vivo* in mouse models. Subretinal injections using these gels resulted in improved distribution of delivered cells when compared to controls [193].

In Shoichet's further work, 1/1 w/w% HA/MC gels improved neural stem and rod cell survival linked to HA's interaction with cell surface adhesion receptor CD44. In this study, functional visual recovery in genetically blind TKO mice was highlighted [194]. Functional repair was again demonstrated using the 0.5/0.5 w/w% HA/MC material, when used to co-transplant RPE and photoreceptor lines into mice with degenerative RPE and photoreceptors induced by sodium iodate ($NaIO_3$) injection. Here, co-transplantation was key to visual recovery [195]. Shoichet's HA/MC systems have also gone on to be modified with Src homology 3 (SH3)-binding peptides to allow for controlled release of insulin-like growth factor 1 (IGF-1), resulting in increased viability in hESC-RPE culture [196]. Of note, the group has described a hyaluronan-furan and bis-maleimide polyethylene glycol material which later gave rise to a hyaluronan-methylfuran material capable of gelling in response to pH. At pH 7.4 the hyaluronan-methylfuran material is capable of encapsulating various cancer cell lines, displaying great potential for applications in tissue engineering [197, 198].

Alginate, a polysaccharide seaweed derivative, is an interesting system due to its crosslinking tunability via ions with a 2+ or greater charge. These crosslinks degrade through exposure to sodium, potassium, phosphate, and magnesium, allowing alginate gels to be cleared over time [199, 200]. RPE cells have been shown to proliferate well in 1.2% calcium crosslinked alginate hydrogels and show normal pigmentation [201, 202]. Further, hiPSC- and hESC-derived embryoid bodies (EBs) were encapsulated in 0.5 and 1 w/v% RGD-alginate hydrogels composed of Glycine-Arginine-Glycine-Aspartate-Serine-Proline (GRGDSP) coupled high guluronic acid, high molecular weight alginate crosslinked with 0.1 M calcium chloride in media. In preliminary work, alginate lacking Arginine-Glycine-Aspartate (RGD) led to reduced retinal structures and abnormal cystic features which promoted interest in RGD incorporation. Growth was compared to Hystem™ (thiolated-HA) and Hystem-C™ (1:1 thiolated HA: thiolated-gelatin) systems, as well as no gel suspension culture controls. EBs were initially grown from hESC/hiPSCs on Matrigel in mTeSR1 media, before being encapsulated in respective gels or suspended in supplemented DMEM/F12 following 12 days of culture. EBs were analyzed at days 30 and 45 [203].

Results revealed both Hystem™ systems to have no significant impact on EB differentiation. However, 0.5% RGD-alginate gels showed the most promise, having increased occurrence of optic vesicles and pigmented RPE. These gels were found to have a higher frequency of RPE as confirmed through increased expression of RPE markers CRALBP using flow cytometry as well as TYR and RPE65 using qualitative real time PCR. 0.5% RGD-alginate gels also increased expression of retinal ganglion marker MATH5 as compared to controls. 1% RGD-alginate gels positively influenced presence of RPE and optic vesicles but did not have a significant impact on other measures of retinal differentiation [203]. Alginate gels modified with antioxidants such as curcumin and taurine, have also been implored for their ability to protect the RPE from oxidative stress. In these studies, both curcumin- and taurine-modified alginate displayed good biocompatibility, cell adhesion, as well as increased expression of type I collagen (indicative of ECM production) and RPE markers CRALBP and RPE65 when cultured with primary RPE cells harvested from rabbits [204, 205].

*In situ* crosslinking Hystem™, used as a control material in the RGD-alginate study described above, has also been explored for its ability to deliver retinal progenitors to the subretinal space. Here, Hystem™ systems delivering retinal progenitors improved distribution in the subretinal space of retinal degenerative Rho -/- mice 3 weeks following injection, showing signs of photoreceptor differentiation through expression of recoverin. *In vitro* culture of retinal progenitors in Hystem™ gels with varying HA concentrations and crosslinking densities, formed neurospheres displaying maintenance of stemness after 15 days through expression of pluripotency markers Pax6 and nestin in most cells [206].

Chitosan hydrochloride and oxidized dextran have been combined into gels using Schiff-base linkages. The produced material (CS-Odex) is described as self healing and compatible with retinal progenitors capable of activating Akt and Erk pathways associated with cell growth and

proliferation. CS-Odex was also found to improve progenitor differentiation into photoreceptors, indicating a potential to aid in visual recovery [207]. Similarly, gelatin-hydroxyphenyl propionic acid (Gtn-HPA) has also been explored for retinal progenitor cell delivery [208]. Gtn-HPA is described as an *in situ* crosslinking hydrogel which undergoes time dependent crosslinking through addition of hydrogen peroxide and horseradish peroxidase. Gtn-HPA is capable of enzymatic degradation over a period of 1-2 weeks via host or supplemented enzymes. In order to explore Gtn-HPA's potential as a scaffold in neural retina delivery, Park et al. combined a 2X working solution of Gtn-HPA in PBS with human retinal progenitor cells prior to addition of the crosslinking catalysts. The gel cell mixture was then seeded onto glass coverslips coated with fibronectin and was allowed to gel for 5 minutes at 37 °C prior to addition of media. Cells seeded on fibronectin cover slips at equal concentrations were used as controls. Over 7 days, cell viability remained above 80% for both Gtn-HPA loaded gels comparable to controls, despite anticipated oxidative stress induced by hydrogen peroxide. Encapsulated cells tested positive for Ki-67, however this mitotic marker was expressed at higher amounts in control cells forming a monolayer [208].

Further, *in vivo* cell delivery in Long Evan rats, was explored using pig retinal progenitors positively expressing green fluorescent protein (GFP). Transscleral injections (4 µL) of cell loaded Gtn-HPA and saline cell suspension controls, were prepared to deliver 40 000 cells to the subretinal space. Successful injection was visualized by bleb formation using a dissecting microscope. Inflammatory response one week post injection in Gtn-HPA groups was lower than saline controls, as marked by low expression of the leukocyte marker CD45 in surrounding retinal layers. As well, subretinal localization of progenitors was improved in Gtn-HPA treated rats as compared to controls. However, persistent retinal detachment was noted with Gtn-HPA treatments. The authors suggest speeding up Gtn-HPA degradation may assist in retinal reattachment and healing in future work [208]. The above studies explore a myriad of primarily natural hydrogels for their ability to support cell growth and be retained within the subretinal space. Hydrogels combine the favourable properties of saline injection and 2D cell carriers for back of the eye delivery. Leveraging the porosity and ease of transplantation yielded by suspension injection with the tunability and mechanical properties of 2D substrates. The *in situ* gelation systems described by Park and the group of Dr. Shoichet, provide a particularly interesting demonstration of the potential for improving cellular entrapment upon injection along with the ease of handling attributed to saline.

#### *1.4.2.1 NIPAAm-based subretinal cell delivery*

Thermoresponsive NIPAAm-based synthetic hydrogels have been proposed in our group as a method of cell delivery to the subretinal space [209-214]. Hydrogels which are able to undergo a sol-gel transition upon injection, may also simultaneously trap and immobilize cells for which they are acting as a carrier. In doing so, loss of cells, aggregation, and efflux into off target sites, such as the vitreous, can be mitigated. In 2010, Fitzpatrick et al. showed that type I bovine

collagen conjugated with pNIPAAm displayed an LCST of 32°C as determined using DSC. Amine end groups on pNIPAAm were reacted with the carboxylic acids of aspartic acid and glutamic acid in type I collagen using EDC/NHS chemistry to form comb-like grafts. The resulting material showed good viability and entrapment of ARPE-19 cells [209].

Mazumder et al. (2012), went on to describe a 90:10 mol% pNIPAAm-*co*-acrylic acid N-hydroxysuccinimide (NAS) material (PNN-10), prepared through free-radical polymerization. The polymer was post modified with HA (PNN-HA), RGDS (PNN-RGDS), as well as both HA and RGDS (PNN-HA.RGDS). Co-polymerization with NAS was predicted to offer sites for bioconjugation throughout the polymer chain, improving formulations which could only support end-functionalization. Having RGDS distributed along the polymer backbone would better mimic ECM and thus improve entrapment of cells [210]. The authors note that several other groups had reported NAS addition to NIPAAm based polymers [104, 215] as well as some NIPAAm-HA materials [216, 217]. However, HA and RGDS combined for this application had not been reported.

DSC of PNN-10 confirmed its LCST to be below physiological at 27°C. PNN-10 that had been modified with RGDS or HA, showed an increased LCST of 31°C. PNN-10 modified with both RGDS and HA had an LCST of 32°C. All polymers were tested at 15 w/v% in PBS and underwent a heat ramp from 0 to 70°C at a rate of 2°C/min in hermetic pans. Preliminary cell culture using ARPE-19 cells was conducte and no significant difference in viability was found between materials as compared to tissue culture plate controls. Viability remained high (above 90%) in all treatments [210].

Subcutaneous injection of 15 w/v% PNN-10, PNN-HA, PNN-RGDS, and PNN-HA.RGDS in PBS, between the shoulder blades of SKH1-E nude mice, revealed that these materials underwent a robust sol-gel transition upon delivery. All materials excluding PNN-10, spread into a thin layer by day 3 following injection. This shows promise for potential use in the subretinal space, where gel spreading could assist with cell distribution and RPE monolayer formation. Additionally, neutrophils, monocytes, lymphocytes, and fibroblasts were evident in histological samples of the dermis of the injection site at day 3. There was no evident infiltration of immune cells in no injection controls. This mild foreign body response was not evident in dermis of day 7, 20, and 40 mice. The liver and spleen were also sectioned 40 days after injection. Results revealed no inflammation, necrosis, neoplasia, or hypertrophy in the livers of all samples. Both the liver and spleen of all samples lacked vacuolated phagocytes indicative of polymer accumulation. Spleens did not show sign of splenomegaly or necrosis [210].

This work demonstrates that PNN-HA.RGDS has the potential to be used as an injectable in the subretinal space [210]. However, this material lacked adequate degradation properties. In response, Fitzpatrick et al. (2012) synthesized NIPAAm, NAS, acrylic acid (AA), and acryloyloxy dimethyl-γ-butyrolactone (DBA) copolymers (pNNAD), with varying amounts of AA. Introduction of DBA was previously shown to increase LCST above physiological through hydrolysis and

subsequent ring opening of the lactone functional group allowing for dissolution of the gel over time [218, 219]. This hydrolysis is slow and therefore ideal for delivery of drugs and biologics. Again, the pNNAD polymers displayed good viability comparable to controls after 96 hours. Subcutaneous injection was conducted using C3H mice for analysis at days 1, 3, and 7 following injection and SKH1-E mice for day 40. Histology of the liver and spleen was devoid of signs of necrosis and inflammation at day 40. Dermis near the site of injection displayed lymphocytes indicative of mild inflammation which subsided by day 7 and was not present in day 40 samples. The authors also explored dexamethasone release from pNNAD gels dissolved at 20 w/v% in a 0.1 mg/mL solution of dexamethasone in PBS. Results were characteristic of sustained low level burst release. Unfortunately, these pNNAD polymers had LCSTs close to room temperature [211, 213]. As such, formulations optimized to have LCSTs closer to physiological may further improve handling of these materials in application.

In response to pNNAD, a copolymer comprised of NIPAAM, AA, polyethylene glycol methyl ether methacrylate (PEGMEMA, MW = 1100 g/mol), and DBA (pNAPD) was synthesized. pNAPD possessed an increased LCST and remained optically transparent upon gelation as compared to pNNAD, making it suitable for subretinal injection [212-214]. Intravitreal injection of pNAPD, dissolved at 5 w/v% in 1X PBS, into the eyes of Sprague Dawley rats, showed no change in the morphology of retinal tissue, immune cell infiltration, or visual performance as compared to saline injection at 0-, 7-, and 14-days following application [214]. These results suggest pNAPD may be well suited for drug and/or cell delivery applications to the posterior segment of the eye.

## 1.5 PEPTIDE MODIFICATION FOR ENHANCED CELL DELIVERY

Peptides encompass a myriad of biomolecules which play important roles *in vivo*. In tissue engineering, short synthetic or recombinant derived sequences have gained particular traction. Namely, adhesion peptides, sequences of amino acid residues involved in the migration and adherence of cells to ECM have shown particular promise. Application of these agents can be used to improve integration of cells on synthetic scaffolds. This work has allowed materials to extend beyond being solely bio-inert upon implantation, by leveraging biomimetic surfaces which can play an active role in tissue integration. Though materials have been designed which are able to promote RPE adhesion without the use of components found in ECM [220, 221], modifying carriers with adhesion proteins continues to be widely used in cell delivery research to form viable and functionally useful substrates. The use of peptide sequences allows for better control of the orientation and density of these agents, a feature not well regulated when grafting full length ECM proteins to materials [222].

Many adhesion sequences have been defined and reviewed for biomaterials research including, but not limited to, IKVAV, REDV, DGEA, PHSRN, RGD(S) and YIGSR [223-225]. RGD is the most widely studied as well as smallest functional adhesion sequence. Innate to ECM proteins such as fibronectin, vitronectin, fibrinogen, as well as laminin and collagen (although other

adhesion peptides dominate within the latter two) RGD is able to bind multiple cell-surface integrins [226-228]. The RGDS tetrapeptide present in fibronectin binds cell surface integrins with high affinity and has been tied to inhibition of thrombosis [222, 229, 230]. Similarly, YIGSR (Tyrosine-Isoleucine-Glycine-Serine-Arginine) is a popular adhesion sequence associated with the basement membrane protein laminin [231, 232]. Found in the β1 chain of laminin, YIGSR has been studied for its anti-angiogenic properties and potential to prevent metastasis [233]. Broadly, both RGDS and YIGSR have been readily employed on synthetic materials to improve cell integration in tissue engineering.

## 1.6 THESIS OBJECTIVES

The aim of this thesis is to explore the synthesis, thermoresponsive nature, and *in vitro* application of a degradable NIPAAm-based hydrogel with the intent of evaluating its potential as a cell delivery agent in treating posterior segment disease, particularly dAMD. Early and dry forms of AMD go without approved treatment, leaving an unmet need for therapeutic agents which can prevent long term progression of disease. Given that dysfunction with the RPE layer correlates with early stages of AMD, RPE transplantation has been proposed as a potential treatment. As noted above, current modalities often rely on bolus injection of cells leading to aggregation and cell death or bulky scaffold transplantation. Whole and partial retinal tissue delivery is dependent on material sourcing and invasive surgical implantation, limiting accessibility of treatment. Improved surgical techniques for cell delivery continue to be problematic, having issues with retinal tearing and inadequate localization. As such, it is believed that a soft hydrogel capable of *in situ* gelation could assist in cell delivery and distribution throughout the subretinal space. The work described herein, serves as a preliminary study of two materials intended to meet this aim.

Chapter 2 discusses the development and characterization of two pNIPAAm-based hydrogel systems modified with adhesion peptides RGDS and YIGSR. Polymer properties are defined using proton nuclear magnetic resonance spectroscopy (NMR) and gel permeation chromatography (GPC). LCST characterization of unmodified materials is explored primarily through differential scanning calorimetry and polymer rheology. Degradation profiles in PBS, have hypothesized pH stability as a potential limiting factor in the modification of the described formulations. Preliminary *in vitro* cytotoxicity assays using model ARPE-19 cells, showcase suitable biocompatibility with some indication of cell movement into certain materials. Further study and materials optimization is required.

Finally, chapter 3 discusses key findings of the described work, highlighting contributions amongst the current literature. **Figure 1.6** serves as a visual representation of the intended application of the materials explored herein.

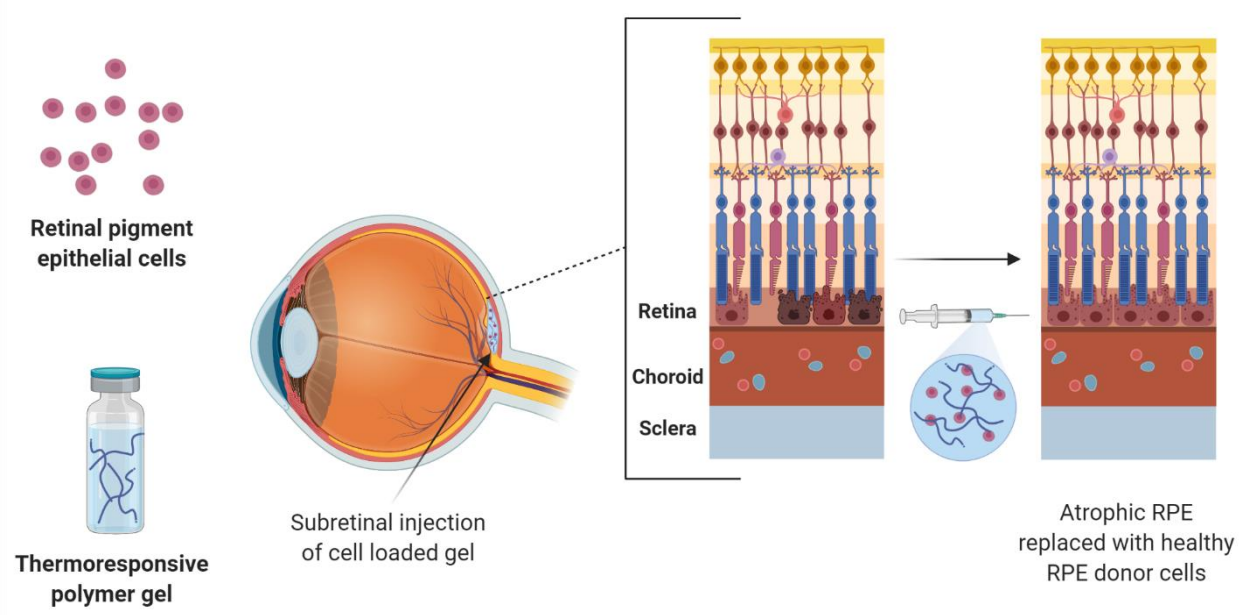


**Figure 1.6.** Visual depiction of RPE delivery to the subretinal space by means of a 3D thermoresponsive hydrogel carrier. Image created using BioRender.com.

# Chapter 2: RGDS AND YIGSR MODIFIED THERMORESPONSIVE HYDROGEL CELL SCAFFOLDS

## 2.1 ABSTRACT

In the current work, two N-isopropylacrylamide (NIPAAm)-based thermoresponsive hydrogels are described with the potential to be used as injectables for subretinal cell delivery. Poly-NIPAAm-*co*-NAS-*co*-PEGMEMA$_{1070}$-*co*-DBA (pNNPD) and Poly-NIPAAm-*co*-NAS-*co*-PEGMEMA$_{510}$-*co*-DBA-*co*-TRIS (pNNP5DT) were individually evaluated for temperature responsive character as well for their effect on two-dimensional ARPE-19 cultures following modification with extracellular matrix adhesion peptides, RGDS and YIGSR. Both pNNPD and pNNP5DT presented with LCSTs below physiological at 24 and 27°C respectively. Oscillation temperature ramps reveal that the Tgel (G' > G'') of pNNPD was approximately 40°C lying outside physiological, where pNNP5DT presented at 35°C. However, pNNP5DT did not retain water content as effectively as pNNPD following gelation. Material modification with YIGSR and/or RGDS indicated that grafting of peptides is not reserved to incorporated NAS. pNNPD is associated with higher viability as compared to pNNP5DT when exposed to cultures of ARPE-19 cells. Fluorescent calcein and ethidium-homodimer 1 imaging revealed materials with higher grafting of RGDS to be associated with potential cell lifting. pNNP5DT-RGDS modified materials displayed notable blank patches and raised agglomerates after 48 h of culture (37°C, 5% $CO_2$), this is hypothesized to be correlated with RPE affinity for RGDS during migration.

## 2.2 INTRODUCTION

Age related macular degeneration (AMD) remains a world leading cause of irreversible central vision loss, predominately affecting those over 50 years of age [234, 235]. AMD is multifactorial and is often categorized on a spectrum beginning with the presence of large extracellular debris (drusen) between the retinal pigment epithelium (RPE) and Bruch's membrane (BrM). Further progression of AMD can lead to choroidal neovascularization [236]. It is projected that by 2040, the worldwide prevalence of AMD will reach 288 million, currently accounting for approximately 8.7% of blindness internationally [3]. The socioeconomic and public health concerns arising from increased prevalence of AMD have promoted a vast body of research surrounding improved treatment [69].

At present, AMD remains untreatable in approximately 90% of patients [57]. Early-stage dry AMD (dAMD) is more common but is generally untreatable, with vitamin supplementation remaining the only clinical recommendation for slowing disease progression [56, 70]. In cases of late-stage wet AMD (wAMD), growth of blood vessels into the retina can lead to subretinal scarring, hemorrhaging, and severe vision loss. To manage wAMD, agents that block vascular endothelial growth factor (VEGF-A) are prescribed to prevent angiogenesis [4, 9]. There is

widespread agreement that RPE degeneration lies at the core of AMD pathogenesis. RPE cells are responsible for maintaining the blood-retinal microenvironment by clearing debris through phagocytosis, producing growth factors that maintain the photoreceptors, and orchestrating cellular responses to stimuli [25, 26]. As dysfunctional RPE tends to occur prior to photoreceptor damage, it is believed that replenishing the RPE may have protective benefits in cases of dAMD [4, 25-27].

RPE delivery has long been considered a point of therapeutic interest due to the role of these cells in maintaining photoreceptors and the blood-retinal microenvironment. However, cell delivery through bolus injections have proven inefficient as leakage, aggregation, and cell death offer limited control over cell fate [191]. Cell scaffolds intended to replace the Bruch's membrane and ensure proper integration have previously been described [107, 115]. Two-dimensional solid sheet scaffolds are often too bulky for application in the layers of the retina. In order to develop a treatment that is conducive with clinical practice, scaffolds must be minimally invasive upon insertion. Subretinal delivery of gel scaffolds has mitigated rigidity issues associated with 2D carriers [192-208], gel systems offer the potential for cell encapsulation with ease of delivery.

The Sheardown lab has previously developed a N-isopropylacrylamide (NIPAAm)-based thermo-responsive hydrogel (pNNPD) which is liquid at room temperature and a gel above 32°C, allowing for *in situ* gelation upon injection [211, 212]. It is hypothesized that modification of this NIPAAm-based polymer with adhesion peptides from extracellular matrix proteins fibronectin and laminin will produce a clear hydrogel scaffold that can deliver RPE cells in the subretinal space. Further investigation of thermoresponsive gels within our lab has also given rise to a formulation based on the components of pNNPD (pNNP5DT). Further, investigation into the potential of this material to deliver RPE cells is of interest.

The development of hydrogel scaffolds for RPE injection may improve clinical outcomes, preventing AMD progression from early stages. It is also expected that such a vehicle for cell delivery can be optimized for stem cell regenerative therapies. A hydrogel which can successfully be applied within the delicate layers of the retina may also present as a suitable method for stem cell delivery for various other pathologies in similarly highly structured tissues. In this chapter, pNNPD and pNNP5DT will be examined as potential systems for RPE cell delivery. This work serves as proof of concept on the capacity of these thermoresponsive hydrogel systems for cell delivery.

## 2.3 MATERIALS

N-isopropylacrylamide (NIPAAm; 97%), acrylic acid N-hydroxysuccinimide (NAS; 99%), polyethylene glycol methyl ether methacrylate (PEGMEMA; MW = 950 g/mol as well as 500 g/mol), benzoyl peroxide (BPO; >98%), (R)-α-Acryloyloxy-β,β-dimethyl-γ-butyrolactone (DBA; 95%), N,N-Dimethylformamide (DMF; 99.8%), Lithium Bromide (LiBr; ≥99%), 98% thiazolyl blue tetrazolium bromide (MTT), Triton™ X-100, Dimethyl sulfoxide (DMSO; Hybri-Max™, sterile-

filtered, BioReagent, suitable for hybridoma, ≥99.7%) were purchased from Sigma. Methacryloxypropyltris(trimethylsiloxy)silane (TRIS) was purchased from Gelest. Reagent grade 1,4-dioxane, anhydrous ethyl ether, toluene, n-hexane, and tetrahydrofuran (THF) were purchased from Caledon. Deuterated water ($D_2O$; 99.9%) and deuterated dimethyl sulfoxide (DMSO-d6; 99.9%) were purchased from Cambridge Isotope Laboratories, Inc. and Sigma respectively. H-Arginine-Glycine-Asparagine-Serine-OH (hydroxy terminated RGDS; 433.42 g/mol) was purchased from abcam and H-Tyrosine-Isoleucine-Glycine-Serine-Arginine-$NH_2$ (amine terminated YIGSR; 593.68 g/mol) was purchased from BACHEM.

10X phosphate buffered saline (PBS; diluted to 1X, pH 7.2-7.4) was purchased from BioShop. Sterile 1X PBS (pH 7.2-7.4) was purchased from McMaster Health Science facilities and used for cell studies as received. An immortalized line of human retinal pigment epithelial cells (ARPE-19) was purchased from ATCC® (CRL-2302™). Dulbecco's Modified Eagle Medium/Nutrient Mixture F-12 (DMEM/F12) was purchased from Gibco™. Complete media was composed of DMEM/F12 supplemented with 10% fetal bovine serum (FBS; Gibco™), in which cells were cultured under $CO_2$ (37°C, 5% $CO_2$) unless otherwise specified. Ethanol (95%) was purchased from Commercial Alcohols by Greenfield Global and was diluted to 70% to be used for disinfection during cell culture. Invitrogen™ LIVE/DEAD™ Viability/Cytotoxicity Kit was purchased from ThermoFisher.

## 2.4 METHODS

### 2.4.1 N-isopropylacrylamide Recrystallization

Prior to polymerization, NIPAAm was purified via recrystallization. 20 g of NIPAAm was weighed in a fume hood and transferred to a 100 mL beaker. 20 mL of toluene was added and the mixture was manually stirred using a scoopula. The mixture was placed in a water bath preheated to 35-40°C and stirred for 1-2 hours, ensuring the NIPAAm was properly dissolved. The beaker was then secured in a large ice bath and 10 mL of n-hexane was pipetted into the mixture prior to incubation in the ice bath for 4 hours. Using a Buchner funnel equipped with a filter and filter paper (no vacuum), the NIPAAm crystals were filtered out of solution, rinsing with n-hexane to ensure adequate transfer. Impurities were removed using 50 mL rinses of n-hexane, repeated until the yellow tint was removed from crystals. The purified NIPAAm was dried in the fumehood overnight. Once dry, recrystallized NIPAAm was transferred into a pre-weighed, opaque, plastic container, covered with parafilm, and stored in the freezer to be used as needed.

### 2.4.2 pNNPD Synthesis *via* Free Radical Polymerization

The base polymer described is composed of an 80:4:4:12 molar ratio of NIPAAm:NAS:$PEGMEMA_{1070}$:DBA [212, 213]. This polymer was synthesized using free radical polymerization using BPO as a thermal initiator. The molecular weight of PEGMEMA was

confirmed by proton nuclear magnetic resonance spectroscopy ($^1$H NMR; Bruker Avance 600 Hz) in DMSO-d6. Masses of monomers to be added were calculated as shown in **Appendix A4**. 1.67 g (0.0148 mol) of recrystallized NIPAAm, 0.125 g (0.000740 mol) NAS, 0.792 g (0.000740 mol) $PEGMEMA_{1070}$, 0.409 g (0.00222 mol) DBA, and 0.0448 g BPO (1 mol% relative to the total moles of all other monomers) were combined in a 100 mL round bottom flask with 30 mL of a 9:1 mixture of 1,4 dioxane:MilliQ water. This flask was then sealed using a rubber septum and covered with parafilm before oxygen purge with nitrogen gas (25 minutes). The flask was then clamped into an oil bath preheated to 70°C and the reaction was allowed to proceed for 24 hours. Following this period, the flask was removed from heat and allowed to cool to room temperature, polymerization was terminated by removing the septum and exposing to oxygen. The mixture was rotovapped at 50°C to remove excess solvent. Once the solution reached a viscosity similar to honey, the product was purified by precipitating twice in 500 mL of chilled anhydrous ethyl ether. To separate precipitate from solvent, the sample was filtered by means of a Buchner funnel and flask using Fisherbrand P8 filter paper under vacuum. The product was re-dissolved in THF prior to the second precipitation. Once complete the powdered polymer was transferred into a pre-weighed sample flask and was allowed to further air dry in the fumehood over 72 hours. The polymer was then covered in parafilm and foil to be stored at -15°C prior to modification.

### 2.4.3 pNNP5DT Synthesis *via* Free Radical Polymerization

The pNNP5DT formulation was composed of an 84.5:5:5:5:0.5 molar ratio of NIPAAm:NAS:$PEGMEMA_{510}$:DBA:TRIS. The molecular weight of $PEGMEMA_{510}$ was confirmed prior to synthesis by $^1$H NMR (Bruker Avance 600 Hz) in DMSO-d6. The mass of monomers to be added was calculated as shown in **Appendix A4**. 2.036 g (0.018 mol) of recrystallized NIPAAm, 0.180 g (0.00106 mol) NAS, 0.543 g (0.00106 mol) $PEGMEMA_{510}$, 0.196 g (0.00106 mol) DBA, 0.045 g (0.000106 mol) TRIS, and 0.0516 g BPO (1 mol% relative to the total moles of all other monomers) were added to a 100 mL round bottom flask with 30 mL of a 9:1 mixture of 1,4 dioxane:MilliQ water. Synthesis by means of free radical polymerization was conducted as described above. Reaction schemes of pNNPD and pNNP5DT synthesis as well as overall structure are summarized in **Figures 2.1 and 2.2**.

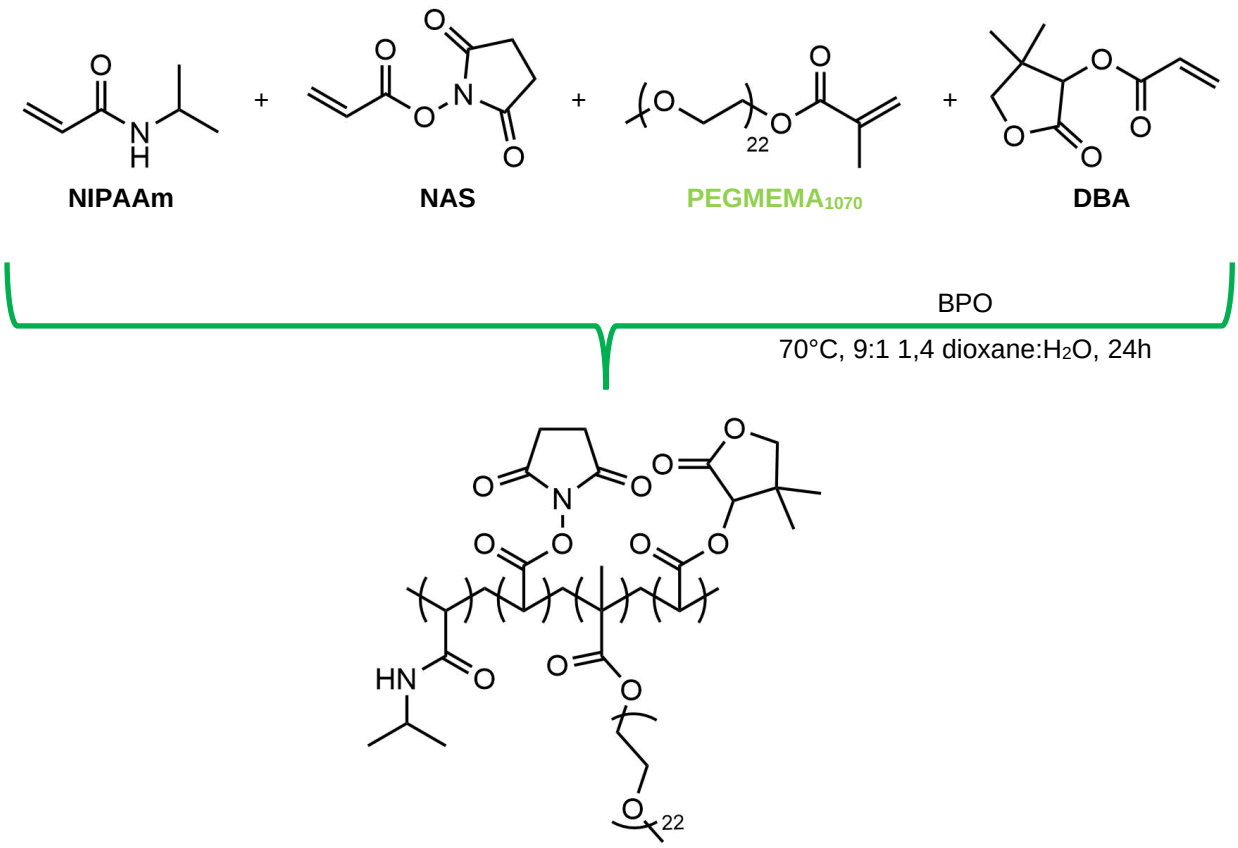


**Figure 2.1.** Scheme of free radical synthesis of pNNPD.

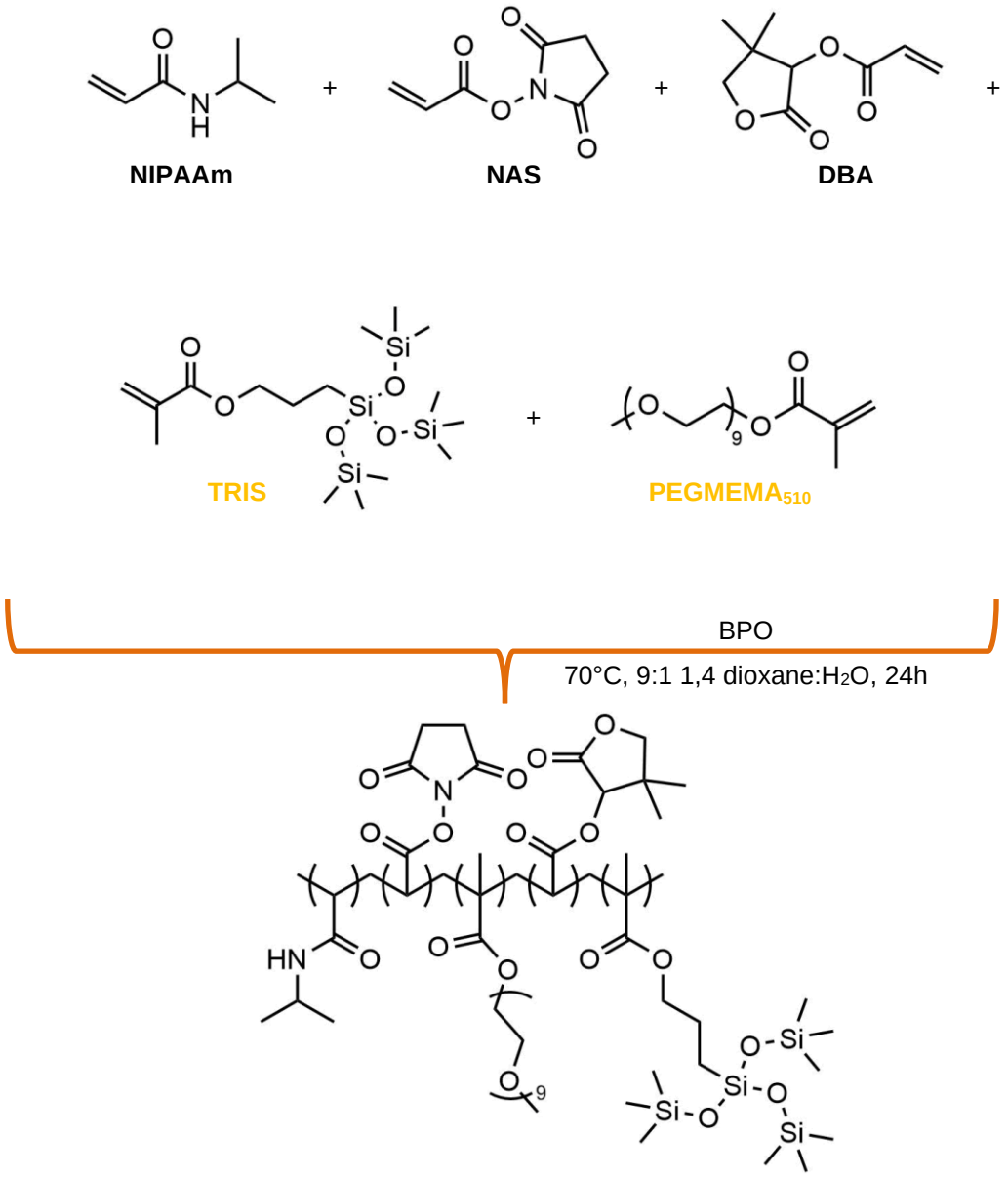


**Figure 2.2.** Scheme of free radical synthesis of pNNP5DT.

### 2.4.4 Gel Permeation Chromatography (GPC)

Gel permeation chromatography (GPC) was used to characterize the molecular weight of materials. A Polymer Laboratories PL-50 GPC equipped with three Phenomenex PhenogelTM columns (300 x 4.6 mm, 5 µm; pore sizes: 100, 500, 104 Å) was used at room temperature. Calibration was performed using linear polyethylene glycol standards (Polymer Laboratories). DMF with 50 mM LiBr was used as the eluent. All samples were filtered using a 0.2 µm Teflon filter prior to analysis.

### 2.4.5 Polymer Post-modification with Extracellular Matrix Adhesion Peptides

Bioconjugation of pNNPD with RGDS and YIGSR was conducted after $^{1}$H NMR (Bruker Avance 600 Hz) in DMSO-d6 of the stock polymers was used to determine the molar percent (mol%) of NAS incorporated during polymerization. Sample calculations are presented in **Appendices A5 and A6**. pNNPD was dissolved at 15 w/v%. Aliquots of peptides were prepared at concentrations of 10 mg/mL in 1X PBS (pH 7.4) and added at molar ratios of 1:2, 1:1, and 2:1 RGDS:NAS; as well as, 1:1:2 RGDS:YIGSR:NAS. These sealed samples were then placed on a shaker at room temperature for 24 h. Samples were then dialyzed in 4 L of purified Milli-Q water with continuous stirring for 72 h using Spectra-Por® Float-A-Lyzer® tubing (molecular weight cut off 20 kDa) to remove any unreacted reagents, water was replaced after 24 h. Following dialysis, samples were collected in glass sample vials, frozen, and freeze dried. $^{1}$H NMR in $D_2O$ was used to confirm modification as $D_2O$ does not interfere with peaks associated with RGDS and YIGSR, where peak shift associated with DMSO-d6 makes quantification difficult. Materials were covered with parafilm and foil, before being stored at -15°C until use.

For pNNP5DT, molar ratios of 1:1 YIGSR to NAS, 1:2 RGDS to NAS, and 1:1 RGDS to NAS were prepared as described above. Alternatively, pNNP5DT materials were modified at 4°C for 72 h with continuous mixing. Samples were again dialyzed, frozen, and freeze dried. $^{1}$H NMR in $D_2O$ was used to confirm degree of modification. Materials were covered with parafilm and foil, before being stored at -15°C until use.

### 2.4.6 MTT Assay

In order to measure potential cytotoxic effects of the hydrogel scaffolds, ARPE-19s (passage 8 pNNP5DT and passage 9 pNNPD) were exposed to scaffolds and analyzed using 98% thiazolyl blue tetrazolium bromide (MTT, Sigma-Aldrich). This colorimetric assay can be used to quantify metabolic activity, as NADPH-dependent oxidoreductase enzymes produced by viable cells reduce MTT to formazan crystals. Formazan crystals can be dissolved in DMSO and an absorbance scan at 590 nm can be used to quantify the relative magnitude of the metabolic activity.

In a Corning® Solid Black, Clear Flat Bottom Polystyrene TC-treated 96-well plate, 20 000 ARPE-19 cells were seeded per well. Cells were cultured in Gibco™ Dulbecco's Modified Eagle Medium/Nutrient Mixture F-12 (DMEM/F12) at 37°C, 5% $CO_2$. 24 hours after seeding, media was

carefully removed from wells, cells were rinsed with 200 µL of sterile 1x PBS aspirating thrice, and 200 µL of incomplete DMEM/F12 (media lacking FBS) was added to each well. Following 24 hours of incubation at 37°C, cells were exposed to respective treatments for an additional 48 and 24 hours. In the case of pNNPD, polymers were pre-dissolved at 20 w/v% (24 h prior, stored at 4°C) and upon treatment 10 µL of polymer was added to respective wells. pNNP5DT materials were dissolved as described above at 10 w/v% and 20 µL of material was exposed to the wells.

Following the desired period of exposure, a 5 mg/mL solution of MTT in sterile 1x PBS was added to an equal volume of DMEM/F12. Positive controls were produced by removing media from untreated cells and applying 100 µL of 0.25% Triton™ X-100 purchased from Sigma, for 5 minutes. 0.25% Triton™ X-100 was then removed and cells rinsed with 200 µL of sterile 1x PBS aspirating thrice. Next, media was gently removed from remaining wells and replaced with 100 µL of the MTT solution and media mixture. Blanks containing neither cells nor treatment were also plated to account for background. The plate was returned to the incubator (37°C, 5% $CO_2$) for 3 hours, after which the MTT mixture was carefully removed from each well as not to disrupt formazan crystals. Formazan was dissolved using 200 µL of DMSO (Hybri-Max™, sterile-filtered, BioReagent, suitable for hybridoma, ≥99.7% purchased from Sigma) in each well. The plate was then covered in foil and allowed to incubate at room temperature for 15 minutes prior to scanning. Absorbance measurements were taken using a TECAN Infinite® M200 PRO NanoQuant Plate Reader at 590 nm absorbance (bandwidth 9 nm, 25 flashes, and multiple reads per well – square-filled, 4 x 4). Percent viability (normalized to negative controls) versus treatment type was plotted with blank subtraction and standard error.

### 2.4.7 LIVE/DEAD Assay

In order to visualize any cytotoxic effects of the materials, ARPE-19s (passage 9) were co-stained with calcein AM and ethidium homodimer-1. The Invitrogen™ LIVE/DEAD™ Viability/Cytotoxicity Kit (ThermoFisher) was used. Calcein AM is non-fluorescent and a cell permeant. In live cells intracellular esterase, particularly acetoxymethyl ester hydrolysis, enzymatically converts calcein AM into green fluorescent calcein. On the contrary, ethidium homodimer-1 is excluded from intact cell membranes. In dying cells with permeable membranes, ethidium homodimer-1 intercalates with nucleic acids producing a red fluorescence.

Cell seeding and culture conditions followed a similar protocol to that described above, however in the case of pNNPD, 50 000 cells were seeded prior to treatment. LIVE/DEAD™ working solution was prepared by adding 20 µL of the supplied Invitrogen™ 2 mM ethidium homodimer-1 stock solution as well as 5 µL of the 4 mM calcein AM stock to 10 mL of sterile 1x PBS (pH 7.4), vortexing to mix. For the positive controls, media was removed from untreated cells and exposed to 100 µL of 0.25% Triton™ X-100 purchased from Sigma, for 5 minutes. Triton™ X-100 was removed and the cells were subsequently washed with 200 µL of sterile 1x PBS aspirating thrice. In remaining negative controls and treated wells, media was gently removed and cells were

washed with 200 µL of sterile 1x PBS, aspirating thrice. 100 µL of 1x PBS was then added to each well along with 100 µL of the prepared LIVE/DEAD™ working solution, aspirating thrice to mix. The plate was then covered with foil and incubated for 45 minutes at room temperature prior to imaging.

Cells were imaged using an Olympus IX51 Inverted Bright Field & Fluorescent microscope. Images were taken at 10X magnification of representative wells, using FITC (calcein) and Texas Red (ethidium homodimer-1) filters. A monochromatic grayscale QImaging Retiga 2000R camera was used for capture while processing used the Olympus cellSens Dimension™ software.

### 2.4.8 ImageJ Counting Protocol

pNNPD dead cell images, taken of each well using an Olympus IX51 Inverted Bright Field & Fluorescent microscope at 10X magnification, were processed using ImageJ. Images were converted to 8-bit from RGB (Red, Green, and Blue) prior to threshold adjustment to ensure all fluorescent artifacts from the original image were properly focussed. Scale and magnification indications were removed from the image prior to counting as not to be included as part of the automated count. The watershed tool was used to separate cell aggregates allowing for more representative counting. Measurements were set to account for area, minimum and maximum gray value, Feret's diameter, and mean gray value. Particles were analyzed and the summary output was then organized using the sort and filter tool in Microsoft Excel. Repetitive low pixel areas were considered background fluorescence and were excluded from the count. A jump in these repeated values was found to occur around 40 pixels across images; as such values above 40 pixels were taken to be more representative of cell area. Areas below 40 pixels were thereby excluded from the count; all images were processed using the same parameters. The number of artifacts remaining were summed and taken as a reflection of cell counts, which were recorded and plotted as an average.

### 2.4.9 Polymer Rheology

Polymer rheology was used to determine lower critical solution temperature (LCST) of materials using a Dynamic Hybrid Rheometer (DHR; TA Instruments DHR-2, New Castle, DE) with software TA instruments TRIOS version 4.4.1. Using a Peltier plate bottom geometry and parallel Peltier plate (20 mm, aluminum) top geometry, inertia, friction, gap temperature, and rotational mapping were calibrated prior to measurement. Oscillation temperature ramps from 15°C to 45°C (1°C/min) at 0.1% oscillation strain, 10 rads/s frequency, and 1000 µm gap, were conducted to explore the effect of temperature on complex viscosity and modulus. Prior to start and after loading approximately 380 µL of dissolved polymer between plates, temperature was set to 15°C for 2 minutes.

### 2.4.10 Differential Scanning Calorimetry (DSC)

Differential scanning calorimetry (DSC; TA Instruments Q200, New Castle, DE) was performed in order to determine the LCST of both pNNPD and pNNP5DT. Approximately 10 mg of pNNPD and pNNP5DT, pre-dissolved in 1X PBS at 20 and 15 w/v% respectively, were loaded into aluminum TZero hermetic pans and measured under nitrogen. Milli-Q water was used as a reference. Samples underwent a custom ramp of 5 to 45°C (1°C/min), remaining isothermal at 45°C for 2 minutes, before a ramp down to 5°C (1°C/min). LCST was taken to be the midpoint between the temperature before and after the endothermal peak of the forward heat flow curve (this value was cross referenced with the exotherm midpoint appearing on the reverse curve).

### 2.4.11 pH Stability Study

Aliquots of pNNPD and pNNP5DT were dissolved in glass sample vials at 20 and 15 w/v% respectively in 1X PBS (pH 7.4), vials were covered with parafilm, wrapped in foil, and stored at 4°C. After 24 hours, vials were vortexed to ensure uniform mixing and pH readings were taken in triplicate using a Fisherbrand™ accumet™ AB250 pH/ISE Benchtop Meter equipped with a Thermo Scientific™ Orion™ PerpHecT™ ROSS™ combination pH Micro Electrode. Vials were returned to 4°C. pH measurements were recorded daily for 7 days and again following 3 months.

### 2.4.12 Statistical Analysis

For cell studies, raw data were collected and analyzed using Microsoft Excel. To test for equal variance, Levene's test of homogeneity of variance was conducted whereby a single-factor analysis of variance (ANOVA; significance level ($\alpha$) of 0.05) was run on the absolute difference of each data point subtracted by the mean of the given data set. If the p-value produced was greater than $\alpha$ in the Levene's test, a single-factor ANOVA assuming equal variances was conducted with an $\alpha$ of 0.05. If $p < \alpha$, Tukey's post-hoc test was conducted to compare all mean pairings.

## 2.5 Results and Discussion

### 2.5.1 Synthesis and Modification of pNNPD and pNNP5DT

Two pNIPAAm-based materials were prepared. The first is based upon an optically transparent formulation previously synthesized by Fitzpatrick and colleagues [212, 213]. Poly-NIPAAm-*co*-NAS-*co*-PEGMEMA$_{1070}$-*co*-DBA (pNNPD) leverages the thermosensitive behaviour of NIPAAm with the potential to elute over time through incorporation of DBA. DBA has been shown to increase LCST through butyrolactone ring opening resulting from hydrolysis [103, 218, 219]. This slow process allows pNIPAAm materials to dissolve and be cleared systemically without production of harmful degradation products [218]. Hydrophilic PEGMEMA was incorporated to increase LCST of pNIPAAm close to physiological and mitigate syneresis by retaining water following coil to globular phase transition. PEGMEMA also played a role in contributing to overall optical transparency. The molecular weight of PEGMEMA ($M_w$ = 1070 g/mol) was confirmed by

$^1$H NMR (**Appendix A1)**. Finally, in order to provide a site for bioconjugation, NAS was incorporated. N-hydroxysuccinimide (NHS) esters are often used in biomaterials as potential sites for protein modification, due to the robust ability of NAS to form stable amide bonds under mild reaction conditions [237-239]. As such, post-modification of pNNPD with adhesion peptides in the presence of a slightly alkaline buffer solution can form stable conjugates with NAS through the primary amines within their sequence. Here, NHS is released as a leaving group [238]. The pNNPD polymer was synthesized by means of free radical polymerization using a BPO initiator as previously described [211-213].

Poly-NIPAAm-*co*-NAS-*co*-PEGMEMA$_{510}$-*co*-DBA-*co*-TRIS (pNNP5DT) differs from pNNPD through the addition of TRIS, which contributes to overall hydrophobicity and oxygen permeability [240-243], as well as the incorporation of a lower molecular weight PEGMEMA (510 g/mol) (**Appendix A1**). pNNP5DT was formulated in an attempt to improve the mechanical properties of pNNPD [212]. The molar feed ratios of each respective monomer in stock pNNPD and pNNP5DT are summarized in **Table 2.1** with final compositions as determined using $^1$H NMR in DMSO-d6 **(Appendices A2 and A5).**

**Table 2.1. Summary of Stock Polymer Composition**

| Polymer Molar Feed Ratio | Composition [a] | $M_n$ [b] (g/mol) | $M_w$ [b] (g/mol) | PDI [b] |
|---|---|---|---|---|
| pNNPD (80: 4: 4: 12) | (80.73: 3.7: 4.22: 11.35) | 25 203 | 82 218 | 3.26 |
| pNNP5DT (84.5: 5: 5: 5: 0.5) | (83.67: 4.73: 5.73: 5.28: 0.59) | 30 327 | 101 993 | 3.36 |

[a] Determined through integration analysis of $^1$H NMR in DMSO-d6; [b] Determined using GPC

To form gels which better mimicked native ECM, pNNPD and pNNP5DT were grafted with adhesion peptides, RGDS and YIGSR. The use of adhesion peptides mitigates impurity issues associated with using full length natural proteins, offering concise sites specific for cell adhesion which can support anchorage during delivery [222]. Preliminary modification of a pNNPD formulation with YIGSR (**Appendix A8**) inspired attempts to improve peptide grafting efficiency through increasing the temperature of post-modification. As such, pNNPD dissolved at 15 w/v% in 1X PBS (pH 7.4), was modified through addition of 10 mg/mL aliquots of RGDS and YIGSR at desired molar equivalents relative to NAS. As opposed to allowing this reaction to proceed at 4°C for 24 h, materials were left to react on a shaker at room temperature (20°C) for this period. Under these conditions, grafting efficiency did appear to improve as compared to preliminary work. For pNNP5DT however, increased viscosity at room temperature required materials to be modified at 4°C. In order to improve grafting efficiency in these materials, a reaction time of 72 h as opposed to 24 h was used. Unmodified pNNPD and pNNP5DT materials underwent the same reaction and dialysis conditions, without addition of adhesion peptide. $^1$H NMR analysis

(**Appendices A3 and A7**) yielded grafting efficiencies for each material. A limitation of this method is inherent peak broadening in $D_2O$ $^1H$ NMR as compared to DMSO-d6, as such the extent of bioconjugation determined using this method serves as an estimate. Material modification results for both pNNPD and pNNP5DT are summarized in **Table 2.2**.

**Table 2.2. Summary of Polymer Modification**

| Sample Name | Adhesion Peptide Modification | Feed Molar Ratio of NAS to Peptide(s) | % NAS Modified Theoretical | % NAS Modified Actual [a] |
|---|---|---|---|---|
| pNNPD-$RGDS_{31}$ | RGDS | 2:1 | 50 | 31 |
| pNNPD-$RGDS_{37}$ | RGDS | 1:1 | 100 | 37 |
| pNNPD-$RGDS_{117}$ | RGDS | 1:2 | 100 | 117* |
| pNNPD-$RGDS_{28}$/$YIGSR_{18}$ | RGDS/YIGSR | 2:1:1 | 50/50 | 28/18 |
| pNNP5DT-$YIGSR_{27}$ | YIGSR | 2:1 | 50 | 27 |
| pNNP5DT-$RGDS_{33}$ | RGDS | 2:1 | 50 | 33* |
| pNNP5DT-$RGDS_{48}$ | RGDS | 1:1 | 100 | 48* |

[a] Determined through integration analysis of $^1H$ NMR in $D_2O$

Materials marked by an asterisk exhibited unusual grafting. For pNNPD-$RGDS_{117}$, pNNP5DT-$RGDS_{33}$, and pNNP5DT-$RGDS_{48}$, RGDS incorporation appears to exceed the amount of NAS modified. In the case of pNNPD-$RGDS_{117}$ this is evident as the percentage of NAS modified exceeds the amount of NAS present within the stock polymer. Referring to **Table 2.3**, further analysis using $PEGMEMA_{1070}$ as an internal standard reveals the molar amount of NAS remaining in pNNPD-$RGDS_{117}$ to be 1.3 mol% as compared to the 3.7 mol% available in the stock. This suggests only 65% of NAS was lost to modification and competing hydrolysis in pNNPD-$RGDS_{117}$. Although, due to peak broadening, the amount of peptide incorporated may be slightly overestimated we also see a reduction in the integration of DBA in pNNPD-$RGDS_{117}$ as compared to other pNNPD materials which underwent the same bioconjugation step.

Similarly, NAS integration analysis relative to the amount of NAS available in stock pNNP5DT suggests only 28% (pNNP5DT-$RGDS_{33}$) and 25% (pNNP5DT-$RGDS_{48}$) of NAS was lost due to modification and competing hydrolysis. These values are notably lower than the molar amounts of RGDS present in both pNNP5DT materials. Unfortunately, reductions of NAS peaks in YIGSR modified materials could not be easily quantified due to unclear overlap of multiple amino acid residues within the YIGSR sequence and the NAS peak of pNNPD and pNNP5DT.

**Table 2.3. Summary of Polymer Composition following Modification**

| Sample | NAS [a] (mol%) | PEGMEMA [a] (mol%) | DBA [a] (mol%) | TRIS [a] (mol%) |
|---|---|---|---|---|
| Unmodified pNNPD | 1.90 | 4.22 | 10.55 | - |
| pNNPD-$RGDS_{31}$ | 1.79 | 4.22 | 10.55 | - |
| pNNPD-$RGDS_{37}$ | 1.62 | 4.22 | 10.85 | - |
| pNNPD-$RGDS_{117}$ | 1.31 | 4.22 | 10.01 | - |
| pNNPD-$RGDS_{28}$/$YIGSR_{18}$ | *overlap* | 4.22 | 10.29 | - |
| Unmodified pNNP5DT | 3.17 | 5.73 | 5.23 | 0.53 |
| pNNP5DT-$YIGSR_{27}$ | *overlap* | 5.73 | 5.19 | 0.51 |
| pNNP5DT-$RGDS_{33}$ | 3.39 | 5.73 | 4.89 | 0.22 |
| pNNP5DT-$RGDS_{48}$ | 3.56 | 5.73 | 5.07 | 0.09 |

[a] Determined through integration analysis of $^1H$ NMR in $D_2O$. NIPAAm shift overlapped with peaks attributed to both PEGMEMA, YIGSR, and RGDS where applicable, as such it was not possible to get an accurate NIPAAm integration in $D_2O$. Similarly, multiple residues composing YIGSR overlapped with NAS. Unmodified pNNPD and pNNP5DT underwent the same reaction conditions as the bioconjugation step of their respective modified materials without the addition of peptide. Differences in molar contributions here may be related to hydrolysis and $D_2O$ peak broadening in $^1H$ NMR.

Irregularities in pNNP5DT-RGDS materials were also evident due to sharp decreases in the contribution of TRIS, to 0.22 mol% in pNNP5DT-$RGDS_{33}$ and 0.09 mol% in pNNP5DT-$RGDS_{48}$ from 0.59 mol% in stock pNNP5DT. DBA once again displayed slight decreases in molar contribution in pNNP5DT-$RGDS_{33}$ and pNNP5DT-$RGDS_{48}$ as compared to unmodified pNNP5DT. Changes in DBA contribution were not as dramatic as that of TRIS. YIGSR modified pNNP5DT displayed a slight decrease in DBA and no change in TRIS, relative to unmodified pNNP5DT. The above suggests potential off-target modification throughout the polymer backbones of both pNNPD and pNNP5DT.

pH measurements of pNNPD and pNNP5DT in **Figure 2.3**, at concentrations comparable to reaction conditions in 1X PBS of the bioconjugation step, show that pH is less than 7 at 24 h for both pNNPD and pNNP5DT, lying outside the slightly alkaline (pH 7.2 to 9) conditions desired for amide bond formation *via* NAS [238]. This reduction in pH can lead to acid hydrolysis of co-monomers in both pNNPD and pNNP5DT, increasing sites available for bioconjugation as a result. In RGDS modified materials, the presence of aspartic acid (D) may further contribute to decreasing acidity during modification as compared to reactions containing only YIGSR.

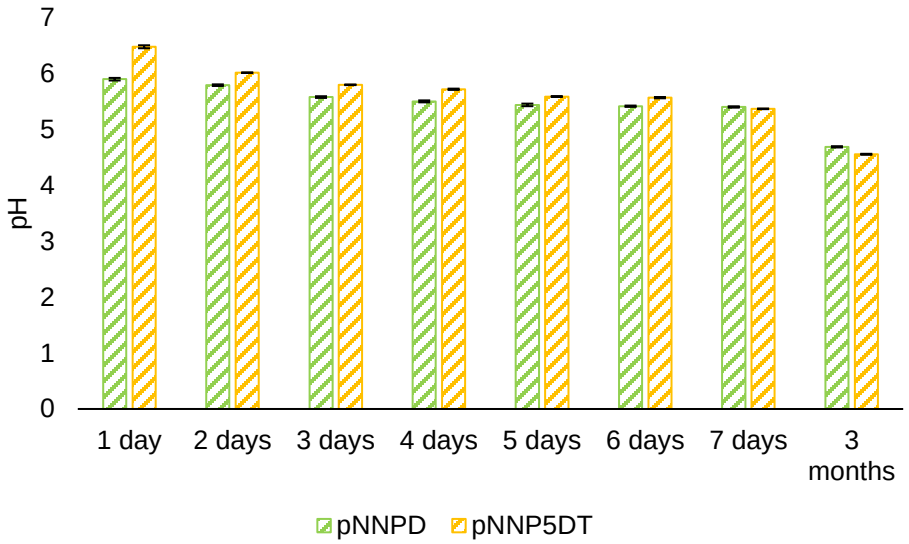


**Figure 2.3.** pH Stability of pNNPD (20 w/v%) and pNNP5DT (15 w/v%) during storage at 4°C. $\sigma_{\bar{x}}$ reflective of an n of 3.

It is hypothesized that various factors may play a role in increased RGDS grafting. Acid hydrolysis of TRIS has not been well defined in the literature. However, TRIS precursor γ-methacryloxypropyltrimethoxysilane (MPS) has been shown to undergo hydrolysis in weakly acidic conditions of pH 4 [244]. Solutions of 2.5% MPS in 2.5% acetic acid and 95% ethanol by volume have been shown to hydrolyze silane ester groups (–Si–O–$CH_3$) to silanol (–Si–OH) almost entirely after 24 hours, followed by oligomer (-Si-O-Si) formation [245]. Although the -Si-O-Si bonds in TRIS are more stable than the silane ester groups of MPS, hydrolysis of various silane coupling agents in weak acids has been well established [246, 247]. As such, it is anticipated that the weakly acidic pH of pNNP5DT dissolved in 1x PBS over 72 h of reaction, may have some effect on the bulky (trimethylsiloxy)silane terminus of TRIS. Sterically, it is hypothesized that this would be less likely than acid catalyzed ester hydrolysis [248]. Hydrolysis of the TRIS ester should theoretically produce 3-tris(trimethylsilyloxy)silylpropan-1-ol as a leaving group, leaving a carboxylic acid available for reaction with free RGDS.

Further, acid hydrolysis mechanisms of γ-butyrolactone in aqueous low acid conditions have been modelled [249]. If any DBA ring-opening has occurred in both pNNPD and pNNP5DT

during peptide modification, a carboxylic acid would be made available once again for reaction with RGDS. Integration analysis of $^{1}$H NMR of both pNNPD and pNNP5DT suggest DBA may be undergoing some low level of slow hydrolysis.

Finally, in the case of pNNPD-RGDS$_{117}$ it is apparent that more RGDS is present than the combined reduction in both NAS and DBA peaks as compared to the stock material. As all materials underwent extensive dialysis, it is unlikely that this is due to the presence of unreacted RGDS. Several studies investigating the self-assembly of amphiphilic materials comprising RGD [250-253], suggest that RGDS grafted to the pNNPD or pNNP5DT may be capable of some form of self-assembly. Self-assembled peptide amphiphiles have previously been proposed as bioinert crosslinking agents in forming stable hydrogels [254]. Self-assembly has also been shown to be influenced by changing pH in the case of peptide amphiphiles having alternating positive and negative charged groups [255, 256]. In the case of RGDS, arginine (R; pKa = 12.5) and aspartic acid (D; pKa = 3.9) are anticipated to possess a positive and negative charged R group respectively, between pH 5 and 7 [257]. Where, YIGSR possesses one positively charged amino acid side chain (R). As such, interaction of grafted peptide sequences and unreacted peptide groups may be forming aggregates through additive intermolecular forces, which later contribute to the appearance of a higher overall grafting efficiency. This phenomenon may be more evident in pNNPD-RGDS$_{117}$ where RGDS was added in excess and, therefore, has a higher potential for interactions between grafted and free RGDS.

The above proposed factors serve as theoretical explanations of why pNNPD-RGDS$_{117}$, pNNP5DT-RGDS$_{33}$, and pNNP5DT-RGDS$_{48}$ present with a higher amount of RGDS than the NAS originally available for modification in stock materials. These hypotheses are not extensive and further investigation is recommended. In future studies, post-modification of pNNPD, pNNP5DT, and similar materials must account for changes in pH in order to ensure off-target copolymers within the backbone are preserved. The potential of off-target grafting during modification had previously been overlooked in the development of pNNPD [212] and this work suggests that bioconjugation is not reserved to NAS within these complex systems. As such pH correction prior to reaction or use of a buffering solution with greater buffering capacity should be used in future studies with this material.

### 2.5.2 Characterization of Thermoresponsivity

LCST was determined using dynamic scanning calorimetry (DSC; TA Instruments Q200, New Castle, DE) of unmodified pNNPD and pNNP5DT at 20 and 15 w/v% respectively. At 20 w/v% pNNP5DT materials were highly viscous and difficult to pipette. As such, these materials were tested at a lower concentration in order to improve workability and handling. pNNP5DT materials were again diluted to improve handling for cell testing and as such crude DSC measurements were taken of these materials, results displayed comparable LCST to the pNNP5DT stock at 15 w/v% (**Appendix A9**). Endotherm and exotherm formation on the heat and cool ramps were

identified for both pNNPD and pNNP5DT. The midpoint of temperatures on either side of the endotherm peak was taken to be LCST. Referring to **Table 2.4**, the LCST of pNNPD is comparable to that reported by Fitzpatrick and colleagues [212, 213]. The LCST of pNNP5DT is higher than pNNPD due to its larger molar concentration of NIPAAm. The values reported are in line with the onset of increased complex viscosity and modulus changes in **Figure 2.4**, measured by means of temperature ramp using a dynamic hybrid rheometer (DHR; TA Instruments DHR-2, New Castle, DE) of pNNPD and pNNP5DT.

**Table 2.4. Summary of Thermoresponsivity**

| Polymer | Concentration in 1X PBS | LCST [a] (°C) | Tgel ± $\sigma_{\bar{x}}$ [b] (°C) | G' at 37°C ± $\sigma_{\bar{x}}$ [b] (Pa) | G' at 37°C ± $\sigma_{\bar{x}}$ [b] (Pa) |
|---|---|---|---|---|---|
| pNNPD | 20 w/v% | 24.06 | 39.94 ± 0.96 | 2.42 ± 0.27 | 5314 ± 307 |
| pNNP5DT | 15 w/v% | 27.29 | 35.04 ± 0.52 | 4.63 ± 0.11 | 4772 ± 1120 |

[a] Determined by DSC; [b] Determined by temperature ramp using DHR ($\sigma_{\bar{x}}$ represents an n of 3).

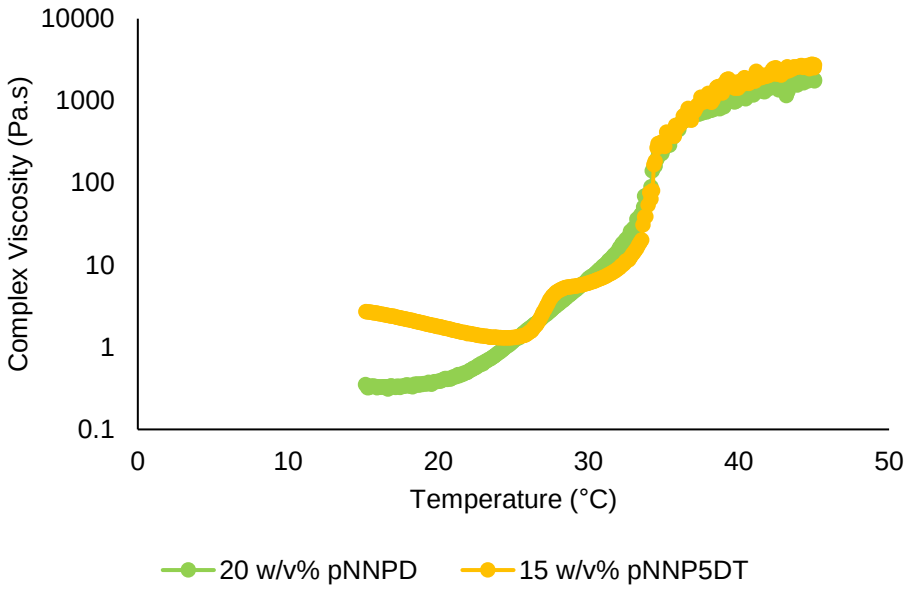


**Figure 2.4.** Representative temperature ramps of pNNPD and pNNP5DT from 15°C to 45°C (1°C/min) with an oscillation strain of 0.1%, frequency of 10 rad/s, and 1000 µm gap. pNNP5DT presents with a higher initial complex viscosity at 20°C and stepwise biphasic gelation beyond its LCST and before Tgel. Whereas, pNNPD displays a gradual increase in viscosity beyond its LCST and before Tgel. Both materials display comparable moduli after complete gelation with pNNP5DT having a slightly higher complex viscosity at 45°C of 2159 ± 425 Pa.s than pNNPD at 2011 ± 157 Pa.s ($\sigma_{\bar{x}}$, represents an n of 3).

Rheology was employed to visualize changes in complex viscosity with increasing temperature. Tgel represents the end of the phase transition in these thermoresponsive materials, whereby modulus changes mark the complete transition from the viscous region into the elastic region. Temperature ramps of pNNPD and pNNP5DT were conducted at 20 w/v% and 15 w/v% respectively. Strain sweeps conducted at 37°C were initially run to determine the Linear Viscoelastic Region (LVR) of both materials. An oscillation strain within the LVR of both materials (0.1%) was selected for further testing by means of oscillation temperature ramp from 15°C to 45°C, in order to ensure any changes in modulus were not dependent on amplitude of deformation. The crossover of storage modulus (G') above the loss modulus (G'') was taken as the Tgel [258-261]. As summarized in **Table 2.4**, the Tgel of pNNPD and pNNP5DT were found to be approximately 40 and 35°C respectively, with the former lying outside physiological temperature. As shown in **Figure 2.4**, a viscosity increase with increasing temperature in pNNPD is shown to be gradual compared to the more step-wise increase observed in pNNP5DT. At 20°C, pNNP5DT is notably more viscous than pNNPD although both materials display comparable viscosities at temperatures above 25°C. G' at 20°C is higher for pNNP5DT at 4.63 ± 0.11 Pa versus that of pNNPD at 2.42 ± 0.27 Pa. Similar to viscosity, modulus of both materials is comparable following gelation with pNNPD and pNNP5DT having G' of 5314 ± 307 Pa and 4772 ± 1120 Pa at 37°C respectively.

It is believed the gelation of pNNPD and pNNP5DT is governed not only by the LCST resulting from the presence of the NIPAAm, but also through the interaction of hydrophilic and hydrophobic groups comprising these copolymer systems [261]. This is supported by endotherm formation appearing prior to complete phase transition in both pNNPD and pNNP5DT. As well, when the molar concentration of DBA in pNNP5DT systems is reduced, biphasic gelation is no longer observed and a single critical gelation event can be seen (**Appendix A10**). This suggests that the hydrophobic/hydrophilic balance is important in regulating pNNP5DT phase transition and associated physical interactions during polymer packing. Cloud point analysis was also attempted to corroborate differences in LCST and Tgel for these materials, however the results were inconclusive due to limited material availability (**Appendix A11**).

**Figure 2.5** displays visual differences in polymers before and after heating at physiological temperature for 10 minutes. High turbidity in pNNP5DT materials as compared to pNNPD was noted. pNNP5DT also appeared to expel some water above its LCST compared to pNNPD which retains its water content. Syneresis occurring in pNNP5DT polymers may be explained by bulky hydrophobic TRIS as well as lower molecular weight $PEGMEMA_{510}$, increasing overall hydrophobic character of the polymer backbone as compared to pNNPD. Longer chain $PEGMEMA_{1070}$ in pNNPD may better assist in water retention following phase transition, reducing the amount of water expelled during aggregation of hydrophobic groups and maintaining optical transparency at 37°C. However, above 40°C pNNPD also loses transparency (not pictured). Materials which better retain water are more desirable for cellular entrapment upon injection, where water expulsion may simultaneously force delivered cells out of the carrier network.

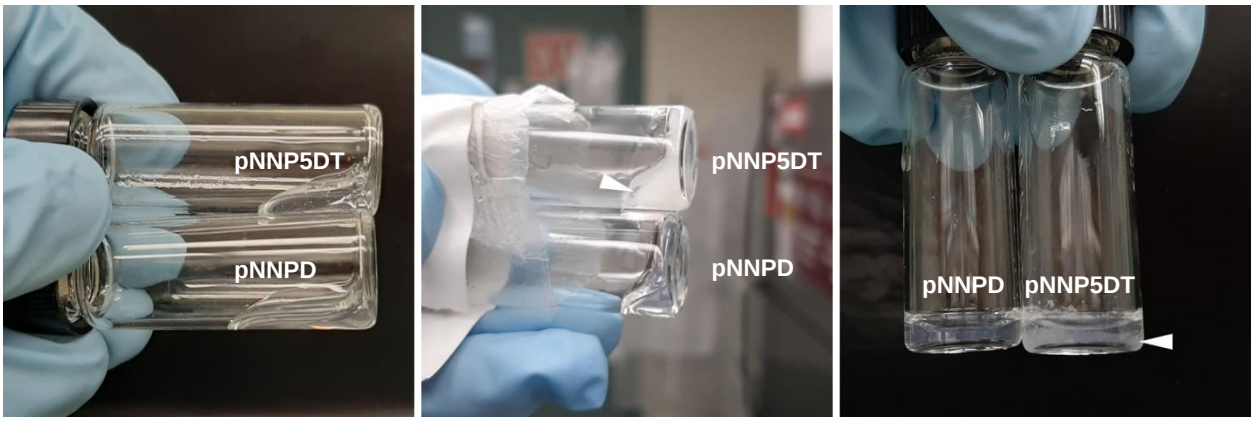


**Figure 2.5.** Photograph displaying visual differences between pNNPD and pNNP5DT at 20°C (left) and after heating for 10 minutes in a water bath at 37°C (middle). pNNP5DT appears more turbid and expels some of its water content above its Tgel (white arrow), where pNNPD retains water at 37°C. While cooling to 20°C following removal from the water bath (right), result of syneresis is evident in pNNP5DT which shows a more turbid material localized to the bottom of the vial (white arrow). This is indicative of increased polymer density following water expulsion above the Tgel of pNNP5DT. pNNPD remains homogenous gel after heating to 37°C and throughout cooling.

Compared to pNNPD, the high initial modulus as well as LCST and Tgel for pNNP5DT may be more suitable for use as an *in situ* gelling cell carrier. However, its physical changes during gelation are not ideal for application in the back of the eye. Namely, pNNP5DT expels some of its water content during polymer collapse producing polymer dense clumps where pNNPD retains its shape. As well, pNNP5DT displays high turbidity at physiological temperatures where pNNPD retains optical transparency below 40°C. Gelation of pNNPD above its LCST is gradual and does not enter the elastic region below physiological temperatures. It is unclear whether G' > G'' crossover is essential for application if modulus and viscosity at 37°C is suitable for delivery to the subretinal space [261]. Both pNNPD and pNNP5DT display comparable complex viscosities beyond 25°C which reflect high flowability; this is desired to achieve even distribution throughout

the subretinal space following injection. It is unclear whether more robust gelation, as shown by pNNP5DT, or gradual gelation, as seen with pNNPD, is best suited for entrapment of cells upon injection.

### 2.5.3 Metabolic Effects of pNNPD and pNNP5DT on ARPE-19s

Metabolic activity of retinal pigment epithelial cells was examined as a measure of cell viability following exposure to modified pNNPD and pNNP5DT polymers. DMEM/F12 lacking FBS and having no dissolved polymer was used as a negative control. PBS added at equal volumes as dissolved polymer treatments was used as a vehicle control. As summarized in **Figure 2.6**, pNNPD polymers displayed high viability across treatments (>80%) after 48 h. Single factor ANOVA ($\alpha$ = 0.05) showed a significant difference among groups (p = 3.34E-13; **Appendices A12.1 and A12.2**). Tukey's post-hoc analysis showed no significant difference between modified polymers and the negative control, although there was a significant decrease in viability of unmodified pNNPD as compared to the negative control. There was no significant difference in viability between cells treated with pNNPD materials with the exception of a significant increase in viability of pNNPD-$RGDS_{31}$ as compared to unmodified pNNPD. Decreases in viability as compared to the PBS vehicle control were found to be significant for all materials, yet there was no significant difference between the negative control and PBS. Due to minimal material availability, this MTT assay unfortunately lacked data for pNNPD-$RGDS_{117}$, however, in a preliminary study conducted in complete DMEM/F12 supplemented with 10% FBS (as opposed to incomplete DMEM/F12 used here – **Appendix A16**), pNNPD-$RGDS_{117}$ showed viability ≥69% at both 24 and 48 hours, which was found to be a significant decrease in viability when compared to all other groups using Tukey's post-hoc analysis ($\alpha$ = 0.05). All other groups showed comparable viability and as such it was determined that FBS in complete DMEM/F12 may lead to an overestimation of viability due to pNNPD interaction with FBS which may have interfered with its interaction with cells.

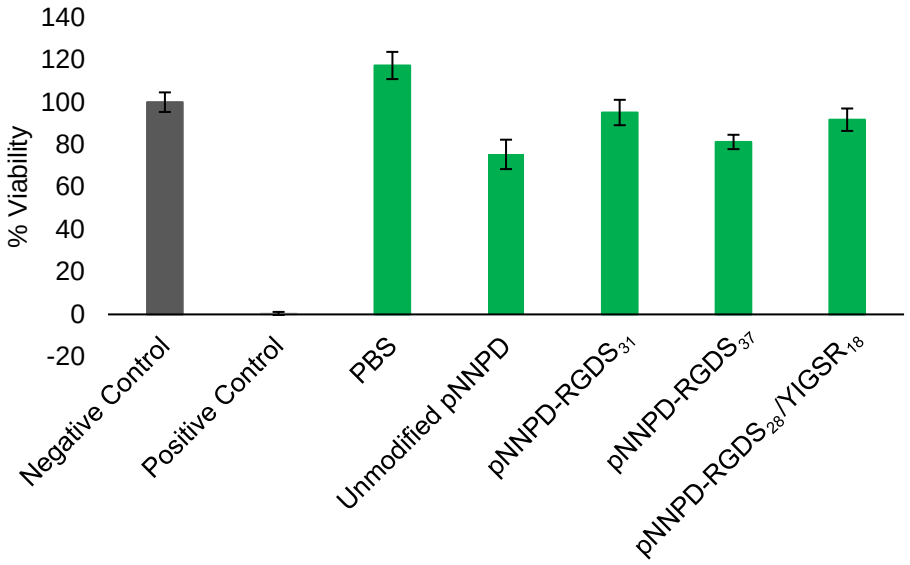


**Figure 2.6.** Cell viability of ARPE-19 cells show high metabolic activity (> 80%) when exposed to 10 µL of 20 w/v% pNNPD in incomplete DMEM/F12 for 48 h of culture (37°C, 5% $CO_2$). $\sigma_{\bar{x}}$ reflective of an n of 4.

In the case of pNNP5DT, summarized in **Figure 2.7**, polymers displayed low viability across treatments (<70%) after 24 and 48 h. Single factor ANOVA ($\alpha$ = 0.05) showed a significant difference among groups ($p_{24h}$ = 9.24E-09, $p_{48h}$ = 3.93E-11; **Appendices A12.3 and A12.4**). Tukey's post-hoc analysis showed that, at 24 h, there was no significant difference between polymers, however, all materials were found to significantly decrease viability as compared to controls. No difference was found between negative and PBS controls. Modification with RGDS was associated with a significant decrease in viability as compared to pNNP5DT-$YIGSR_{27}$, however, there was no significant difference in viability between pNNP5DT-$RGDS_{33}$ and pNNP5DT-$RGDS_{48}$. At 48 h, decreases in viability were found to be significant across all groups relative to negative and PBS controls, with no difference in viability between the negative control and PBS vehicle control. No difference was noted between RGDS modified materials. As well, both pNNP5DT-$RGDS_{33}$ and pNNP5DT-$RGDS_{48}$ displayed a significant decrease in viability as compared to pNNP5DT-$YIGSR_{27}$. pNNP5DT-$RGDS_{48}$ showed a significant decrease in viability as compared to unmodified pNNP5DT, although there was no significant difference in viability between unmodified pNNP5DT and the other modified pNNP5DT materials.

Considering the results of MTT analysis alone, pNNPD is not associated with drastic decreases in ARPE-19 metabolic viability as compared to pNNP5DT. It is unclear what may induce low metabolic activity in pNNP5DT materials. However, it is hypothesized that syneresis could contribute to cell asphyxiation, resulting in the formation of regions where thin layers of polymer coat confluent cells. These regions would likely have reduced the transfer of oxygen and nutrients. Alternatively, pNNPD which is able to retain water content at 37°C, is less polymer

dense than pNNP5DT and therefore more permeable. Results of the MTT analysis should be considered holistically with fluorescent LIVE/DEAD imaging.

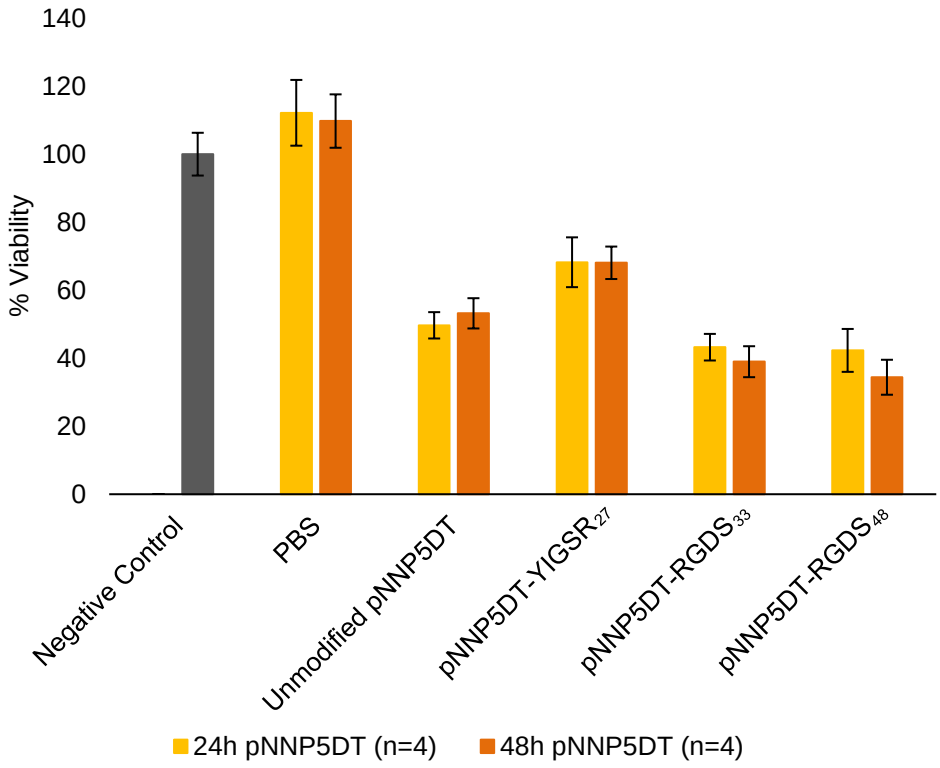


**Figure 2.7.** Cell viability of ARPE-19 cells show low metabolic activity (> 70%) when exposed to 20 µL of 10 w/v% pNNP5DT in incomplete DMEM/F12 for 24 and 48 h of culture (37°C, 5% CO2). $\sigma_{\bar{x}}$ reflective of an n of 4.

### 2.5.4 Cytotoxicity of pNNPD and pNNP5DT on ARPE-19s

In order to further understand the changes in viability demonstrated by the MTT analysis, visualization by means of LIVE/DEAD staining with calcein AM and ethidium homodimer-1 (Invitrogen™) was conducted. The results are shown in **Figure 2.8**, which depicts representative images taken at 10X magnification of pNNPD treated ARPE-19 cultures. Images display comparable LIVE/DEAD staining across all pNNPD materials as compared to controls. Regions where cells appear raised and more spherical can be noted in materials modified with peptide. Distinct patchiness is evident in pNNPD-$RGDS_{117}$. Single factor ANOVA ($\alpha = 0.05$) displayed no significant difference between ImageJ dead cell counts of all treatment groups ($p = 0.23$, **Figure 2.9**; **Appendix A13**).

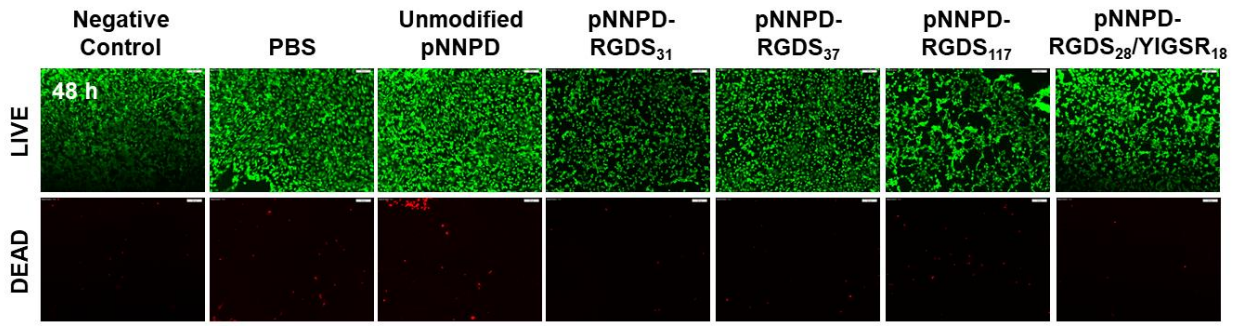


**Figure 2.8.** Representative fluorescent images (10X magnification) of ARPE-19 cells stained with calcein (live cells - green) and ethidium homodimer (dead cells – red) following treatment with 10 µL of 20 w/v% pNNPD in sterile 1X PBS for 48 h (images taken from an n of 3). Polymer treatments show comparable staining as controls with some patch regions noted in pNNPD-RGDS$_{117}$.

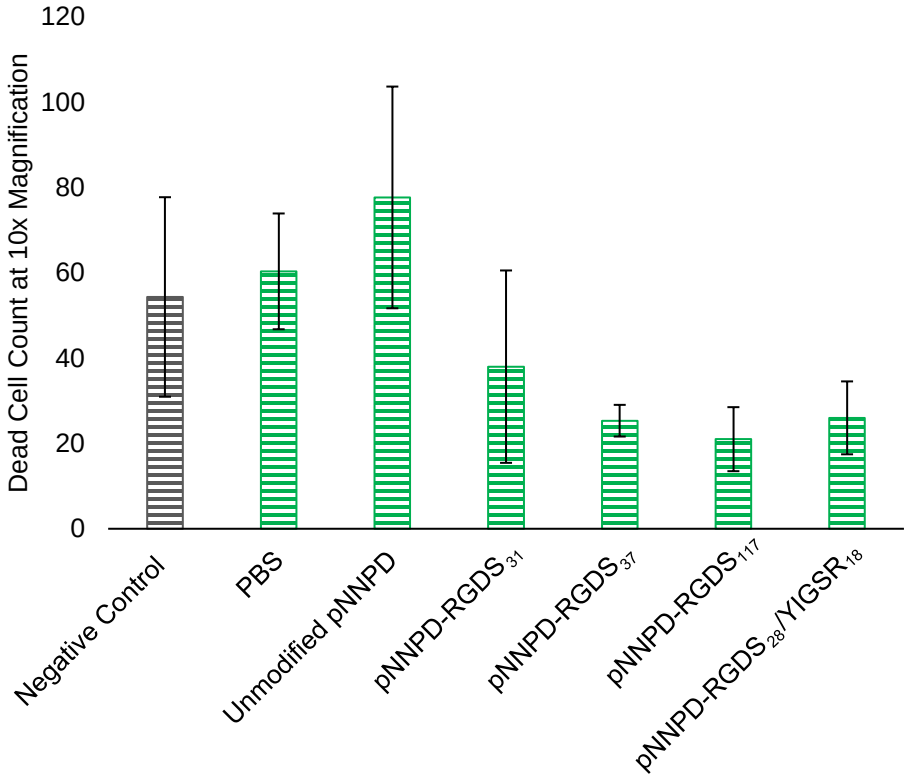


**Figure 2.9.** Dead cell counts of ARPE-19 cells following treatment with 10 µL of 20 w/v% pNNPD in sterile 1X PBS for 48 h, processed from fluorescent images using ImageJ. $\sigma_{\bar{x}}$ reflective of an n of 3.

Alternatively, as shown in **Figure 2.10**, visualization of pNNP5DT treated cells elucidates notable patchiness and apparent cell lifting in RGDS modified pNNP5DT-$RGDS_{33}$ and pNNP5DT-$RGDS_{48}$. This phenomenon was consistently visualized in independent repeated trials (**Appendix A15**). In **Figure 2.11**, images taken at 20X magnification of raised agglomerates found in wells treated with pNNP5DT-$RGDS_{33}$ and pNNP5DT-$RGDS_{48}$ reveal these regions to be primarily composed of lifted live cells. This suggests that cells leaving the surface of the tissue culture plate are not lysed prior to lifting. Dead cell counts using ImageJ were not collected for pNNP5DT treated materials as this apparent cell lifting was anticipated to interfere in providing an accurate representation of cytotoxicity. Attempts were made to compare relative fluorescence between pNNP5DT treatments using a fluorescence intensity scan (TECAN Infinite® M200 PRO NanoQuant Plate Reader) at an excitation of 485 nm and emission of 530 nm (live stain) as well as an excitation of 530 nm and emission of 645 nm (dead stain), as per the Invitrogen™ LIVE/DEAD™ Viability/Cytotoxicity Kit plate reader protocol. Again, cell lifting interfered with the accuracy of acquired measurements (data not shown).

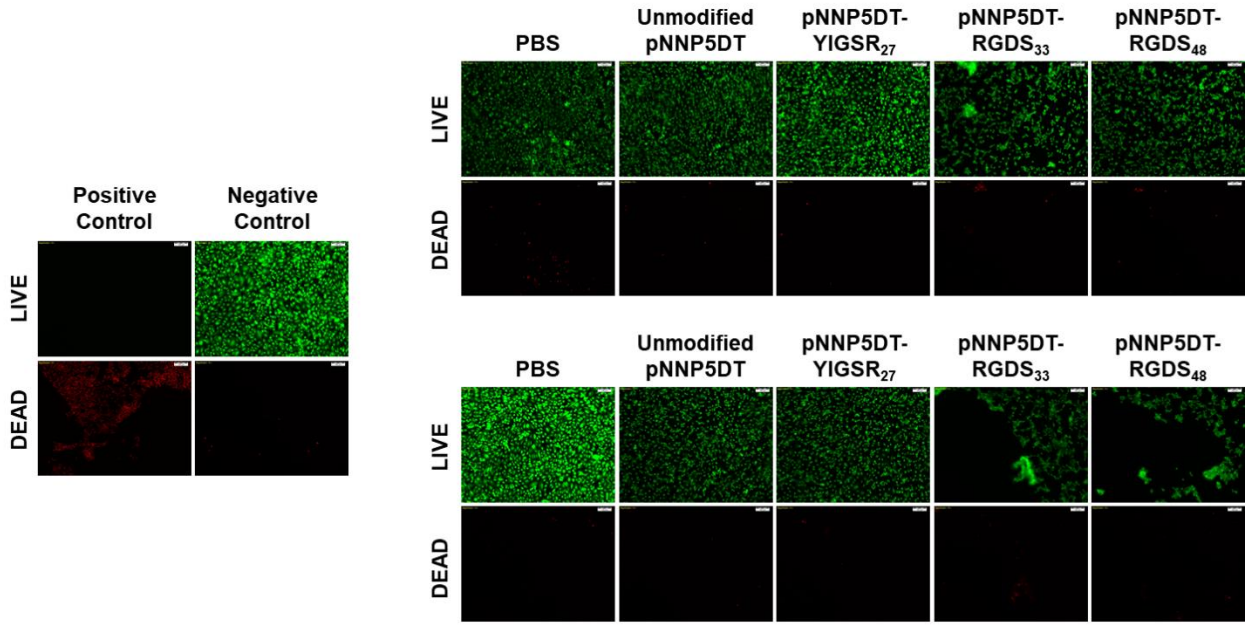


**Figure 2.10.** Representative fluorescent images (10X magnification) of ARPE-19 cells stained with calcein (live cells - green) and ethidium homodimer (dead cells – red) following treatment with 20 µL of 10 w/v% pNNP5DT in sterile 1X PBS for 24 and 48 h (images taken from an n of 4).

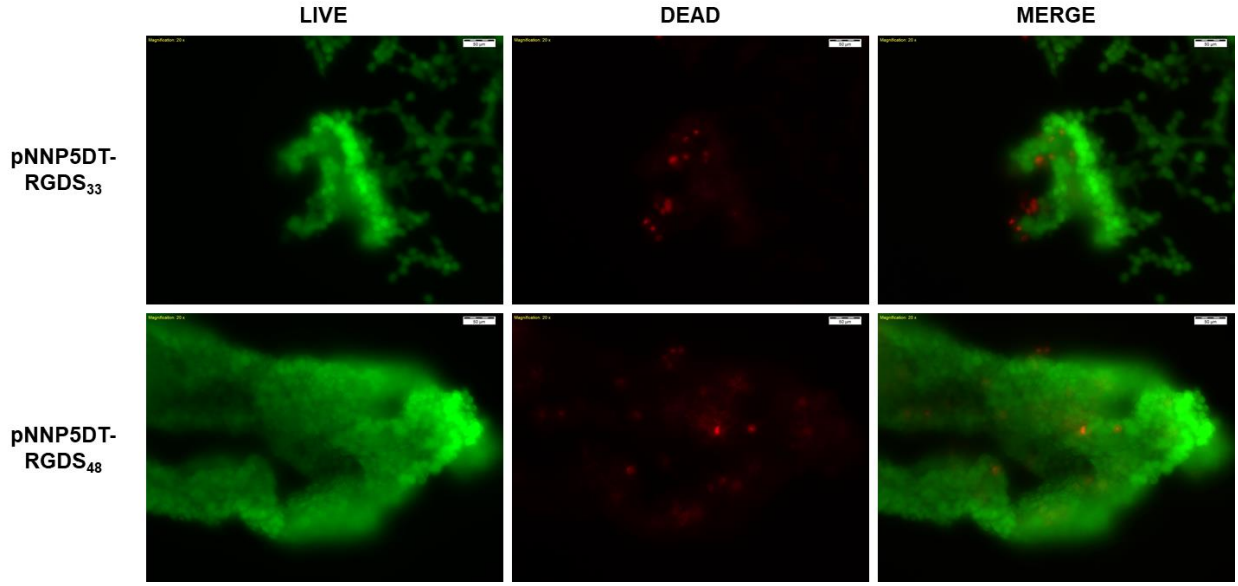


**Figure 2.11.** Fluorescent images (20X magnification) of raised agglomerates found in wells treated with either pNNP5DT-RGDS$_{33}$ or pNNP5DT-RGDS$_{48}$. Agglomerates appear to be composed primarily of live ARPE-19 cells.

Cell lifting evident in cultures exposed to pNNP5DT-RGDS$_{33}$ and pNNP5DT-RGDS$_{48}$ may be explained by possible migration of ARPE-19 cells from the tissue culture plate into the overlying polymer. RPE cells have been shown to migrate in response to fibronectin gradients [262-264], and fibronectin homeostasis is well documented in retinal ECM formation as well as at the onset of retinal disease, including proliferative vitreoretinopathy, AMD, and diabetic retinopathy [265]. *In vitro* cultures of RPE R-50 on surfaces coated with fibronectin, laminin, type I collagen, type IV collagen, and bovine serum albumin as a control, displayed comparable levels of cell adhesion on fibronectin and laminin. However, brightfield imaging of morphology 60 minutes after seeding revealed RPE R-50 cells spread most effectively on fibronectin as compared to all other surface coatings [266]. Migration of aged and fetal human RPE cells has also been shown to be consistently better on human fibronectin resurfaced culture plates as compared to those with human laminin [267].

The role of fibronectin in migration is further demonstrated by the presence of the RGD specific α5β1 receptor in adult and fetal human RPE, with the α5-subunit primarily found on the apical membrane and the β1-subunit equally localized to the apical and basolateral membranes [268]. Furthermore, human fetal RPE were shown to secrete fibronectin to the apical surface at concentrations 450 times greater than that seen on the basal side. When exposed to an α5β1 antagonist (JSM6427), human fetal RPE showed significantly inhibited ability to attach to fibronectin, but there was no change in their attachment to laminin, type I collagen, and type IV collagen. JSM6427 was also found to inhibit cell migration, induced by basic fibroblast growth

factor and platelet-derived growth factor-BB, as well as cell proliferation. These disruptions were attributed to F-actin and cytoskeleton abnormalities in proliferating cells treated with JSM6427, including the accumulation of F-actin circumferentially as well as the loss of interlocking tight junctions [268]. F-actin disruption in proliferative over quiescent cells by JSM6427, is complemented by the finding that RPE express ten times less α5 and β1 integrins when quiescent than when proliferative [269].

In this work, the affinity of RPE for fibronectin during migration may explain increased lifting in materials modified with RGDS compared with those modified with YIGSR. Differences in lifting seen between pNNPD and pNNP5DT materials modified with RGDS, may result from syneresis during pNNP5DT gelation. The polymer expelling water content, produces regions which have a higher polymer density. As a result, potential cell adhesion and migration into modified pNNP5DT is higher relative to the highly flowable pNNPD at 37°C. pNNPD may require increased RGDS modification to encourage cell adhesion, as indicated by lifting being most notable in pNNPD-$RGDS_{117}$. LIVE/DEAD staining also reveals a potential flaw in using the MTT assay with these materials. If cells are robustly moving into certain RGDS modified materials, cells may be removed from wells during washing and before formazan crystal formation which is expected to lower viability readings by virtue of decreased cell number as compared to controls. In order to confirm whether or not cells are in fact migrating into overlying material, future studies using confocal microscopy would be beneficial in visualizing cell response following exposure to pNNPD or pNNP5DT. As well, a deeper evaluation of the ability of cells to migrate through and out of these materials is recommended, a preliminary migration assay is described in **Appendix A16** and serves as a basis for future study.

## 2.6 SUMMARY

Cell adhesion peptides RGDS and YIGSR, derived from the ECM proteins fibronectin and laminin, were used to modify NIPAAm-based thermoresponsive gels pNNPD and pNNP5DT with the goal of improving suitability of these gels as injectable cell carriers. Neat pNNP5DT displayed an LCST and Tgel that would make it suitable for use at physiological temperatures whereas pNNPD possessed a Tgel at 40°C. Both materials were shown to have comparable complex viscosities and modulus above 25°C, although pNNP5DT has a G' that is twice that of pNNPD at 20°C. Despite having a more favourable response to temperature for application as an *in situ* gelling cell carrier, forming an elastic gel around physiological, pNNP5DT did not retain its water content and optical transparency unlike pNNPD at 37°C. Metabolic activity of ARPE-19 cells cultured in DMEM/F12 was significantly reduced when cultured with pNNP5DT materials and was associated with lower cell viability than observed with all pNNPD materials. This is believed to be a product of syneresis in pNNP5DT which is hypothesized to interfere with nutrient transport. pNNPD materials maintained high viability of ARPE-19 cells (> 80%) across modifications. Fluorescent LIVE/DEAD imaging revealed that analysis of metabolic activity may have also been

impacted by potential cell lifting in RGDS modified materials. pNNP5DT-$RGDS_{33}$, pNNP5DT-$RGDS_{48}$, and pNNPD-$RGDS_{117}$ showed signs of cell lifting and migration into polymeric matrices. This is anticipated to be related to affinity of RPE for the fibronectin derived RGDS during migration.

Overall, the results of the present study indicate that a formulation which combines the benefits of both pNNPD and pNNP5DT may have improved character for cell delivery to the subretinal space. As well, high molar concentrations of RGDS modification may be best suited for RPE delivery as compared to YIGSR. This work serves as foundation for further optimization using the monomers and bioconjugation agents described herein. This study also suggests that peptide modification may not be reserved to NAS. In systems possessing multiple co-monomers, groups which are susceptible to hydrolysis due to decreasing pH caused by competing NAS hydrolysis, may become subject to off-target grafting. Here, changes in $^{1}H$ NMR of DBA and TRIS peaks are indicative of potential reaction. As well, amphiphilic peptides may be subject to self-assembly further contributing to the overall amount of peptide incorporated. Careful modulation of pH during reaction is therefore recommended to ensure modification is controlled to NAS sites to allow for reproducible levels of peptide to be present in the polymer matrices. These results provide insight into the future development of pNIPAAm-based thermoresponsive gels intended for use as *in situ* gelling injectable cell carriers and highlights important considerations for subretinal delivery of RPE cells.

# Chapter 3: CONCLUSIONS

Retinal cell delivery has been investigated for its ability to rescue vision and prevent further progression of degeneration in dAMD. The use of *in situ* gelling soft hydrogels offers the potential for minimally invasive cell transplant with improved cell distribution as compared to two-dimensional platforms and saline injections. The work herein describes the study of two pNIPAAm-based hydrogels as potential subretinal cell carriers.

A comparison of the thermoresponsivity of pNNPD and pNNP5DT revealed that pNNP5DT possesses desirable thermoresponsive character by virtue of its LCST (27°C) and Tgel (35°C) both of which occur below physiological temperature. However, pNNP5DT did not conserve transparency and water retention at 37°C as was seen with pNNPD. pNNPD, having an LCST around 24°C, possessed a Tgel above physiological at 40°C. It is unclear whether or not complete formation of an elastic gel is a requirement for cell delivery. If modulus is favourable for cellular entrapment upon injection, a Tgel above physiological may be unimportant. However, the high initial viscosity of pNNP5DT at room temperature and robust viscosity changes leading to formation of an elastic gel below 37°C, may further aid in entrapping cells prior to injection as compared to pNNPD which has a G' two times lower at 20°C and displays gradual gelation above its LCST.

In terms of cell compatibility, pNNPD yields higher viability of ARPE-19 cells than pNNP5DT. Taken holistically with evidence of syneresis, decreases in cell viability are thought to be a result of areas of increased polymer density interfering with oxygen and nutrient permeability in cultures treated with pNNP5DT. Fluorescent imaging using calcein and ethidium-homodimer 1 as LIVE/DEAD stains, revealed that pNNP5DT-RGDS modified materials show evidence of cell lifting. As well, lifting defined by spherical cell shape and some patchiness was noted in pNNPD-$RGDS_{117}$. It is hypothesized that cell lifting in pNNP5DT may again be a product of regions of increased polymer density, allowing cells to more easily adhere to and move into overlying material, as compared to the highly flowable pNNPD at 37°C. This is corroborated by higher concentrations of RGDS being required in the pNNPD materials before cell lifting is observed.

This work also elucidates potential off-target grafting of adhesion peptides in materials possessing complex copolymer formulations susceptible to acid-catalyzed hydrolysis. Decreasing pH of pNNPD and pNNP5DT was attributed to increased acrylic acid content produced as a result of NAS hydrolysis over time. Increased bioconjugation in pNNPD and pNNP5DT materials indicates interaction of peptides with other groups within the polymer backbone (namely DBA and TRIS) as well as possible additive intermolecular interactions between grafted and free adhesion sequences.

Overall, a material which combines the optical transparency and water retention of pNNPD with slightly increased modulus as anticipated in the polymer dense regions of pNNP5DT,

may be better suited for cell delivery to the subretinal space. A preference for RGDS over YIGSR may also be important in RPE cell delivery specifically, as indicated by potential cell lifting being preferential with RGDS modified materials compared to YIGSR of similar grafting concentrations in pNNP5DT. This work highlights important considerations in the development of pNIPAAm-based cell carriers for RPE cell delivery to the subretinal space and elucidates potential off-target grafting not previously considered. Further study is recommended in order to develop *in situ* gelling materials which can be applied in the treatment of degenerative retinal disorders.

# APPENDIX A

## A1. $^1$H NMR OF PEGMEMA$_{510}$ AND PEGMEMA$_{1070}$ IN DMSO-D6

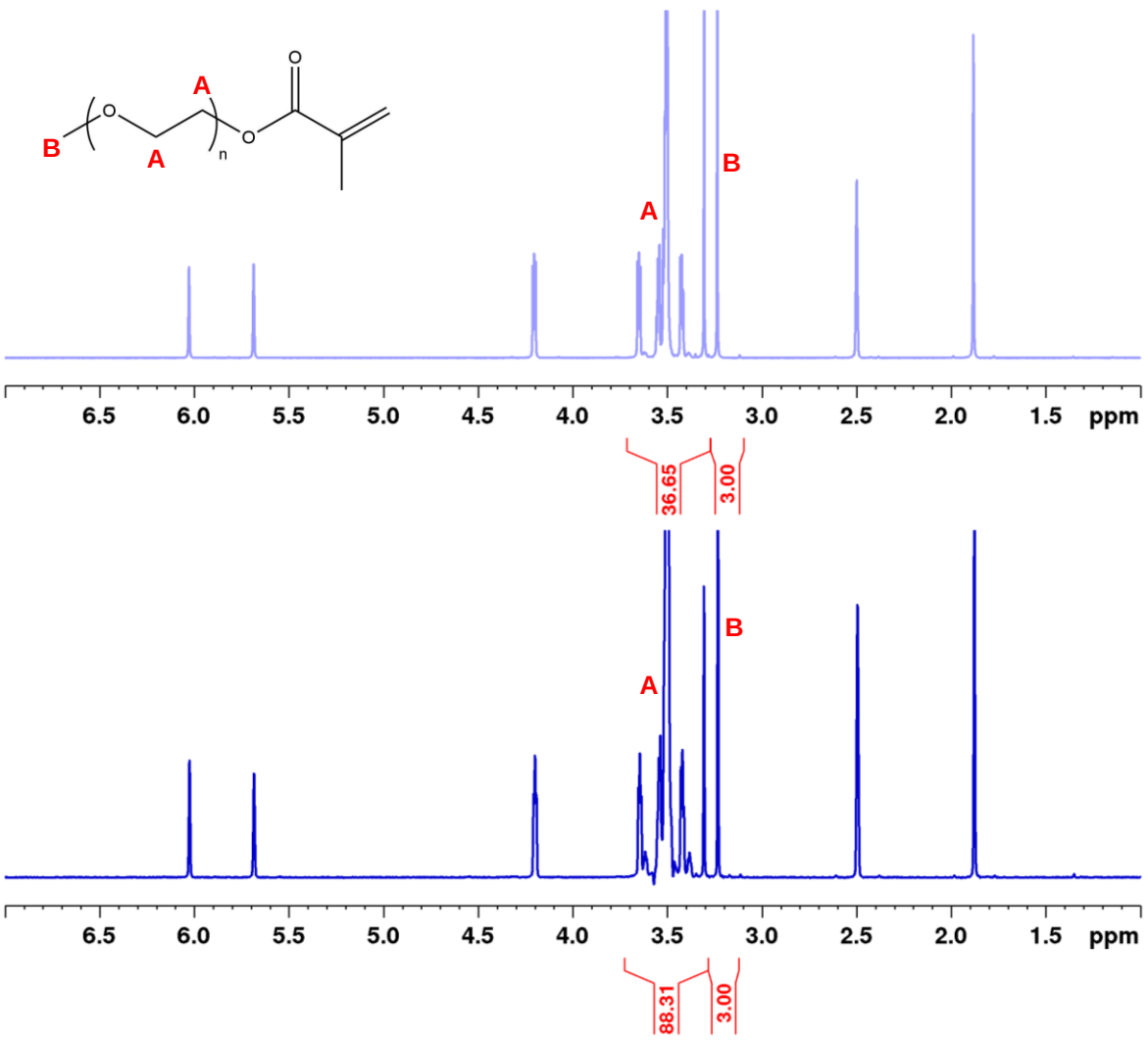


**Figure A1.** $^1$H NMR (Bruker Avance 600 Hz) of PEGMEMA$_{510}$ (top) and PEGMEMA$_{1070}$ (bottom) in DMSO-d6. Integration of terminal -$CH_3$ peak was calibrated to 3, using the associated integration of the PEGMEMA repeating unit the number of repeat units was derived and used to determine molecular weight (g/mol).

## A2. $^{1}$H NMR OF STOCK PNNPD AND PNNP5DT IN DMSO-D6

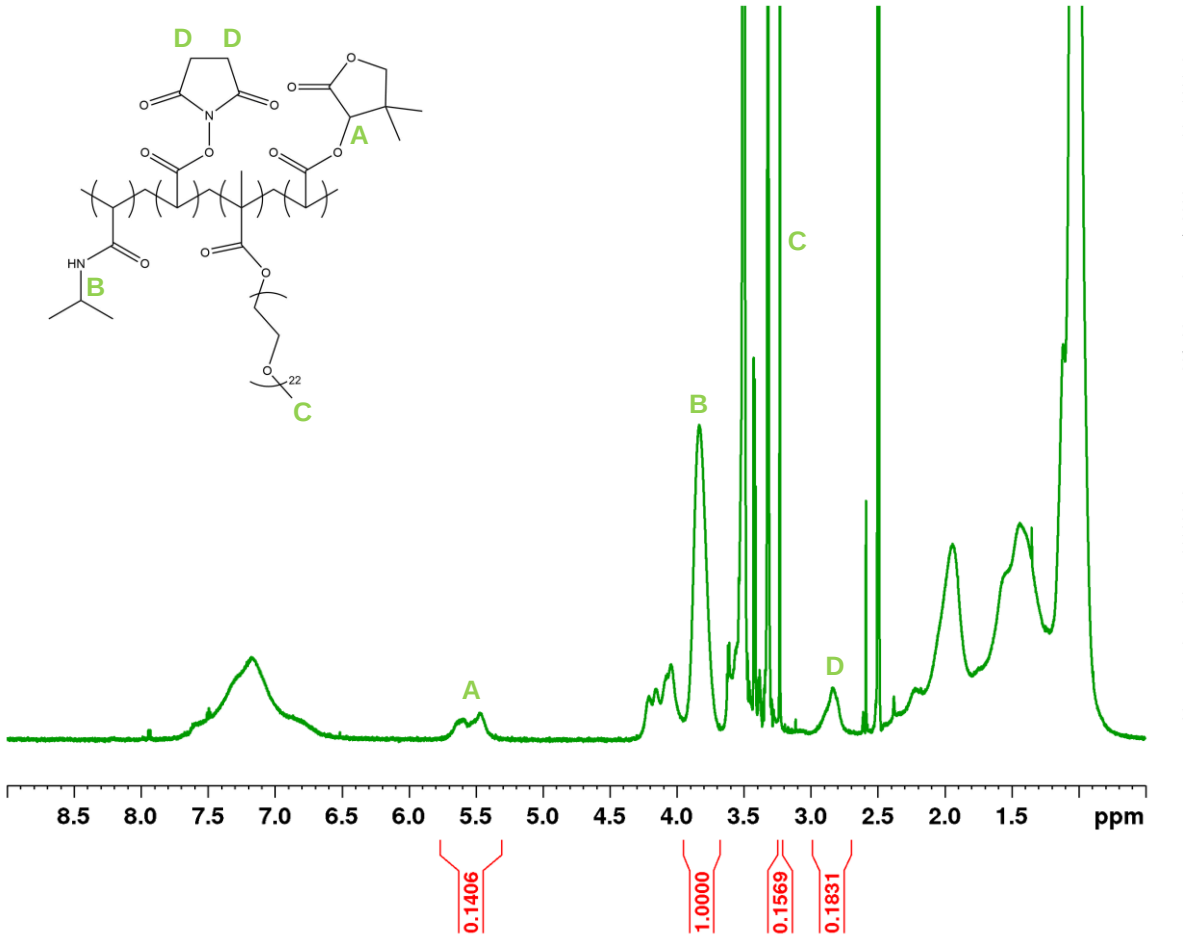


**Figure A2.** $^{1}$H NMR (Bruker Avance 600 Hz) of stock pNNPD in DMSO-d6.

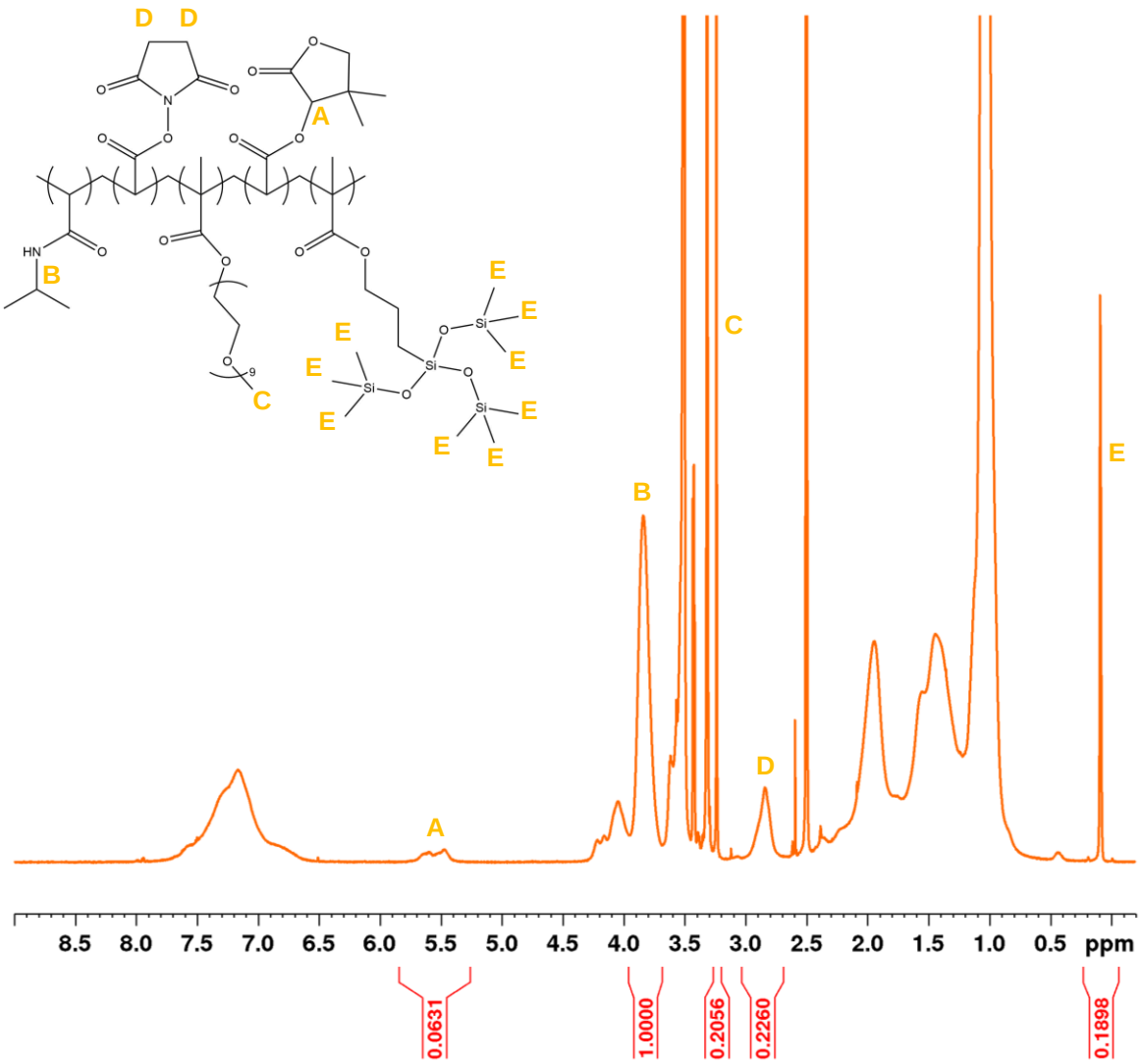


**Figure A3.** $^{1}$H NMR (Bruker Avance 600 Hz) of stock pNNP5DT in DMSO-d6.

## A3. $^1$H NMR OF RGDS/YIGSR MODIFIED PNNPD AND PNNP5DT IN $D_2O$

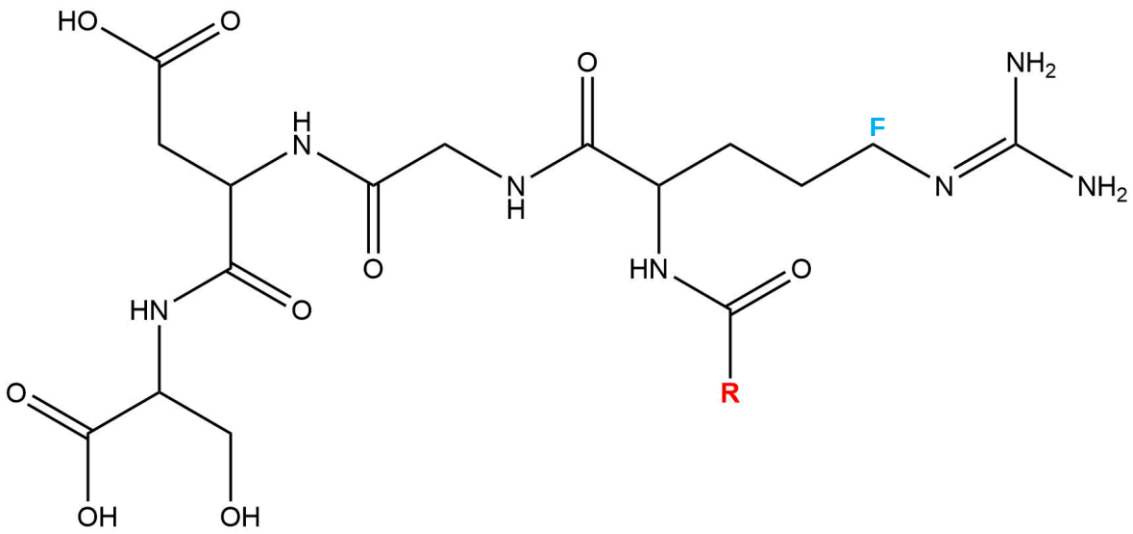


**Figure A4.** Molecular Structure of RGDS conjugated to either pNNPD or pNNP5DT (denoted R) through an amide bond. Carbon groups marked with a F indicate the site of $^1$H NMR (Bruker Avance 600 Hz; $D_2O$) proton peaks used to quantify amount of RGDS grafted (-$CH_2$; 3.23 ppm).

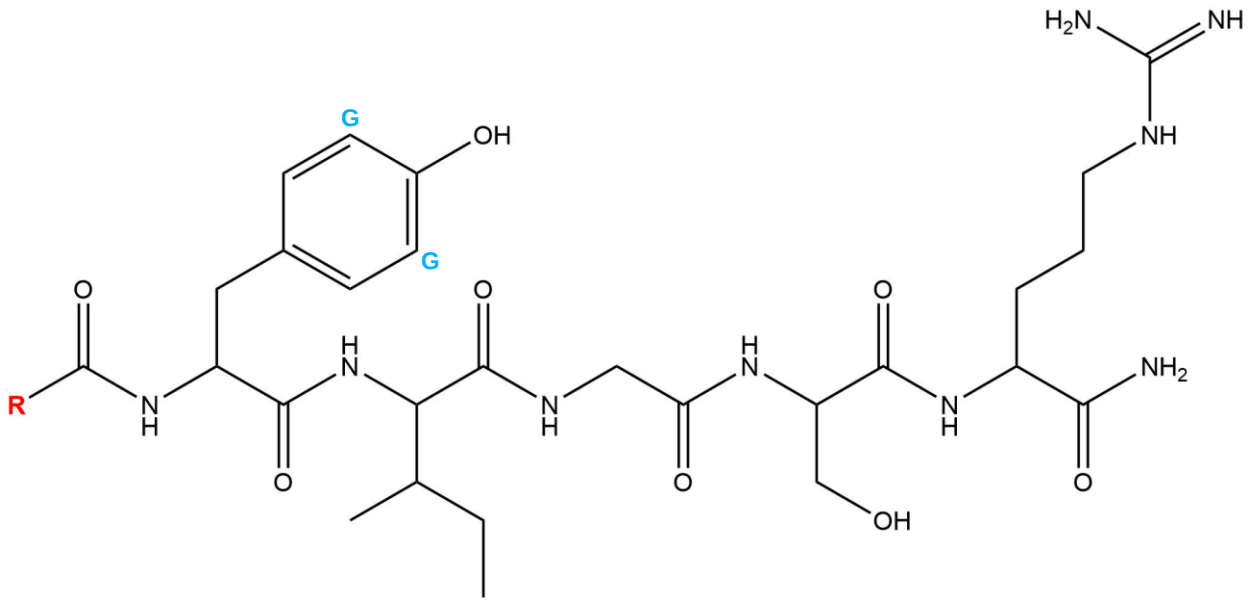


**Figure A5.** Molecular Structure of YIGSR conjugated to either pNNPD or pNNP5DT (denoted R) through an amide bond. Carbon groups marked with a G indicate the site of $^{1}H$ NMR (Bruker Avance 600 Hz; $D_2O$) proton peaks used to quantify amount of YIGSR grafted (C2 and C6 of tyrosine ring; 6.8 ppm).

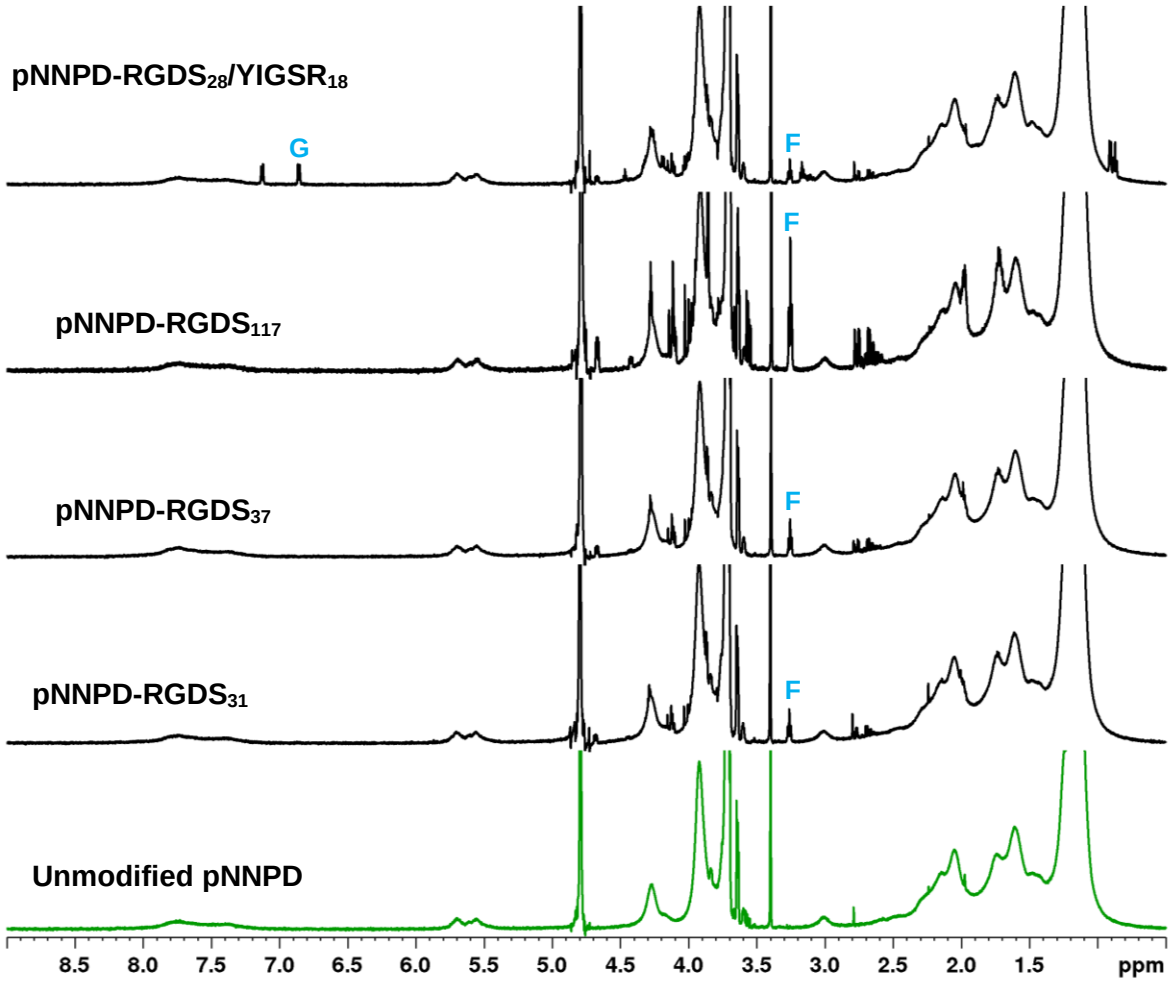


**Figure A6.** $^{1}H$ NMR in $D_2O$ of pNNPD materials following modification with adhesion peptides RGDS and YIGSR. $PEGMEMA_{1070}$ was used as an internal standard to allow for approximate molar contributions of isolated co-monomers to be identified. As such, the integration for $PEGMEMA_{1070}$ (terminal $-CH_3$ peak at 3.4 ppm) was calibrated to 12.66 (4.22 mol% * 3 protons). Peaks of interest are defined as follows NAS ($-CH_2$) peak around 2.9-3.1 ppm, DBA (-CH) peak at 5.4–5.8 ppm, TRIS (protons of nine terminal methyl groups) peak at 0.1 ppm, RGDS (denoted F, $-CH_2$ on arginine residue) peak at 3.23 ppm, and YIGSR (denoted G, protons on C2 and C6 of tyrosine residue) peak at 6.8 ppm. Refer to **Table A1** for associated integrations.

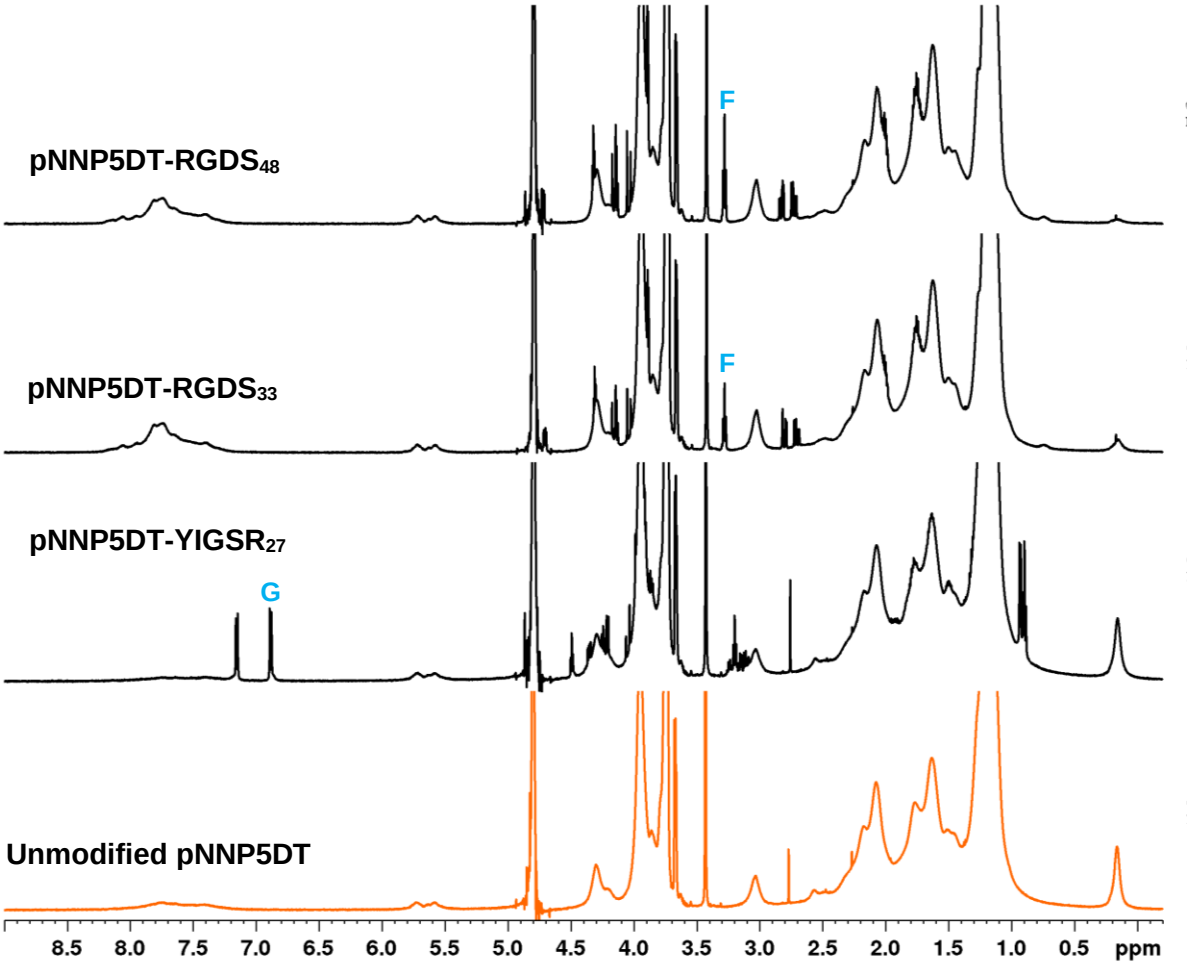


**Figure A7.** $^{1}H$ NMR (Bruker Avance 600 Hz) in $D_2O$ of pNNP5DT materials following modification with adhesion peptides RGDS and YIGSR. $PEGMEMA_{1070}$ was used as an internal standard to allow for approximate molar contributions of isolated co-monomers to be identified. As such, the integration for $PEGMEMA_{1070}$ (terminal $-CH_3$ peak at 3.4 ppm) was calibrated to 17.19 (5.73 mol% * 3 protons). Peaks of interest are defined as follows NAS ($-CH_2$) peak at 2.9–3.1 ppm, DBA (-CH) peak at 5.4–5.8 ppm, TRIS (protons of nine terminal methyl groups) peak at 0.1 ppm, RGDS (denoted F, $-CH_2$ on arginine residue) peak at 3.23 ppm, and YIGSR (denoted G, protons on C2 and C6 of tyrosine residue) peak at 6.8 ppm. Refer to **Table A1** for associated integrations.

**Table A1. Summary of $^1$H NMR Integrations following Modification***

| Sample | NAS | PEGMEMA | DBA | TRIS | RGDS | YIGSR |
|---|---|---|---|---|---|---|
| pNNPD | 7.6080 | 12.6600 | 10.5532 | - | - | - |
| pNNPD-$RGDS_{31}$ | 7.1792 | 12.6600 | 10.5528 | - | 2.3164 | - |
| pNNPD-$RGDS_{37}$ | 6.4607 | 12.6600 | 10.8467 | - | 2.7254 | - |
| pNNPD-$RGDS_{117}$ | 5.2313 | 12.6600 | 10.0128 | - | 8.6811 | - |
| pNNPD-$RGDS_{28}$/$YIGSR_{18}$ | *overlap* | 12.6600 | 10.2903 | - | 2.0702 | 1.3196 |
| pNNP5DT | 12.6630 | 17.1900 | 5.2317 | 14.3782 | - | - |
| pNNP5DT-$YIGSR_{27}$ | *overlap* | 17.1900 | 5.1918 | 13.8246 | | 2.5623 |
| pNNP5DT-$RGDS_{33}$ | 13.5462 | 17.1900 | 4.8978 | 5.8630 | 3.0940 | - |
| pNNP5DT-$RGDS_{48}$ | 14.2278 | 17.1900 | 5.0682 | 2.4215 | 4.5688 | - |

*$^1$H NMR (Bruker Avance 600 Hz) $D_2O$ as solvent; NAS integration could not be well defined due to multiple YIGSR residues overlapping with peak; for stacked spectra refer to **Figures A6 and A7**.

## A4. Sample Calculation Molar Feed Ratio Polymer Synthesis

To determine the mass (g) to be added of each monomer to synthesize 3 g of pNNPD with a molar feed ratio of 80:4:4:12:

***Step 1***

$$\text{NIPAAm} = (0.8)(113.16\ \text{g/mol})(\text{x})$$
$$\text{NAS} = (0.04)(169.136\ \text{g/mol})(\text{x})$$
$$\text{PEGMEMA}_{1070} = (0.04)(1070\ \text{g/mol})(\text{x})$$
$$\text{DBA} = (0.12)(184.19\ \text{g/mol})(\text{x})$$

***Step 2***

$$(0.8)(113.16\ \text{g/mol})(\text{x}) + (0.04)(169.136\ \text{g/mol})(\text{x}) + (0.04)(1070\ \text{g/mol})(\text{x}) + (0.12)(184.19\ \text{g/mol})(\text{x}) = 3\ \text{g}$$
$$162.19624\text{x} = 3\ \text{g}$$
$$\text{x} = 0.018496$$

***Step 3***

$$\text{NIPAAm} = (0.8)(113.16\ \text{g/mol})(0.018496) = \mathbf{1.67\ g}$$
$$\text{NAS} = (0.04)(169.136\ \text{g/mol})(0.018496) = \mathbf{0.125\ g}$$
$$\text{PEGMEMA}_{1070} = (0.04)(1070\ \text{g/mol})(0.018496) = \mathbf{0.792\ g}$$
$$\text{DBA} = (0.12)(184.19\ \text{g/mol})(0.018496) = \mathbf{0.409\ g}$$

## A5. Sample Calculation for Determining Molar Contribution using $^1$H NMR

To determine the molar contributions of each incorporated monomer, integration analysis using TopSpin 4.0.6 was conducted. Referring to **Figure A2**, DMSO-d6 peak was calibrated to 2.5 ppm. With NIPAAm -CH peak at 3.7–4.0 ppm (B; 1 proton), NAS $CH_2$ peaks at 2.9–3.1 ppm (D; 4 protons), PEGMEMA -$CH_3$ terminal peak at 3.4 ppm (C; 3 protons), and DBA -CH peak at 5.4–5.8 ppm (A; 1 proton). As such, the integration of NIPAAm was calibrated to 1. Integrations were then divided by the number of protons represented by the analyzed peak to determine monomer contributions:

$$\text{NIPAAm} = \frac{1}{1} = \mathbf{1}$$

$$\text{NAS} = \frac{0.1831}{4} = \mathbf{0.045775}$$

$$\text{PEGMEMA}_{1070} = \frac{0.1569}{3} = \mathbf{0.0523}$$

$$\text{DBA} = \frac{0.1406}{1} = \mathbf{0.1406}$$

These values were then weighted to 100 percent as follows:

***Step 1***

$$1 + 0.045775 + 0.0523 + 0.1406 = 1.238675$$

***Step 2***

$$\text{NIPAAm contribution} = \left(\frac{1}{1.238675}\right) * 100 = 80.73\%$$

$$\text{NAS contribution} = \left(\frac{0.045775}{1.238675}\right) * 100 = 3.7\%$$

$$\text{PEGMEMA}_{1070}\text{ contribution} = \left(\frac{0.0523}{1.238675}\right) * 100 = 4.22\%$$

$$\text{DBA contribution} = \left(\frac{0.1406}{1.238675}\right) * 100 = 11.35\%$$

## A6. Sample Calculation for Polymer Modification per mole of NAS

To modify polymers based upon the molar concentration of NAS, each monomer contribution was divided by the contribution of NAS as follows:

$$\frac{\text{NIPAAm contribution}}{\text{NAS contribution}} = \frac{80.73}{3.7} = \mathbf{21.8}$$

$$\frac{\text{NAS contribution}}{\text{NAS contribution}} = \frac{3.7}{3.7} = \mathbf{1}$$

$$\frac{\text{PEGMEMA}_{1070}\text{ contribution}}{\text{NAS contribution}} = \frac{4.22}{3.7} = \mathbf{1.1}$$

$$\frac{\text{DBA contribution}}{\text{NAS contribution}} = \frac{11.35}{3.7} = \mathbf{3.1}$$

The above quotients were then multiplied by the molecular weight of their associated monomer as follows:

$$\text{NIPAAm contribution} = 21.8 * 113.16\ \text{g/mol} = \mathbf{2466.888\ g/mol}$$
$$\text{NAS contribution} = 1 * 169.136\ \text{g/mol} = \mathbf{169.136\ g/mol}$$
$$\text{PEGMEMA}_{1070}\text{ contribution} = 1.1 * 1070\ \text{g/mol} = \mathbf{1177\ g/mol}$$
$$\text{DBA contribution} = 3.1 * 184.19\ \text{g/mol} = \mathbf{570.989\ g/mol}$$

Molecular weight contributions were then summed to find the molecular weight of the polymer per one mole of NAS:

$$2466.888 + 169.136 + 1177 + 570.989 = \mathbf{4384.013\ g/mol}$$

Finally, to reveal the approximate number of moles of NAS available for modification, the desired mass of polymer was divided by the above molecular weight per on mole of NAS. This value was then used as needed to determine the required mass of adhesion peptide to be added to meet the desired molar feed ratio. In the case of pNNPD to be modified with a 1:1 molar feed ratio of NAS to RGDS:

***Step 1***

$$\frac{\text{Mass of pNNPD to be modified}}{\text{Molecular weight of pNNPD per one mole NAS}} = \frac{0.1\ \text{g}}{4384.013\ \text{g/mol}} = \mathbf{0.00002281\ mol}$$

***Step 2***

$$\text{Moles of NAS available} * \text{Desired amount of NAS modified} * \text{Molecular weight of RGDS} = \boldsymbol{x}$$
$$0.00002281 * 1 * 433.42\ \text{g/mol} = \mathbf{0.00989\ g}$$

## A7. Sample Calculation for Determining %NAS Modified

In order to determine the grafting efficiency of adhesion peptides on NAS, integration analysis of $^1$H NMRs of modified polymers in $D_2O$ were conducted. The molar contribution of PEGMEMA was used as an internal standard. For pNNPD, the integration of $PEGMEMA_{1070}$ would be set to 12.66 (4.22% * 3 protons), allowing the integrations taken from peaks associated with RGDS and YIGSR to be directly compared to the initial molar contribution of NAS in stock pNNPD (calculated above).

For example, consider pNNPD-$RGDS_{31}$. Using TopSpin 4.0.6 we take the integration of the -$CH_2$ triplet of RGDS's arginine residue around 3.23 ppm (F; 2 protons) and compare this pseudo molar percentage with the amount of NAS in the stock polymer:

$$\text{RGDS} = \frac{2.3164}{2} = \mathbf{1.1582}$$
$$\%\ \text{NAS Modified} = \frac{1.1582}{3.7} * 100 = \mathbf{31}\%$$

## A8. Preliminary 1-pNNPD Modified with YIGSR

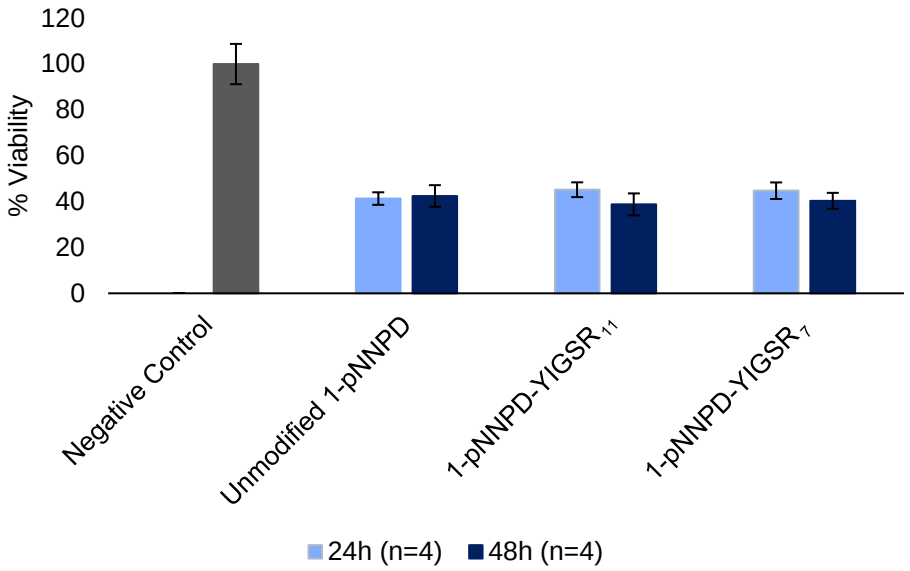


**Figure A8.** 1-pNNPD was synthesized by free radical polymerization with a molar feed ratio of 80:4:4:12. 1-pNNPD underwent dialysis following precipitation and prior to freeze drying for 72 h changing water each day, this step was removed in the synthesis of pNNPD and pNNP5DT as it likely contributed to NAS hydrolysis. Integration analysis of $^{1}H$ NMR (Bruker Avance 600 Hz) in DMSO-d6 revealed a final composition of 82.4: 2.4: 4.1: 11.1. Low NAS molar contribution is attributed to extensive dialysis. Still, materials were dissolved at 15 w/v% in 1X PBS and H-YIGSR-$NH_2$ (10 mg/mL in 1X PBS) was added at a 1:1 and 2:1 NAS to YIGSR molar ratio as previously described. 1-pNNPD materials were equipped with stir bars and left to react for 24 h at 4°C with constant stirring. Following this period materials were dialyzed again for 72 h to remove unreacted YIGSR before being freeze dried. $^{1}H$ NMR integration analysis in $D_2O$ using $PEGMEMA_{1070}$ as an internal standard revealed 11% NAS modified from theoretical 100% NAS modified feed ratio (1-pNNPD-$YIGSR_{11}$) and 7% NAS modified from theoretical 50% NAS modified feed ratio (1-pNNPD-$YIGSR_7$). Cell viability of ARPE-19 (passage 7) cells after treatment with 10 µL of 5 w/v% 1-pNNPD for 24 and 48 h of culture (37°C, 5% CO2; seeding density of 50 000 cells per well; absorbance measured at 570 nm using Thermo Scientific Multiskan GO and Thermo Scientific SkanIt software with blank subtraction) show low metabolic activity (> 50%) across materials. Materials failed Levene's test for homogeneity of variance and as such were analyzed by means of two-tailed two sample t-tests assuming unequal variances ($\alpha = 0.05$; **Appendices A8.1 and A8.2**). All 1-pNNPD materials were found to be significantly different as compared to the negative control at both 24 and 48 h. There was no significant difference between 1-pNNPD materials. $\sigma_{\bar{x}}$ is reflective of an n of 4.

## A8.1. Levene's Test 1-pNNPD MTT Assay

***24h 1-pNNPD MTT Assay Levene's Test***

SUMMARY

| *Groups* | *Count* | *Sum* | *Average* | *Variance* |
|---|---|---|---|---|
| Negative Control | 4 | 0.8327 | 0.208175 | 0.02253 |
| Unmodified 1-pNNPD | 4 | 0.1361 | 0.034025 | 0.000231 |
| 1-pNNPD-YIGSR$_{11}$ | 4 | 0.2341 | 0.058525 | 0.000682 |
| 1-pNNPD-YIGSR$_{7}$ | 4 | 0.29335 | 0.073338 | 0.003687 |

ANOVA

| *Source of Variation* | *SS* | *df* | *MS* | *F* | *P-value* | *F crit* |
|---|---|---|---|---|---|---|
| Between Groups | 0.07327 | 3 | 0.024423 | 3.600867 | 0.046076 | 3.490295 |
| Within Groups | 0.081391 | 12 | 0.006783 | | | |
| | | | | | | |
| Total | 0.154661 | 15 | | | | |

***48h 1-pNNPD MTT Assay Levene's Test***

SUMMARY

| *Groups* | *Count* | *Sum* | *Average* | *Variance* |
|---|---|---|---|---|
| Negative Control | 4 | 0.8327 | 0.208175 | 0.02253 |
| Unmodified 1-pNNPD | 4 | 0.5206 | 0.13015 | 0.009313 |
| 1-pNNPD-YIGSR$_{11}$ | 4 | 0.55285 | 0.138213 | 0.010188 |
| 1-pNNPD-YIGSR$_{7}$ | 4 | 0.31845 | 0.079612 | 0.003856 |

ANOVA

| *Source of Variation* | *SS* | *df* | *MS* | *F* | *P-value* | *F crit* |
|---|---|---|---|---|---|---|
| Between Groups | 0.033564 | 3 | 0.011188 | 0.975262 | 0.436554 | 3.490295 |
| Within Groups | 0.137661 | 12 | 0.011472 | | | |
| | | | | | | |
| Total | 0.171225 | 15 | | | | |

**A8.2. Summary of Two-Sample t-Tests Assuming Unequal Variances**

| *Sample Set* | *Comparison* | *df* | *t Stat* | *Two-tailed p-value* | *Significant ($p < \alpha$)* |
|---|---|---|---|---|---|
| 24 h | Negative Control – Unmodified 1-pNNPD | 3 | 9.334435 | 0.002603 | yes |
| | Negative Control – 1-pNNPD-YIGSR$_{11}$ | 3 | 8.541981 | 0.003371 | yes |
| | Negative Control - 1-pNNPD-YIGSR$_{7}$ | 3 | 8.339256 | 0.00113 | yes |
| | Unmodified 1-pNNPD - 1-pNNPD-YIGSR$_{11}$ | 5 | -2.0977 | 0.090016 | no |
| | Unmodified 1-pNNPD - 1-pNNPD-YIGSR$_{7}$ | 4 | -1.39148 | 0.236471 | no |
| | 1-pNNPD-YIGSR$_{11}$ - 1-pNNPD-YIGSR$_{7}$ | 5 | 0.15286 | 0.884486 | no |
| 48 h | Negative Control – Unmodified 1-pNNPD | 5 | 7.83079 | 0.000545 | yes |
| | Negative Control – 1-pNNPD-YIGSR$_{11}$ | 5 | 8.192473 | 0.000441 | yes |
| | Negative Control - 1-pNNPD-YIGSR$_{7}$ | 4 | 8.937193 | 0.000867 | yes |
| | Unmodified 1-pNNPD - 1-pNNPD-YIGSR$_{11}$ | 6 | 0.641554 | 0.544876 | no |
| | Unmodified 1-pNNPD - 1-pNNPD-YIGSR$_{7}$ | 5 | 0.460164 | 0.664717 | no |
| | 1-pNNPD-YIGSR$_{11}$ - 1-pNNPD-YIGSR$_{7}$ | 5 | -0.31962 | 0.762179 | no |

## A9. DSC (TA INSTRUMENTS Q200) OF PNNP5DT MATERIALS INTENDED FOR CELL STUDIES

**Table A2. LCST of pNNP5DT Materials following use in Cell Studies**

| Polymer | Concentration in 1X PBS | LCST (°C) |
|---|---|---|
| pNNP5DT | 10 w/v% | 26.24 |
| pNNP5DT-YIGSR$_{27}$ | 10 w/v% | 25.03 |
| pNNP5DT-RGDS$_{33}$ | 10 w/v% | 26.40 |
| pNNP5DT-RGDS$_{48}$ | 10 w/v% | 26.00 |

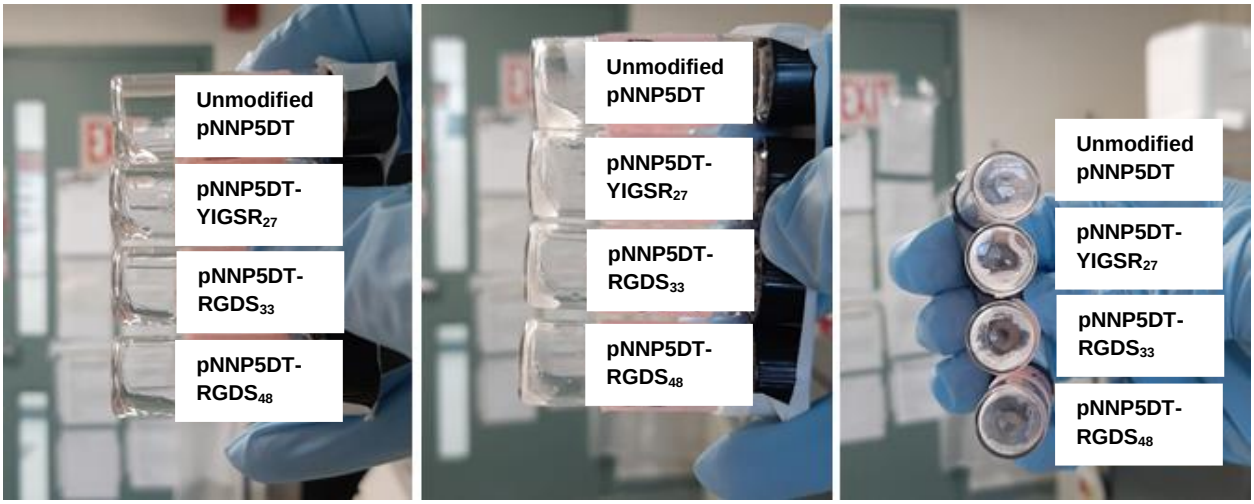


**Figure A9.** Photograph displaying visual differences between pNNP5DT materials at 20°C (left) and after heating for 10 minutes in a water bath at 37°C (middle). pNNP5DT-RGDS materials appear less viscous at room temperature compared to unmodified pNNP5DT and pNNP5DT-YIGSR$_{27}$, likely due to lower molar concentrations of bulky hydrophobic TRIS. All pNNP5DT materials display evidence of syneresis noted by dense polymer clumps found in vials following heating above Tgel (right).

## A10. Rheology (TA Instruments DHR-2) of pNNP5DT and pNNP5DT-low DBA

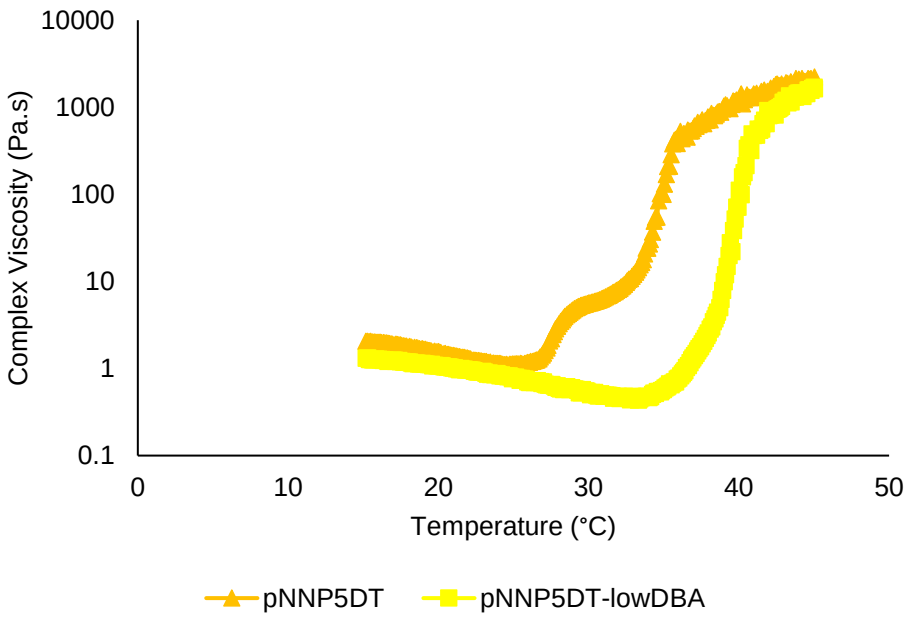


**Figure A10.** Complex viscosity during temperature ramp of pNNP5DT and pNNP5DT-lowDBA from 15°C to 45°C (1°C/min) with an oscillation strain of 1%, frequency of 10 rad/s, and 1000 µm gap. pNNP5DT-lowDBA was found to have a molar composition of 88.6: 4.13: 6.57: 0.22: 0.48. Higher NIPAAm incorporation and lower hydrophobic DBA appears to have an influence on gelation profile. Tgel for pNNP5DT-lowDBA marked by G'>G'' crossover lies around 40.57°C as compared to pNNP5DT in this ramp at 35.8°C (comparable to triplicate Tgel measurements summarized in **Table 2.4**). pNNP5DT-lowDBA is not paired with notable gelation events occurring prior to Tgel as compared to pNNP5DT, indicating that DBA incorporation may play a role in monomer hydrophilic/hydrophobic balance during polymer packing occurring above LCST. DSC LCST measurements were not collected for pNNP5DT-lowDBA, it is hypothesized that endotherm formation in this material may overlap with where Tgel appears here.

## A11. Attempted Cloud Point Analysis of pNNPD and pNNP5DT

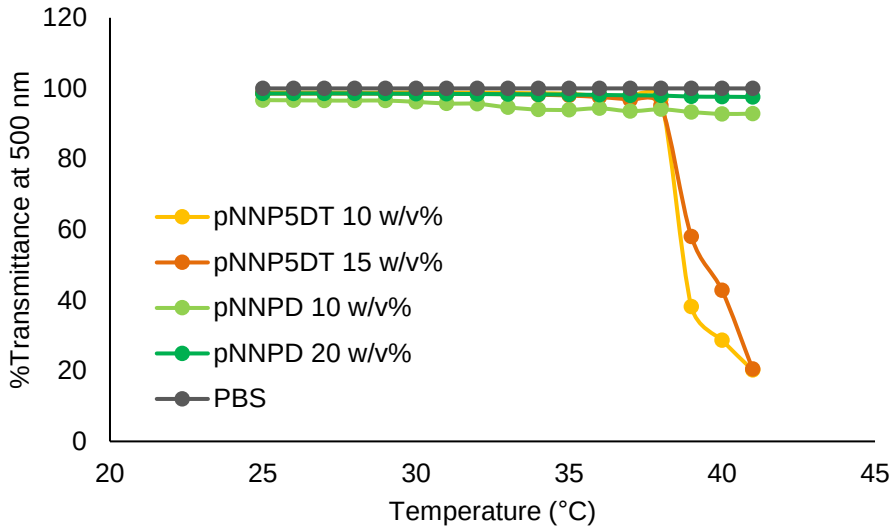


**Figure A11.** Attempted turbidimetry using cloud point as a marker for phase transition. Absorbance measurements were taken using a TECAN Infinite® M200 PRO NanoQuant Plate Reader at 500 nm absorbance (bandwidth 9 nm, 25 flashes, and multiple reads per well – square-filled, 4 x 4) in a Corning® Solid Black, Clear Flat Bottom Polystyrene TC-treated 96-well plate. 100 µL of polymer was seeded per well. Temperature ramp from 25°C to 42°C (was confined to the range of the plate reader). Cloud point was taken as the temperature at which materials displayed 95% transmittance. Improper heat transfer across the plate was anticipated to yield cloud points at higher values than respective LCST and Tgel measurements determined via DSC and DHR analysis. Various attempts were made to improve protocol, such as increasing time spent at each temperature before reading. When time was increased to 10 minutes at each temperature before reading, evaporation led to variable cloud point measurements (data not shown). Ultraviolet-Visible Spectrophotometry using crystal cuvettes would allow for better heat transfer during temperature ramp and is recommended given material availability to determine cloud point.

## A12. STATISTICAL ANALYSIS MTT ASSAYS

### A12.1. Levene's Test pNNPD MTT Assay

***48h pNNPD MTT Assay Levene's Test***

SUMMARY

| *Groups* | *Count* | *Sum* | *Average* | *Variance* |
|---|---|---|---|---|
| Negative Control | 4 | 0.2847 | 0.071175 | 0.001416 |
| Positive Control | 4 | 0.0654 | 0.01635 | 1.64E-05 |
| PBS | 4 | 0.41245 | 0.103113 | 0.006336 |
| Unmodified pNNPD | 4 | 0.4526 | 0.11315 | 0.015369 |
| pNNPD-$RGDS_{31}$ | 4 | 0.3876 | 0.0969 | 0.007665 |
| pNNPD-$RGDS_{37}$ | 4 | 0.1837 | 0.045925 | 0.000556 |
| pNNPD-$RGDS_{28}$/$YIGSR_{18}$ | 4 | 0.4178 | 0.10445 | 8.64E-05 |

ANOVA

| *Source of Variation* | *SS* | *df* | *MS* | *F* | *P-value* | *F crit* |
|---|---|---|---|---|---|---|
| Between Groups | 0.031182 | 6 | 0.005197 | 1.156901 | 0.365655 | 2.572712 |
| Within Groups | 0.094335 | 21 | 0.004492 | | | |
| Total | 0.125516 | 27 | | | | |

### A12.2. Single-Factor ANOVA and Tukey's post-hoc Analysis pNNPD MTT Assay

***48h pNNPD MTT Assay ANOVA and Tukey's post-hoc***

SUMMARY

| *Groups* | *Count* | *Sum* | *Average* | *Variance* |
|---|---|---|---|---|
| Negative Control | 4 | 6.7409 | 1.685225 | 0.008171 |
| Positive Control | 4 | 1.2046 | 0.30115 | 0.000373 |
| PBS | 4 | 7.7019 | 1.925475 | 0.020512 |
| Unmodified pNNPD | 4 | 5.372 | 1.343 | 0.032439 |
| pNNPD-$RGDS_{31}$ | 4 | 6.4694 | 1.61735 | 0.020185 |
| pNNPD-$RGDS_{37}$ | 4 | 5.6983 | 1.424575 | 0.003368 |
| pNNPD-$RGDS_{28}$/$YIGSR_{18}$ | 4 | 6.2816 | 1.5704 | 0.014633 |

ANOVA

| *Source of Variation* | *SS* | *df* | *MS* | *F* | *P-value* | *F crit* |
|---|---|---|---|---|---|---|
| Between Groups | 6.577736 | 6 | 1.096289 | 76.98611 | 3.34E-13 | 2.572712 |
| Within Groups | 0.299042 | 21 | 0.01424 | | | |
| Total | 6.876778 | 27 | | | | |

| | |
|---|---|
| $Q_{crit}$ | 4.597 |
| n | 4 |
| Pooled variance (MSw) | 0.01424 |
| sqrt(MSw/n) | 0.059666 |

| *Comparison* | *Absolute Difference Between Means* | *Q* | *Significant ($Q > Q_{crit}$)* |
|---|---|---|---|
| Negative Control - Positive Control | 1.384075 | 23.19707 | yes |
| Negative Control - PBS | 0.24025 | 4.026586 | no |
| Negative Control - Unmodified pNNPD | 0.342225 | 5.735685 | yes |
| Negative Control - pNNPD-$RGDS_{31}$ | 0.067875 | 1.137584 | no |
| Negative Control - pNNPD-$RGDS_{37}$ | 0.26065 | 4.368489 | no |
| Negative Control - pNNPD-$RGDS_{28}$/$YIGSR_{18}$ | 0.114825 | 1.924465 | no |
| Positive Control - PBS | 1.624325 | 27.22366 | yes |
| Positive Control - Unmodified pNNPD | 1.04185 | 17.46139 | yes |
| Positive Control - pNNPD-$RGDS_{31}$ | 1.3162 | 22.05949 | yes |
| Positive Control - pNNPD-$RGDS_{37}$ | 0.5009 | 8.395075 | yes |
| Positive Control - pNNPD-$RGDS_{28}$/$YIGSR_{18}$ | 1.26925 | 21.27261 | yes |
| Positive Control - Unmodified | 0.582475 | 9.762271 | yes |
| PBS - pNNPD-$RGDS_{31}$ | 0.308125 | 5.16417 | yes |
| PBS - pNNPD-$RGDS_{37}$ | 0.5009 | 8.395075 | yes |
| PBS - pNNPD-$RGDS_{28}$/$YIGSR_{18}$ | 0.355075 | 5.951051 | yes |
| Unmodified pNNPD - pNNPD-$RGDS_{31}$ | 0.27435 | 4.598101 | yes |
| Unmodified pNNPD - pNNPD-$RGDS_{37}$ | 0.081575 | 1.367196 | no |
| Unmodified pNNPD - pNNPD-$RGDS_{28}$/$YIGSR_{18}$ | 0.2274 | 3.81122 | no |
| pNNPD-$RGDS_{31}$ - pNNPD-$RGDS_{37}$ | 0.192775 | 3.230906 | no |
| pNNPD-$RGDS_{31}$ - pNNPD-$RGDS_{28}$/$YIGSR_{18}$ | 0.04695 | 0.786881 | no |
| pNNPD-$RGDS_{37}$ - pNNPD-$RGDS_{28}$/$YIGSR_{18}$ | 0.145825 | 2.444024 | no |

### A12.3. Levene's Test pNNP5DT MTT Assay

***24h pNNP5DT MTT Assay Levene's Test***

SUMMARY

| *Groups* | *Count* | *Sum* | *Average* | *Variance* |
|---|---|---|---|---|
| Negative Control | 4 | 0.7059 | 0.176475 | 0.002321 |
| PBS | 4 | 0.5637 | 0.140925 | 0.009839 |
| Unmodified pNNP5DT | 4 | 0.1322 | 0.03305 | 0.000613 |
| pNNP5DT-YIGSR$_{27}$ | 4 | 0.5315 | 0.132875 | 0.005204 |
| pNNP5DT-RGDS$_{33}$ | 4 | 0.204 | 0.051 | 0.000965 |
| pNNP5DT-RGDS$_{48}$ | 4 | 0.4708 | 0.1177 | 0.008014 |

ANOVA

| *Source of Variation* | *SS* | *df* | *MS* | *F* | *P-value* | *F crit* |
|---|---|---|---|---|---|---|
| Between Groups | 0.061398 | 5 | 0.01228 | 2.733382 | 0.05237 | 2.772853 |
| Within Groups | 0.080864 | 18 | 0.004492 | | | |
| Total | 0.142263 | 23 | | | | |

***48h pNNP5DT MTT Assay Levene's Test***

SUMMARY

| *Groups* | *Count* | *Sum* | *Average* | *Variance* |
|---|---|---|---|---|
| Negative Control | 4 | 0.51285 | 0.128213 | 0.010684 |
| PBS | 4 | 0.2834 | 0.07085 | 0.003214 |
| Unmodified pNNP5DT | 4 | 0.18105 | 0.045263 | 0.002331 |
| pNNP5DT-YIGSR$_{27}$ | 4 | 0.1207 | 0.030175 | 0.000138 |
| pNNP5DT-RGDS$_{33}$ | 4 | 0.285 | 0.07125 | 0.00375 |
| pNNP5DT-RGDS$_{48}$ | 4 | 0.38565 | 0.096413 | 0.004349 |

ANOVA

| *Source of Variation* | *SS* | *df* | *MS* | *F* | *P-value* | *F crit* |
|---|---|---|---|---|---|---|
| Between Groups | 0.024819 | 5 | 0.004964 | 1.217351 | 0.341091 | 2.772853 |
| Within Groups | 0.073395 | 18 | 0.004078 | | | |
| Total | 0.098214 | 23 | | | | |

## A12.4. Single-Factor ANOVA and Tukey's post-hoc Analysis pNNP5DT MTT Assay

***24h pNNP5DT MTT Assay ANOVA and Tukey's post-hoc***

SUMMARY

| *Groups* | *Count* | *Sum* | *Average* | *Variance* |
|---|---|---|---|---|
| Negative Control | 4 | 6.8233 | 1.705825 | 0.043846 |
| PBS | 4 | 7.3594 | 1.83985 | 0.036318 |
| Unmodified pNNP5DT | 4 | 3.63 | 0.9075 | 0.002069 |
| pNNP5DT-YIGSR$_{27}$ | 4 | 4.7369 | 1.184225 | 0.028745 |
| pNNP5DT-RGDS$_{33}$ | 4 | 3.246 | 0.8115 | 0.004433 |
| pNNP5DT-RGDS$_{48}$ | 4 | 3.1898 | 0.79745 | 0.026485 |

ANOVA

| *Source of Variation* | *SS* | *df* | *MS* | *F* | *P-value* | *F crit* |
|---|---|---|---|---|---|---|
| Between Groups | 4.254771 | 5 | 0.850954 | 35.98225 | 9.24E-09 | 2.772853 |
| Within Groups | 0.425687 | 18 | 0.023649 | | | |
| Total | 4.680458 | 23 | | | | |

| | |
|---|---|
| $Q_{crit}$ | 4.494 |
| n | 4 |
| Pooled variance (MSw) | 0.023649 |
| sqrt(MSw/n) | 0.076892 |

| *Comparison* | *Absolute Difference Between Means* | *Q* | *Significant ($Q > Q_{crit}$)* |
|---|---|---|---|
| Negative Control - PBS | 0.134025 | 1.743038 | no |
| Negative Control - Unmodified | 0.798325 | 10.38247 | yes |
| Negative Control - pNNP5DT-YIGSR$_{27}$ | 0.5216 | 6.783575 | yes |
| Negative Control - pNNP5DT-RGDS$_{33}$ | 0.894325 | 11.63098 | yes |
| Negative Control - pNNP5DT-RGDS$_{48}$ | 0.908375 | 11.81371 | yes |
| PBS - Unmodified pNNP5DT | 0.93235 | 12.12551 | yes |
| PBS - pNNP5DT-YIGSR$_{27}$ | 0.655625 | 8.526613 | yes |
| PBS - pNNP5DT-RGDS$_{33}$ | 1.02835 | 13.37402 | yes |
| PBS - pNNP5DT-RGDS$_{48}$ | 1.0424 | 13.55675 | yes |
| Unmodified pNNP5DT - pNNP5DT-YIGSR$_{27}$ | 0.276725 | 3.598897 | no |
| Unmodified pNNP5DT - pNNP5DT-RGDS$_{33}$ | 0.096 | 1.248511 | no |
| Unmodified pNNP5DT - pNNP5DT-RGDS$_{48}$ | 0.11005 | 1.431235 | no |
| pNNP5DT-YIGSR$_{27}$ - pNNP5DT-RGDS$_{33}$ | 0.372725 | 4.847408 | yes |
| pNNP5DT-YIGSR$_{27}$ - pNNP5DT-RGDS$_{48}$ | 0.386775 | 5.030132 | yes |
| pNNP5DT-RGDS$_{33}$ - pNNP5DT-RGDS$_{48}$ | 0.01405 | 0.182725 | no |

***48h pNNP5DT MTT Assay ANOVA and Tukey's post-hoc***

SUMMARY

| *Groups* | *Count* | *Sum* | *Average* | *Variance* |
|---|---|---|---|---|
| Negative Control | 4 | 6.6337 | 1.658425 | 0.032602 |
| PBS | 4 | 7.2144 | 1.8036 | 0.009907 |
| Unmodified pNNP5DT | 4 | 3.8405 | 0.960125 | 0.005063 |
| pNNP5DT-YIGSR$_{27}$ | 4 | 4.7271 | 1.181775 | 0.001352 |
| pNNP5DT-RGDS$_{33}$ | 4 | 2.9914 | 0.74785 | 0.010518 |
| pNNP5DT-RGDS$_{48}$ | 4 | 2.7185 | 0.679625 | 0.016743 |

ANOVA

| *Source of Variation* | *SS* | *df* | *MS* | *F* | *P-value* | *F crit* |
|---|---|---|---|---|---|---|
| Between Groups | 4.411403 | 5 | 0.882281 | 69.48532 | 3.93407E-11 | 2.772853 |
| Within Groups | 0.228553 | 18 | 0.012697 | | | |
| Total | 4.639955 | 23 | | | | |

| | |
|---|---|
| $Q_{crit}$ | 4.494 |
| n | 4 |
| Pooled variance (MSw) | 0.012697 |
| sqrt(MSw/n) | 0.056341 |

| *Comparison* | *Absolute Difference Between Means* | *Q* | *Significant ($Q > Q_{crit}$)* |
|---|---|---|---|
| Negative Control - PBS | 0.145175 | 2.576708 | no |
| Negative Control - Unmodified | 0.6983 | 12.39411 | yes |
| Negative Control - pNNP5DT-YIGSR$_{27}$ | 0.47665 | 8.460046 | yes |
| Negative Control - pNNP5DT-RGDS$_{33}$ | 0.910575 | 16.16177 | yes |
| Negative Control - pNNP5DT-RGDS$_{48}$ | 0.9788 | 17.37269 | yes |
| PBS - Unmodified pNNP5DT | 0.843475 | 14.97081 | yes |
| PBS - pNNP5DT-YIGSR$_{27}$ | 0.621825 | 11.03675 | yes |
| PBS - pNNP5DT-RGDS$_{33}$ | 1.05575 | 18.73848 | yes |
| PBS - pNNP5DT-RGDS$_{48}$ | 1.123975 | 19.9494 | yes |
| Unmodified pNNP5DT - pNNP5DT-YIGSR$_{27}$ | 0.22165 | 3.934059 | no |
| Unmodified pNNP5DT - pNNP5DT-RGDS$_{33}$ | 0.212275 | 3.767663 | no |
| Unmodified pNNP5DT - pNNP5DT-RGDS$_{48}$ | 0.2805 | 4.978586 | yes |
| pNNP5DT-YIGSR$_{27}$ - pNNP5DT-RGDS$_{33}$ | 0.433925 | 7.701722 | yes |
| pNNP5DT-YIGSR$_{27}$ - pNNP5DT-RGDS$_{48}$ | 0.50215 | 8.912646 | yes |
| pNNP5DT-RGDS$_{33}$ - pNNP5DT-RGDS$_{48}$ | 0.068225 | 1.210924 | no |

## A13. Statistical Analysis LIVE/DEAD Assay

### A13.1. Levene's Test pNNPD ImageJ Dead Cell Count

***48h pNNPD ImageJ Dead Cell Count Levene's Test***

SUMMARY

| *Groups* | *Count* | *Sum* | *Average* | *Variance* |
|---|---|---|---|---|
| Negative Control | 3 | 87.33333 | 29.11111 | 369.1481 |
| PBS | 3 | 47.33333 | 15.77778 | 178.9259 |
| Unmodified pNNPD | 3 | 102.6667 | 34.22222 | 268.5926 |
| pNNPD-RGDS$_{31}$ | 3 | 90 | 30 | 175 |
| pNNPD-RGDS$_{37}$ | 3 | 14.66667 | 4.888889 | 5.481481 |
| pNNPD-RGDS$_{117}$ | 3 | 26 | 8.666667 | 56.33333 |
| pNNPD-RGDS$_{28}$/YIGSR$_{18}$ | 3 | 34 | 11.33333 | 26.33333 |

ANOVA

| *Source of Variation* | *SS* | *df* | *MS* | *F* | *P-value* | *F crit* |
|---|---|---|---|---|---|---|
| Between Groups | 2489.608 | 6 | 414.9347 | 2.689853 | 0.059624 | 2.847726 |
| Within Groups | 2159.63 | 14 | 154.2593 | | | |
| Total | 4649.238 | 20 | | | | |

## A13.2. Single-Factor ANOVA pNNPD ImageJ Dead Cell Count

***48h pNNPD ImageJ Dead Cell Count ANOVA***

SUMMARY

| *Groups* | *Count* | *Sum* | *Average* | *Variance* |
|---|---|---|---|---|
| Negative Control | 3 | 163 | 54.33333 | 1640.333 |
| PBS | 3 | 181 | 60.33333 | 552.3333 |
| Unmodified pNNPD | 3 | 233 | 77.66667 | 2025.333 |
| pNNPD-$RGDS_{31}$ | 3 | 114 | 38 | 1525 |
| pNNPD-$RGDS_{37}$ | 3 | 76 | 25.33333 | 41.33333 |
| pNNPD-$RGDS_{117}$ | 3 | 63 | 21 | 169 |
| pNNPD-$RGDS_{28}$/$YIGSR_{18}$ | 3 | 78 | 26 | 219 |

ANOVA

| *Source of Variation* | *SS* | *df* | *MS* | *F* | *P-value* | *F crit* |
|---|---|---|---|---|---|---|
| Between Groups | 8221.143 | 6 | 1370.19 | 1.553923 | 0.232261 | 2.847726 |
| Within Groups | 12344.67 | 14 | 881.7619 | | | |
| Total | 20565.81 | 20 | | | | |

## A14. pNNPD MTT Assay in DMEM/F12 Supplemented with 10% FBS

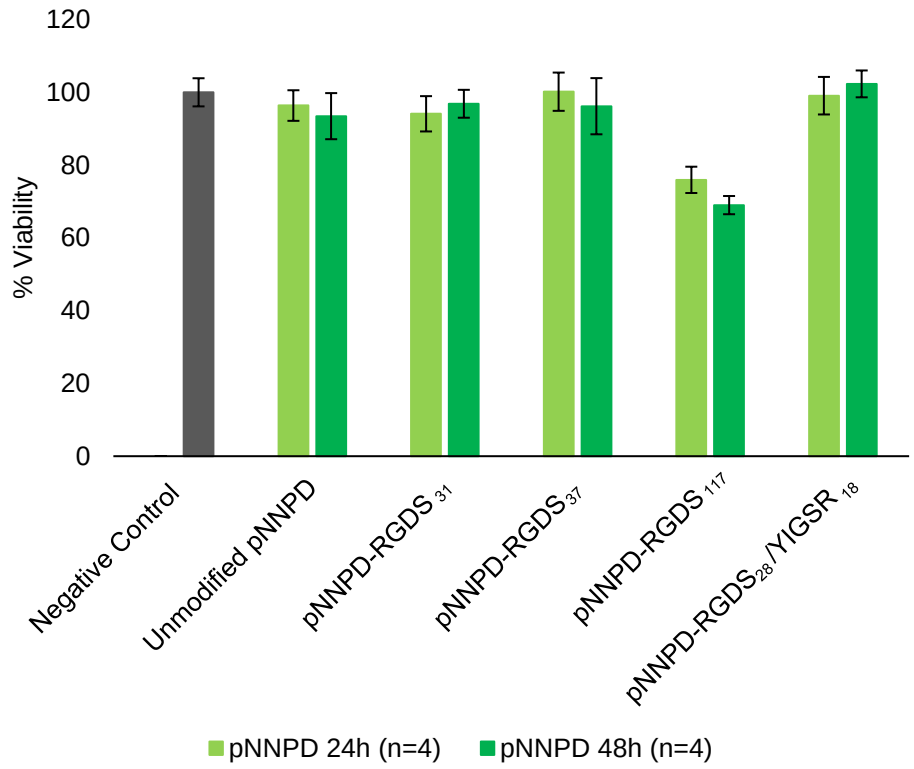


**Figure A12.** Cell viability of ARPE-19 (passage 7) cells after treatment with 10 µL of 20 w/v% pNNPD for 24 and 48 h of culture (37°C, 5% CO2; seeding density of 50 000 cells per well; absorbance measured at 570 nm using Thermo Scientific Multiskan GO and Thermo Scientific SkanIt software with blank subtraction) show high metabolic activity (> 90%) across materials at both 24 and 48 h, with the exception of pNNPD-RGDS$_{117}$ which displayed 76 ± 3.6% and 69 ± 2.5% viability at 24 and 48 h respectively. Single factor ANOVA ($\alpha = 0.05$) displayed a significant difference among groups ($p_{24h}$ = 1.64E-3, $p_{48h}$ = 3.91E-4) leading to Tukey's post-hoc analysis (**Appendices A14.1 and A14.2**). There was no significant difference between groups with the exception of pNNPD-RGDS$_{117}$ which was found to have a significant decrease in viability as compared to all materials and the negative control. $\sigma_{\bar{x}}$ is reflective of an n of 4.

## A14.1. Levene's Test pNNPD MTT Assay in Complete Media

***24h pNNPD MTT Assay Levene's Test (Complete Media)***

SUMMARY

| *Groups* | *Count* | *Sum* | *Average* | *Variance* |
|---|---|---|---|---|
| Negative Control | 4 | 0.4071 | 0.101775 | 0.002903 |
| Unmodified pNNPD | 4 | 0.45385 | 0.113463 | 0.006845 |
| pNNPD-$RGDS_{31}$ | 4 | 0.6099 | 0.152475 | 0.006843 |
| pNNPD-$RGDS_{37}$ | 4 | 0.61105 | 0.152763 | 0.013978 |
| pNNPD-$RGDS_{117}$ | 4 | 0.3857 | 0.096425 | 0.007196 |
| pNNPD-$RGDS_{28}$/$YIGSR_{18}$ | 4 | 0.62115 | 0.155288 | 0.011004 |

ANOVA

| *Source of Variation* | *SS* | *df* | *MS* | *F* | *P-value* | *F crit* |
|---|---|---|---|---|---|---|
| Between Groups | 0.0154 | 5 | 0.00308 | 0.378924 | 0.856597 | 2.772853 |
| Within Groups | 0.146307 | 18 | 0.008128 | | | |
| Total | 0.161707 | 23 | | | | |

***48h pNNPD MTT Assay Levene's Test (Complete Media)***

SUMMARY

| *Groups* | *Count* | *Sum* | *Average* | *Variance* |
|---|---|---|---|---|
| Negative Control | 4 | 0.4071 | 0.101775 | 0.002903 |
| Unmodified pNNPD | 4 | 0.7875 | 0.196875 | 0.023515 |
| pNNPD-$RGDS_{31}$ | 4 | 0.3629 | 0.090725 | 0.006197 |
| pNNPD-$RGDS_{37}$ | 4 | 0.9607 | 0.240175 | 0.040983 |
| pNNPD-$RGDS_{117}$ | 4 | 0.2058 | 0.05145 | 0.002498 |
| pNNPD-$RGDS_{28}$/$YIGSR_{18}$ | 4 | 0.3916 | 0.0979 | 0.000206 |

ANOVA

| *Source of Variation* | *SS* | *df* | *MS* | *F* | *P-value* | *F crit* |
|---|---|---|---|---|---|---|
| Between Groups | 0.104601 | 5 | 0.02092 | 1.645047 | 0.198977 | 2.772853 |
| Within Groups | 0.228908 | 18 | 0.012717 | | | |
| Total | 0.333509 | 23 | | | | |

## A14.2. Single-Factor ANOVA and Tukey's post-hoc Analysis pNNPD MTT Assay in DMEM/F12 Supplemented with 10% FBS

***24h pNNPD MTT Assay ANOVA and Tukey's post-hoc (Complete Media)***

SUMMARY

| *Groups* | *Count* | *Sum* | *Average* | *Variance* |
|---|---|---|---|---|
| Negative Control | 4 | 9.4606 | 2.36515 | 0.016714 |
| Unmodified pNNPD | 4 | 9.1168 | 2.2792 | 0.02401 |
| pNNPD-$RGDS_{31}$ | 4 | 8.9018 | 2.22545 | 0.037841 |
| pNNPD-$RGDS_{37}$ | 4 | 9.476 | 2.369 | 0.045093 |
| pNNPD-$RGDS_{117}$ | 4 | 7.1847 | 1.796175 | 0.019593 |
| pNNPD-$RGDS_{28}$/$YIGSR_{18}$ | 4 | 9.3728 | 2.3432 | 0.043157 |

ANOVA

| *Source of Variation* | *SS* | *df* | *MS* | *F* | *P-value* | *F crit* |
|---|---|---|---|---|---|---|
| Between Groups | 0.964183 | 5 | 0.192837 | 6.20693 | 0.001638 | 2.772853 |
| Within Groups | 0.559223 | 18 | 0.031068 | | | |
| Total | 1.523406 | 23 | | | | |

| | |
|---|---|
| $Q_{crit}$ | 4.494 |
| n | 4 |
| Pooled variance (MSw) | 0.031068 |
| sqrt(MSw/n) | 0.088131 |

| *Comparison* | *Absolute Difference Between Means* | *Q* | *Significant ($Q > Q_{crit}$)* |
|---|---|---|---|
| Negative Control - Unmodified pNNPD | 0.08595 | 0.975258 | no |
| Negative Control - pNNPD-RGDS$_{31}$ | 0.1397 | 1.585149 | no |
| Negative Control - pNNPD-RGDS$_{37}$ | 0.00385 | 0.043685 | no |
| Negative Control - pNNP5DT-RGDS$_{117}$ | 0.568975 | 6.456051 | yes |
| Negative Control - pNNPD-RGDS$_{28}$/YIGSR$_{18}$ | 0.02195 | 0.249062 | no |
| Unmodified pNNPD - pNNPD-RGDS$_{31}$ | 0.05375 | 0.609891 | no |
| Unmodified pNNPD - pNNPD-RGDS$_{37}$ | 0.0898 | 1.018943 | no |
| Unmodified pNNPD - pNNP5DT-RGDS$_{117}$ | 0.483025 | 5.480792 | yes |
| Unmodified pNNPD - pNNPD-RGDS$_{28}$/YIGSR$_{18}$ | 0.064 | 0.726196 | no |
| pNNPD-RGDS$_{31}$ - pNNPD-RGDS$_{37}$ | 0.14355 | 1.628834 | no |
| pNNPD-RGDS$_{31}$ - pNNP5DT-RGDS$_{117}$ | 0.429275 | 4.870901 | yes |
| pNNPD-RGDS$_{31}$ - pNNPD-RGDS$_{28}$/YIGSR$_{18}$ | 0.11775 | 1.336087 | no |
| pNNPD-RGDS$_{37}$ - pNNP5DT-RGDS$_{117}$ | 0.572825 | 6.499736 | yes |
| pNNPD-RGDS$_{37}$ - pNNPD-RGDS$_{28}$/YIGSR$_{18}$ | 0.0258 | 0.292748 | no |
| pNNPD-RGDS$_{117}$ - pNNPD-RGDS$_{28}$/YIGSR$_{18}$ | 0.547025 | 6.206988 | yes |

***48h pNNPD MTT Assay ANOVA and Tukey's post-hoc (Complete Media)***

SUMMARY

| *Groups* | *Count* | *Sum* | *Average* | *Variance* |
|---|---|---|---|---|
| Negative Control | 4 | 9.4606 | 2.36515 | 0.016714 |
| Unmodified pNNPD | 4 | 8.8407 | 2.210175 | 0.075195 |
| pNNPD-RGDS$_{31}$ | 4 | 9.1627 | 2.290675 | 0.017172 |
| pNNPD-RGDS$_{37}$ | 4 | 9.0995 | 2.274875 | 0.117895 |
| pNNPD-RGDS$_{117}$ | 4 | 6.5277 | 1.631925 | 0.006028 |
| pNNPD-RGDS$_{28}$/YIGSR$_{18}$ | 4 | 9.6793 | 2.419825 | 0.012986 |

ANOVA

| *Source of Variation* | *SS* | *df* | *MS* | *F* | *P-value* | *F crit* |
|---|---|---|---|---|---|---|
| Between Groups | 1.648918 | 5 | 0.329784 | 8.043875 | 0.000391 | 2.772853 |
| Within Groups | 0.737966 | 18 | 0.040998 | | | |
| | | | | | | |
| Total | 2.386884 | 23 | | | | |

| | |
|---|---|
| $Q_{crit}$ | 4.494 |
| n | 4 |
| Pooled variance (MSw) | 0.040998 |
| sqrt(MSw/n) | 0.10124 |

| *Comparison* | *Absolute Difference Between Means* | *Q* | *Significant ($Q > Q_{crit}$)* |
|---|---|---|---|
| Neg - Unmodified | 0.154975 | 1.530769 | no |
| Neg - pNNPD-RGDS$_{31}$ | 0.074475 | 0.735629 | no |
| Neg - pNNPD-RGDS$_{37}$ | 0.090275 | 0.891694 | no |
| Neg - pNNP5DT-RGDS$_{117}$ | 0.733225 | 7.242448 | yes |
| Neg - pNNPD-RGDS$_{28}$/YIGSR$_{18}$ | 0.054675 | 0.540054 | no |
| Unmodified - pNNPD-RGDS$_{31}$ | 0.0805 | 0.795141 | no |
| Unmodified - pNNPD-RGDS$_{37}$ | 0.0647 | 0.639076 | no |
| Unmodified - pNNP5DT-RGDS$_{117}$ | 0.57825 | 5.711679 | yes |
| Unmodified - pNNPD-RGDS$_{28}$/YIGSR$_{18}$ | 0.20965 | 2.070823 | no |
| pNNPD-RGDS$_{31}$ - pNNPD-RGDS$_{37}$ | 0.0158 | 0.156065 | no |
| pNNPD-RGDS$_{31}$ - pNNP5DT-RGDS$_{117}$ | 0.65875 | 6.50682 | yes |
| pNNPD-RGDS$_{31}$ - pNNPD-RGDS$_{28}$/YIGSR$_{18}$ | 0.12915 | 1.275682 | no |
| pNNPD-RGDS$_{37}$ - pNNP5DT-RGDS$_{117}$ | 0.64295 | 6.350755 | yes |
| pNNPD-RGDS$_{37}$ - pNNPD-RGDS$_{28}$/YIGSR$_{18}$ | 0.14495 | 1.431747 | no |
| pNNPD-RGDS$_{117}$ - pNNPD-RGDS$_{28}$/YIGSR$_{18}$ | 0.7879 | 7.782502 | yes |

## A15. pNNP5DT LIVE/DEAD IMAGES OF INDEPENDENT REPLICATE TRIALS

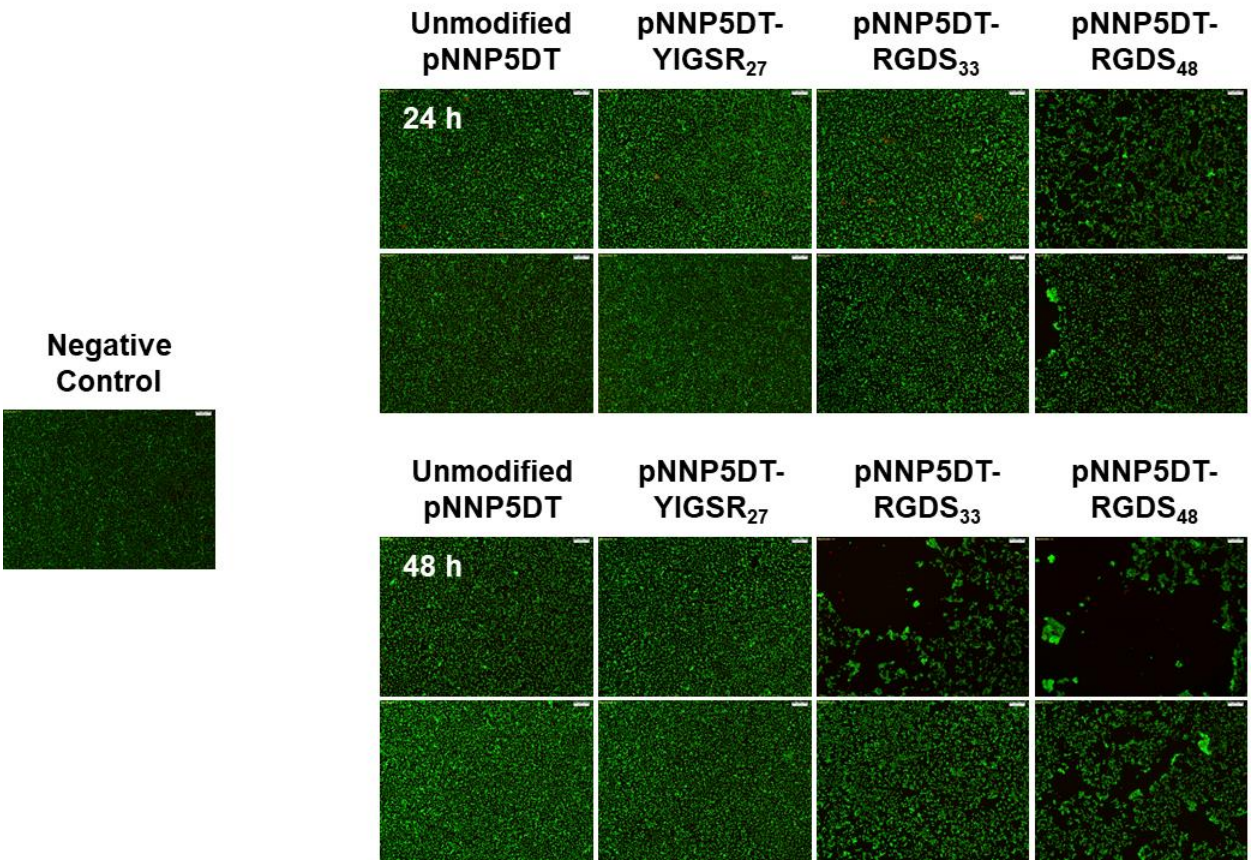


**Figure A13.** Representative merged fluorescent images of two independent studies whereby ARPE-19 cells (passage 9) were stained with calcein (live cells - green) and ethidium homodimer (dead cells – red) following treatment with 10 µL of 20 w/v% pNNP5DT in sterile 1X PBS for 24 and 48 h. Images were taken from an n of 4 within each experiment (4X magnification) and reflect cytotoxicity trials independent from those featured in Chapter 2. Characteristic patchiness believed to be associated with cell lifting in pNNP5DT-RGDS$_{33}$ and pNNP5DT-RGDS$_{48}$ are observed repeatably.

## A16. Preliminary pNNPD Migration Study

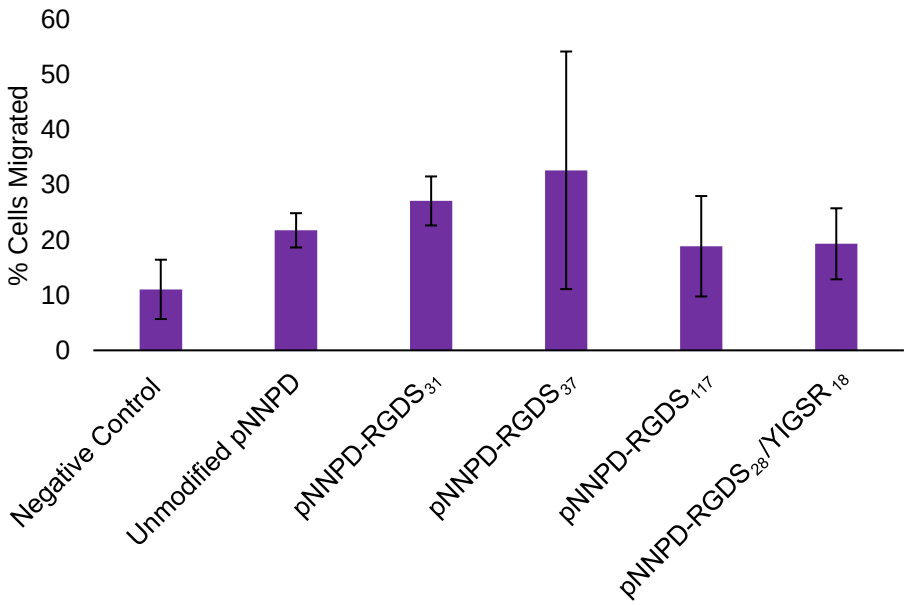


**Figure A14.** Preliminary pNNPD migration study was designed whereby 150 µL of Corning® Matrigel® Matrix (VWR) was mixed in equal parts with DMEM/F12 lacking FBS supplementation (incomplete media) and seeded into transwell inserts (0.4 µm) fitted for a Falcon® 24-well Clear Flat Bottom Polystyrene TC-treated plate. Matrigel filled inserts were allowed to gel overnight at 4°C. Following this period, 400 µL of DMEM/F12 supplemented with 10% FBS (complete media) was added to each well and cell inserts were placed into wells containing complete media. pNNPD materials dissolved at 20 w/v% in sterile 1X PBS were pipette into 0.5 mL sterile microcentrifuge tubes to which ARPE-19 (passage 9) resuspended in incomplete media was added in equal volumes (bringing pNNPD concentration to 10 w/v%). Cells were pre-counted using a hemocytometer. Microcentrifuge tubes containing both polymer and cells were gently vortexed to suspend cells throughout solution. 10 µL of each pNNPD material doped with cells was then seeded onto the Matrigel filled transwell inserts (for a total of 25 000 cells per well) and was incubated at 37°C (5% $CO_2$) for approximately 22 h before 200 µL of incomplete media was added above gels. 24 h following initial pNNPD cell seeding, incomplete media was carefully removed from transwell inserts as not to disrupt underlying Matrigel matrices and to ensure removal of excess pNNPD. ARPE-19s which had penetrated Matrigel matrices were recovered through addition of 300 µL Corning® Cell Recovery Solution (VWR), aspirating thrice, and transferring to sterile 1.5 mL microcentrifuge tubes to incubate for 20 minutes at 4°C. Vials were then centrifuged at 5000 rpm for 3 minutes and supernatant containing cell recovery solution and dissolved Matrigel were decanted. Pellets were resuspended in 50 µL sterile 1X PBS and 50 µL 0.4% Trypan Blue (Gibco™) to allow for Trypan Blue exclusion cell counts of total cells migrated per well. Counts were plotted as percent of total cells migrated from original seeding density. Single factor ANOVA ($\alpha = 0.05$) displayed no significant difference in migration across groups ($p = 0.76$; **Appendix A16.1**). This study served as a rough preliminary trial to explore methods of evaluating *in vitro* migration from polymers into materials resembling native ECM, as such this protocol requires significant optimization and larger sample size. $\sigma_{\bar{x}}$ is reflective of an n of 2, an assumption of equal variances is taken.

## A16.1. Single-Factor ANOVA pNNPD Preliminary Migration Assay

***24h pNNPD Preliminary Migration Assay ANOVA***

SUMMARY

| *Groups* | *Count* | *Sum* | *Average* | *Variance* |
|---|---|---|---|---|
| Negative Control | 2 | 9960 | 4980 | 11712800 |
| PBS | 2 | 19600 | 9800 | 3920000 |
| Unmodified pNNPD | 2 | 24400 | 12200 | 8000000 |
| pNNPD-$RGDS_{31}$ | 2 | 29400 | 14700 | 1.88E+08 |
| pNNPD-$RGDS_{37}$ | 2 | 17000 | 8500 | 33620000 |
| pNNPD-$RGDS_{117}$ | 2 | 17400 | 8700 | 16820000 |
| pNNPD-$RGDS_{28}$/$YIGSR_{18}$ | 2 | 9960 | 4980 | 11712800 |

ANOVA

| *Source of Variation* | *SS* | *df* | *MS* | *F* | *P-value* | *F crit* |
|---|---|---|---|---|---|---|
| Between Groups | 1.12E+08 | 5 | 22360533 | 0.51158 | 0.760515 | 4.387374 |
| Within Groups | 2.62E+08 | 6 | 43708800 | | | |
| Total | 3.74E+08 | 11 | | | | |

# REFERENCES

[1] C.L. VanPutte, J.L. Regan, A.F. Russo, Seeley's anatomy & physiology, 10th ed., McGraw-Hill2014.
[2] M.F. Land, R.D. Fernald, The evolution of eyes, Annual review of neuroscience 15(1) (1992) 1-29.
[3] W.L. Wong, X. Su, X. Li, C.M.G. Cheung, R. Klein, C.-Y. Cheng, T.Y. Wong, Global prevalence of age-related macular degeneration and disease burden projection for 2020 and 2040: a systematic review and meta-analysis, The Lancet Global Health 2(2) (2014) e106-e116.
[4] E.K. de Jong, M.J. Geerlings, A.I. den Hollander, Age-related macular degeneration, The New England Journal of Medicine (2006) 1474-1485.
[5] M. Goldstein, A. Loewenstein, A. Barak, A. Pollack, A. Bukelman, H. Katz, A. Springer, A.P. Schachat, N.M. Bressler, S.B. Bressler, Results of a multicenter clinical trial to evaluate the preferential hyperacuity perimeter for detection of age-related macular degeneration, Retina (Philadelphia, Pa.) 25(3) (2005) 296-303.
[6] M. Amsler, L'examen qualitatif de la fonction maculaire, Ophthalmologica 114(4-5) (1947) 248-261.
[7] L. Fäs, N. Bodmer, L. Bachmann, M. Thiel, M. Schmid, Diagnostic accuracy of the Amsler grid and the preferential hyperacuity perimetry in the screening of patients with age-related macular degeneration: systematic review and meta-analysis, Eye 28(7) (2014) 788-796.
[8] F.L. Ferris, M.D. Davis, T.E. Clemons, L.Y. Lee, E.Y. Chew, A.S. Lindblad, R.C. Milton, S.B. Bressler, R. Klein, A simplified severity scale for age-related macular degeneration: AREDS Report No. 18, Archives of ophthalmology (Chicago, Ill.: 1960) 123(11) (2005) 1570-1574.
[9] L.S. Lim, P. Mitchell, J.M. Seddon, F.G. Holz, T.Y. Wong, Age-related macular degeneration, The Lancet 379(9827) (2012) 1728-1738.
[10] T.J. Heesterbeek, L. Lorés-Motta, C.B. Hoyng, Y.T. Lechanteur, A.I. den Hollander, Risk factors for progression of age-related macular degeneration, Ophthalmic and Physiological Optics 40(2) (2020) 140-170.
[11] X. Han, P. Gharahkhani, P. Mitchell, G. Liew, A.W. Hewitt, S. MacGregor, Genome-wide meta-analysis identifies novel loci associated with age-related macular degeneration, Journal of human genetics 65(8) (2020) 657-665.
[12] R. Ratnapriya, E.Y. Chew, Age-related macular degeneration—clinical review and genetics update, Clinical genetics 84(2) (2013) 160-166.
[13] J.B. MH, M. Yaseri, M. Soheilian, Association of combined complement factor H Y402H and ARMS2/LOC387715 A69S polymorphisms with age-related macular degeneration: an updated meta-analysis, Ophthalmic Genetics (2020) 1-7.
[14] S.G. Schwartz, B.M. Hampton, J.L. Kovach, M.A. Brantley Jr, Genetics and age-related macular degeneration: a practical review for the clinician, Clinical Ophthalmology (Auckland, NZ) 10 (2016) 1229.
[15] D.A. Schaumberg, S.E. Hankinson, Q. Guo, E. Rimm, D.J. Hunter, A prospective study of 2 major age-related macular degeneration susceptibility alleles and interactions with modifiable risk factors, Archives of Ophthalmology 125(1) (2007) 55-62.
[16] L.G. Fritsche, R.N. Fariss, D. Stambolian, G.R. Abecasis, C.A. Curcio, A. Swaroop, Age-related macular degeneration: genetics and biology coming together, Annual review of genomics and human genetics 15 (2014) 151-171.
[17] R. Klein, K.J. Cruickshanks, S.D. Nash, E.M. Krantz, F.J. Nieto, G.H. Huang, J.S. Pankow, B.E. Klein, The prevalence of age-related macular degeneration and associated risk factors, Archives of ophthalmology 128(6) (2010) 750-758.
[18] U. Chakravarthy, T.Y. Wong, A. Fletcher, E. Piault, C. Evans, G. Zlateva, R. Buggage, A. Pleil, P. Mitchell, Clinical risk factors for age-related macular degeneration: a systematic review and meta-analysis, BMC ophthalmology 10(1) (2010) 31.

[19] G.P. Zlateva, J.C. Javitt, S.N. Shah, Z. Zhou, J.G. Murphy, Comparison of comorbid conditions between neovascular AGE–RELATED macular degeneration patients and a control cohort in the Medicare population, Retina 27(9) (2007) 1292-1299.
[20] D. Olson, X. Zhang, M.F. Ward, P. Le, O.M. Ismail, Z.B. Poole, J.C. Donaldson, E. Van Buren, F.-C. Lin, J.N. Ulrich, Rates of comorbid anxiety and depression in patients with age-related macular degeneration, Journal of VitreoRetinal Diseases 3(4) (2019) 211-214.
[21] R. Eramudugolla, J. Wood, K.J. Anstey, Co-morbidity of depression and anxiety in common age-related eye diseases: a population-based study of 662 adults, Frontiers in aging neuroscience 5 (2013) 56.
[22] C.A. McCarty, B.N. Mukesh, C.L. Fu, P. Mitchell, J.J. Wang, H.R. Taylor, Risk factors for age-related maculopathy: the Visual Impairment Project, Archives of ophthalmology 119(10) (2001) 1455-1462.
[23] F.L. Ferris III, C. Wilkinson, A. Bird, U. Chakravarthy, E. Chew, K. Csaky, S.R. Sadda, B.I.f.M.R.C. Committee, Clinical classification of age-related macular degeneration, Ophthalmology 120(4) (2013) 844-851.
[24] S.R. Sadda, U. Chakravarthy, D.G. Birch, G. Staurenghi, E.C. Henry, C. Brittain, Clinical endpoints for the study of geographic atrophy secondary to age-related macular degeneration, Retina (Philadelphia, Pa.) 36(10) (2016) 1806.
[25] K.L. Pennington, M.M. DeAngelis, Epidemiology of age-related macular degeneration (AMD): associations with cardiovascular disease phenotypes and lipid factors, Eye and vision 3(1) (2016) 34.
[26] K. Kaarniranta, H. Uusitalo, J. Blasiak, S. Felszeghy, R. Kannan, A. Kauppinen, A. Salminen, D. Sinha, D. Ferrington, Mechanisms of mitochondrial dysfunction and their impact on age-related macular degeneration, Progress in retinal and eye research 79 (2020) 100858.
[27] M. Zhang, N. Jiang, Y. Chu, O. Postnikova, R. Varghese, A. Horvath, A.K. Cheema, N. Golestaneh, Dysregulated metabolic pathways in age-related macular degeneration, Scientific reports 10(1) (2020) 1-14.
[28] I. Bhutto, G. Lutty, Understanding age-related macular degeneration (AMD): relationships between the photoreceptor/retinal pigment epithelium/Bruch's membrane/choriocapillaris complex, Molecular aspects of medicine 33(4) (2012) 295-317.
[29] M.J. Barron, M.A. Johnson, R.M. Andrews, M.P. Clarke, P.G. Griffiths, E. Bristow, L.-P. He, S. Durham, D.M. Turnbull, Mitochondrial abnormalities in ageing macular photoreceptors, Investigative ophthalmology & visual science 42(12) (2001) 3016-3022.
[30] N.D. Wangsa-Wirawan, R.A. Linsenmeier, Retinal oxygen: fundamental and clinical aspects, Archives of ophthalmology 121(4) (2003) 547-557.
[31] B.S. Winkler, M.E. Boulton, J.D. Gottsch, P. Sternberg, Oxidative damage and age-related macular degeneration, Molecular vision 5 (1999) 32.
[32] J. Blasiak, Senescence in the pathogenesis of age-related macular degeneration, Cellular and Molecular Life Sciences 77(5) (2020) 789-805.
[33] K. Petrukhin, Pharmacological inhibition of lipofuscin accumulation in the retina as a therapeutic strategy for dry AMD treatment, Drug Discovery Today: Therapeutic Strategies 10(1) (2013) e11-e20.
[34] S.C. Finnemann, L.W. Leung, E. Rodriguez-Boulan, The lipofuscin component A2E selectively inhibits phagolysosomal degradation of photoreceptor phospholipid by the retinal pigment epithelium, Proceedings of the National Academy of Sciences 99(6) (2002) 3842-3847.
[35] J.C. Booij, B. Jacoline, S.M. Swagemakers, A.J. Verkerk, A.H. Essing, P.J. Van Der Spek, A.A. Bergen, A new strategy to identify and annotate human RPE-specific gene expression, PloS one 5(5) (2010) e9341.
[36] A.C. Bird, N.M. Bressler, S.B. Bressler, I.H. Chisholm, G. Coscas, M.D. Davis, P.T. de Jong, C. Klaver, B. Klein, R. Klein, An international classification and grading system for age-related maculopathy and age-related macular degeneration, Survey of ophthalmology 39(5) (1995) 367-374.

[37] L.V. Johnson, W.P. Leitner, M.K. Staples, D.H. Anderson, Complement activation and inflammatory processes in Drusen formation and age related macular degeneration, Experimental eye research 73(6) (2001) 887-896.
[38] M. Nozaki, B.J. Raisler, E. Sakurai, J.V. Sarma, S.R. Barnum, J.D. Lambris, Y. Chen, K. Zhang, B.K. Ambati, J.Z. Baffi, Drusen complement components C3a and C5a promote choroidal neovascularization, Proceedings of the National Academy of Sciences 103(7) (2006) 2328-2333.
[39] R.F. Mullins, S.R. Russell, D.H. Anderson, G.S. Hageman, Drusen associated with aging and age-related macular degeneration contain proteins common to extracellular deposits associated with atherosclerosis, elastosis, amyloidosis, and dense deposit disease, The FASEB Journal 14(7) (2000) 835-846.
[40] D.H. Anderson, R.F. Mullins, G.S. Hageman, L.V. Johnson, A role for local inflammation in the formation of drusen in the aging eye, American journal of ophthalmology 134(3) (2002) 411-431.
[41] J.M. Isas, V. Luibl, L.V. Johnson, R. Kayed, R. Wetzel, C.G. Glabe, R. Langen, J. Chen, Soluble and mature amyloid fibrils in drusen deposits, Investigative ophthalmology & visual science 51(3) (2010) 1304-1310.
[42] T. Dentchev, A.H. Milam, V.M.-Y. Lee, J.Q. Trojanowski, J.L. Dunaief, Amyloid-β is found in drusen from some age-related macular degeneration retinas, but not in drusen from normal retinas, American journal of ophthalmology 136(4) (2003) 787-787.
[43] N.S. Bora, B. Matta, V.V. Lyzogubov, P.S. Bora, Relationship between the complement system, risk factors and prediction models in age-related macular degeneration, Molecular immunology 63(2) (2015) 176-183.
[44] F.G. Holz, S. Schmitz-Valckenberg, M. Fleckenstein, Recent developments in the treatment of age-related macular degeneration, The Journal of clinical investigation 124(4) (2014) 1430-1438.
[45] M. Shibuya, Vascular endothelial growth factor and its receptor system: physiological functions in angiogenesis and pathological roles in various diseases, The Journal of Biochemistry 153(1) (2013) 13-19.
[46] P. Carmeliet, V. Ferreira, G. Breier, S. Pollefeyt, L. Kieckens, M. Gertsenstein, M. Fahrig, A. Vandenhoeck, K. Harpal, C. Eberhardt, Abnormal blood vessel development and lethality in embryos lacking a single VEGF allele, Nature 380(6573) (1996) 435-439.
[47] N. Ferrara, K. Carver-Moore, H. Chen, M. Dowd, L. Lu, K.S. O'Shea, L. Powell-Braxton, K.J. Hillan, M.W. Moore, Heterozygous embryonic lethality induced by targeted inactivation of the VEGF gene, Nature 380(6573) (1996) 439-442.
[48] M. Shibuya, VEGF-VEGFR signals in health and disease, Biomolecules & therapeutics 22(1) (2014) 1.
[49] H.-P. Gerber, F. Condorelli, J. Park, N. Ferrara, Differential transcriptional regulation of the two vascular endothelial growth factor receptor genes Flt-1, but not Flk-1/KDR, is up-regulated by hypoxia, Journal of Biological Chemistry 272(38) (1997) 23659-23667.
[50] J.E. Park, H.H. Chen, J. Winer, K.A. Houck, N. Ferrara, Placenta growth factor. Potentiation of vascular endothelial growth factor bioactivity, in vitro and in vivo, and high affinity binding to Flt-1 but not to Flk-1/KDR, Journal of Biological Chemistry 269(41) (1994) 25646-25654.
[51] G.-H. Fong, J. Rossant, M. Gertsenstein, M.L. Breitman, Role of the Flt-1 receptor tyrosine kinase in regulating the assembly of vascular endothelium, Nature 376(6535) (1995) 66-70.
[52] R.L. Kendall, K.A. Thomas, Inhibition of vascular endothelial cell growth factor activity by an endogenously encoded soluble receptor, Proceedings of the National Academy of Sciences 90(22) (1993) 10705-10709.
[53] L. Luo, H. Uehara, X. Zhang, S.K. Das, T. Olsen, D. Holt, J.M. Simonis, K. Jackman, N. Singh, T.R. Miya, Photoreceptor avascular privilege is shielded by soluble VEGF receptor-1, Elife 2 (2013) e00324.
[54] N. Ferrara, Vascular Endothelial Growth Factor: Basic Science and Clinical Progress, Endocrine Reviews 25(4) (2004) 581-611.
[55] R. Kannan, N. Zhang, P.G. Sreekumar, C.K. Spee, A. Rodriguez, E. Barron, D.R. Hinton, Stimulation of apical and basolateral VEGF-A and VEGF-C secretion by oxidative stress in polarized retinal pigment epithelial cells, Molecular vision 12 (2006) 1649-1659.

[56] A.-R.E.D.S.R. Group, A randomized, placebo-controlled, clinical trial of high-dose supplementation with vitamins C and E, beta carotene, and zinc for age-related macular degeneration and vision loss: AREDS report no. 8, Archives of ophthalmology 119(10) (2001) 1417.
[57] GlobalData, Age-Related Macular Degeneration: Global Drug Forecast and Market Analysis to 2026, 2018, p. 319.
[58] A. Ide, Vascularization of the Brown-Pearce rabbit epithelioma transplant as seen in the transparent ear chamber, Am. J. Roentg. 42 (1939) 891.
[59] G.H. Algire, H.W. Chalkley, F.Y. Legallais, H.D. Park, Vasculae reactions of normal and malignant tissues in vivo. I. vascular reactions of mice to wounds and to normal and neoplastic transplants, JNCI: Journal of the National Cancer Institute 6(1) (1945) 73-85.
[60] H. Hurwitz, L. Fehrenbacher, W. Novotny, T. Cartwright, J. Hainsworth, W. Heim, J. Berlin, A. Baron, S. Griffing, E. Holmgren, Bevacizumab plus irinotecan, fluorouracil, and leucovorin for metastatic colorectal cancer, New England journal of medicine 350(23) (2004) 2335-2342.
[61] E.S. Gragoudas, A.P. Adamis, E.T. Cunningham Jr, M. Feinsod, D.R. Guyer, Pegaptanib for neovascular age-related macular degeneration, New england journal of medicine 351(27) (2004) 2805-2816.
[62] N. Ferrara, R.S. Kerbel, Angiogenesis as a therapeutic target, Nature 438(7070) (2005) 967-974.
[63] H. Xu, M. Chen, Targeting the complement system for the management of retinal inflammatory and degenerative diseases, European journal of pharmacology 787 (2016) 94-104.
[64] M.P. Kawa, A. Machalinska, D. Roginska, B. Machalinski, Complement system in pathogenesis of AMD: dual player in degeneration and protection of retinal tissue, Journal of immunology research 2014 (2014).
[65] M. Landowski, U. Kelly, M. Klingeborn, M. Groelle, J.-D. Ding, D. Grigsby, C.B. Rickman, Human complement factor H Y402H polymorphism causes an age-related macular degeneration phenotype and lipoprotein dysregulation in mice, Proceedings of the National Academy of Sciences 116(9) (2019) 3703-3711.
[66] K.B. Ebrahimi, N. Fijalkowski, M. Cano, J.T. Handa, Decreased membrane complement regulators in the retinal pigmented epithelium contributes to age-related macular degeneration, The Journal of pathology 229(5) (2013) 729-742.
[67] H.P. Scholl, P.C. Issa, M. Walier, S. Janzer, B. Pollok-Kopp, F. Börncke, L.G. Fritsche, N.V. Chong, R. Fimmers, T. Wienker, Systemic complement activation in age-related macular degeneration, PloS one 3(7) (2008) e2593.
[68] B.L. Yaspan, D.F. Williams, F.G. Holz, C.D. Regillo, Z. Li, A. Dressen, M. van Lookeren Campagne, K.N. Le, R.R. Graham, T. Beres, Targeting factor D of the alternative complement pathway reduces geographic atrophy progression secondary to age-related macular degeneration, Science translational medicine 9(395) (2017).
[69] M.J. Ammar, J. Hsu, A. Chiang, A.C. Ho, C.D. Regillo, Age-related macular degeneration therapy: a review, Current opinion in ophthalmology 31(3) (2020) 215-221.
[70] A.-R.E.D.S.R. Group, Lutein+ zeaxanthin and omega-3 fatty acids for age-related macular degeneration: the Age-Related Eye Disease Study 2 (AREDS2) randomized clinical trial, Jama 309(19) (2013) 2005-2015.
[71] N.A. Peppas, A.G. Mikos, Preparation methods and structure of hydrogels, Hydrogels in medicine and pharmacy 1 (1986) 1-27.
[72] A.S. Hoffman, Hydrogels for biomedical applications, Advanced drug delivery reviews 64 (2012) 18-23.
[73] M.W. Tibbitt, K.S. Anseth, Hydrogels as extracellular matrix mimics for 3D cell culture, Biotechnology and bioengineering 103(4) (2009) 655-663.
[74] L. Klouda, A.G. Mikos, Thermoresponsive hydrogels in biomedical applications, European journal of pharmaceutics and biopharmaceutics 68(1) (2008) 34-45.

[75] A. Gandhi, A. Paul, S.O. Sen, K.K. Sen, Studies on thermoresponsive polymers: Phase behaviour, drug delivery and biomedical applications, asian journal of pharmaceutical sciences 10(2) (2015) 99-107.
[76] E. Ruel-Gariepy, J.-C. Leroux, In situ-forming hydrogels—review of temperature-sensitive systems, European Journal of Pharmaceutics and Biopharmaceutics 58(2) (2004) 409-426.
[77] B. Jeong, S.W. Kim, Y.H. Bae, Thermosensitive sol–gel reversible hydrogels, Advanced drug delivery reviews 64 (2012) 154-162.
[78] L. Klouda, Thermoresponsive hydrogels in biomedical applications: A seven-year update, European Journal of Pharmaceutics and Biopharmaceutics 97 (2015) 338-349.
[79] E.H. Sprecht, A. Neuman, H.T. Neher, Preparation of Acrylamides, Rohm & Haas Company, United States, 1956.
[80] N.H.J. Shearer, H.W.J. Coover, Amide Rodent Repellent Comeposmons, Eastman Kodak Company, United States, 1957.
[81] M. Heskins, J.E. Guillet, Solution properties of poly (N-isopropylacrylamide), Journal of Macromolecular Science—Chemistry 2(8) (1968) 1441-1455.
[82] S. Fujishige, K. Kubota, I. Ando, Phase transition of aqueous solutions of poly (N-isopropylacrylamide) and poly (N-isopropylmethacrylamide), The Journal of Physical Chemistry 93(8) (1989) 3311-3313.
[83] K. Kubota, S. Fujishige, I. Ando, Solution properties of poly (N-isopropylacrylamide) in water, Polymer Journal 22(1) (1990) 15-20.
[84] F. Ilmain, T. Tanaka, E. Kokufuta, Volume transition in a gel driven by hydrogen bonding, Nature 349(6308) (1991) 400-401.
[85] H.G. Schild, Poly (N-isopropylacrylamide): experiment, theory and application, Progress in polymer science 17(2) (1992) 163-249.
[86] Z. Ahmed, E.A. Gooding, K.V. Pimenov, L. Wang, S.A. Asher, UV resonance Raman determination of molecular mechanism of poly (N-isopropylacrylamide) volume phase transition, The Journal of Physical Chemistry B 113(13) (2009) 4248-4256.
[87] I. Juurinen, S. Galambosi, A.G. Anghelescu-Hakala, J. Koskelo, V. Honkimaki, K. Hamalainen, S. Huotari, M. Hakala, Molecular-level changes of aqueous poly (N-isopropylacrylamide) in phase transition, The Journal of Physical Chemistry B 118(20) (2014) 5518-5523.
[88] S.A. Deshmukh, S.K. Sankaranarayanan, K. Suthar, D.C. Mancini, Role of solvation dynamics and local ordering of water in inducing conformational transitions in poly (N-isopropylacrylamide) oligomers through the LCST, The Journal of Physical Chemistry B 116(9) (2012) 2651-2663.
[89] S.A. Deshmukh, G. Kamath, K.J. Suthar, D.C. Mancini, S.K. Sankaranarayanan, Non-equilibrium effects evidenced by vibrational spectra during the coil-to-globule transition in poly (N-isopropylacrylamide) subjected to an ultrafast heating–cooling cycle, Soft matter 10(10) (2014) 1462-1480.
[90] L.J. Abbott, A.K. Tucker, M.J. Stevens, Single chain structure of a poly (N-isopropylacrylamide) surfactant in water, The Journal of Physical Chemistry B 119(9) (2015) 3837-3845.
[91] M. Podewitz, Y. Wang, P.K. Quoika, J.R. Loeffler, M. Schauperl, K.R. Liedl, Coil–Globule Transition Thermodynamics of Poly (N-isopropylacrylamide), The Journal of Physical Chemistry B 123(41) (2019) 8838-8847.
[92] Y. Pei, J. Chen, L. Yang, L. Shi, Q. Tao, B. Hui, J. Li, The effect of pH on the LCST of poly (N-isopropylacrylamide) and poly (N-isopropylacrylamide-co-acrylic acid), Journal of Biomaterials Science, Polymer Edition 15(5) (2004) 585-594.
[93] T. Okano, N. Yamada, H. Sakai, Y. Sakurai, A novel recovery system for cultured cells using plasma-treated polystyrene dishes grafted with poly (N-isopropylacrylamide), Journal of biomedical materials research 27(10) (1993) 1243-1251.
[94] N. Yamada, T. Okano, H. Sakai, F. Karikusa, Y. Sawasaki, Y. Sakurai, Thermo-responsive polymeric surfaces; control of attachment and detachment of cultured cells, Die Makromolekulare Chemie, Rapid Communications 11(11) (1990) 571-576.

[95] T. Umemoto, M. Yamato, K. Nishida, T. Okano, Regenerative medicine of cornea by cell sheet engineering using temperature-responsive culture surfaces, Chinese Science Bulletin 58(35) (2013) 4349-4356.
[96] K. Nishida, M. Yamato, Y. Hayashida, K. Watanabe, K. Yamamoto, E. Adachi, S. Nagai, A. Kikuchi, N. Maeda, H. Watanabe, Corneal reconstruction with tissue-engineered cell sheets composed of autologous oral mucosal epithelium, New England Journal of Medicine 351(12) (2004) 1187-1196.
[97] T. Götze, M. Valtink, M. Nitschke, S. Gramm, T. Hanke, K. Engelmann, C. Werner, Cultivation of an immortalized human corneal endothelial cell population and two distinct clonal subpopulations on thermo-responsive carriers, Graefe's Archive for Clinical and Experimental Ophthalmology 246(11) (2008) 1575-1583.
[98] K. Mokhtarinia, M.S. Nourbakhsh, E. Masaeli, M. Entezam, F. Karamali, M.H. Nasr-Esfahani, Switchable phase transition behavior of thermoresponsive substrates for cell sheet engineering, Journal of Polymer Science Part B: Polymer Physics 56(23) (2018) 1567-1576.
[99] N. Yaji, M. Yamato, J. Yang, T. Okano, S. Hori, Transplantation of tissue-engineered retinal pigment epithelial cell sheets in a rabbit model, Biomaterials 30(5) (2009) 797-803.
[100] R.A. Stile, W.R. Burghardt, K.E. Healy, Synthesis and characterization of injectable poly (N-isopropylacrylamide)-based hydrogels that support tissue formation in vitro, Macromolecules 32(22) (1999) 7370-7379.
[101] Z. Li, X. Guo, S. Matsushita, J. Guan, Differentiation of cardiosphere-derived cells into a mature cardiac lineage using biodegradable poly (N-isopropylacrylamide) hydrogels, Biomaterials 32(12) (2011) 3220-3232.
[102] D. Neradovic, W.L. Hinrichs, J.J. Kettenes-van den Bosch, W.E. Hennink, Poly (N-isopropylacrylamide) with hydrolyzable lactic acid ester side groups: a new type of thermosensitive polymer, Macromolecular Rapid Communications 20(11) (1999) 577-581.
[103] Z. Cui, B.H. Lee, C. Pauken, B.L. Vernon, Degradation, cytotoxicity, and biocompatibility of NIPAAm-based thermosensitive, injectable, and bioresorbable polymer hydrogels, Journal of Biomedical Materials Research Part A 98(2) (2011) 159-166.
[104] J. Guan, Y. Hong, Z. Ma, W.R. Wagner, Protein-reactive, thermoresponsive copolymers with high flexibility and biodegradability, Biomacromolecules 9(4) (2008) 1283-1292.
[105] D.J. Overstreet, H.D. Dhruv, B.L. Vernon, Bioresponsive copolymers of poly (N-isopropylacrylamide) with enzyme-dependent lower critical solution temperatures, Biomacromolecules 11(5) (2010) 1154-1159.
[106] Q.Q. Dou, S.S. Liow, E. Ye, R. Lakshminarayanan, X.J. Loh, Biodegradable thermogelling polymers: working towards clinical applications, Advanced healthcare materials 3(7) (2014) 977-988.
[107] N.C. Hunt, D. Hallam, V. Chichagova, D.H. Steel, M. Lako, The application of biomaterials to tissue engineering neural retina and retinal pigment epithelium, Advanced Healthcare Materials 7(23) (2018) 1800226.
[108] P. Royo, W. Quay, Retinal transplantation from fetal to maternal mammalian eye, Growth 23 (1959) 313.
[109] M. Del Cerro, H.H. Yeh, A. Marrero-Rodriguez, E. Lazar, C. del Cerro, Intraocular transplantation of cell layers derived from neonatal rat retina, Brain research 535(1) (1990) 25-32.
[110] M. del Cerro, J.R. Ison, G.P. Bowen, E. Lazar, C. del Cerro, Intraretinal grafting restores visual function in light-blinded rats, Neuroreport: An International Journal for the Rapid Communication of Research in Neuroscience (1991).
[111] P. Gouras, J. Du, M. Gelanze, R. Kwun, H. Kjeldbye, R. Lopez, Transplantation of photoreceptors labeled with tritiated thymidine into RCS rats, Investigative ophthalmology & visual science 32(5) (1991) 1704-1707.

[112] R. Aramant, M. Seiler, B. Ehinger, A. Bergström, B. Gustavii, P. Brundin, A. Adolph, Transplantation of human embryonic retina to adult rat retina, Restorative Neurology and Neuroscience 2(1) (1990) 9-22.
[113] R. Aramant, M. Seiler, Cryopreservation and transplantation of immature rat retina into adult rat retina, Developmental brain research 61(2) (1991) 151-159.
[114] R.B. Aramant, M.J. Seiler, Human embryonic retinal cell transplants in athymic immunodeficient rat hosts, Cell Transplantation 3(6) (1994) 461-474.
[115] T.-C. Lin, M. Stevanovic, L.P. Foltz, D.O. Clegg, M.S. Humayun, Stem Cell-Derived Retinal Cells for Transplantation, Macular Surgery, Springer2020, pp. 423-437.
[116] S.T. Schuschereba, M.S. Silverman, Retinal cell and photoreceptor transplantation between adult New Zealand red rabbit retinas, Experimental neurology 115(1) (1992) 95-99.
[117] S. Mohand-Said, D. Hicks, M. Simonutti, D. Tran-Minh, A. Deudon-Combe, H. Dreyfus, M.S. Silverman, J.M. Ogilvie, T. Tenkova, J. Sahel, Photoreceptor transplants increase host cone survival in the retinal degeneration (rd) mouse, Ophthalmic research 29(5) (1997) 290-297.
[118] F. Ghosh, K. Arner, B. Ehinger, Transplant of full-thickness embryonic rabbit retina using pars plana vitrectomy, Retina (Philadelphia, Pa.) 18(2) (1998) 136-142.
[119] F. Ghosh, B. Juliusson, K. Arnér, B. Ehinger, Partial and full-thickness neuroretinal transplants, Experimental eye research 68(1) (1999) 67-74.
[120] J. Wassélius, F. Ghosh, Adult rabbit retinal transplants, Investigative ophthalmology & visual science 42(11) (2001) 2632-2638.
[121] M.J. Seiler, R.B. Aramant, Intact sheets of fetal retina transplanted to restore damaged rat retinas, Investigative ophthalmology & visual science 39(11) (1998) 2121-2131.
[122] R.B. Aramant, M.J. Seiler, S.L. Ball, Successful cotransplantation of intact sheets of fetal retina with retinal pigment epithelium, Investigative ophthalmology & visual science 40(7) (1999) 1557-1564.
[123] R.B. Aramant, M.J. Seiler, Transplanted sheets of human retina and retinal pigment epithelium develop normally in nude rats, Experimental eye research 75(2) (2002) 115-125.
[124] N.D. Radtke, R.B. Aramant, H.M. Petry, P.T. Green, D.J. Pidwell, M.J. Seiler, Vision improvement in retinal degeneration patients by implantation of retina together with retinal pigment epithelium, American journal of ophthalmology 146(2) (2008) 172-182. e1.
[125] M. Silverman, S. Hughes, Transplantation of photoreceptors to light-damaged retina, Investigative ophthalmology & visual science 30(8) (1989) 1684-1690.
[126] M.J. Seiler, R.B. Aramant, Cell replacement and visual restoration by retinal sheet transplants, Progress in retinal and eye research 31(6) (2012) 661-687.
[127] G. Fujii, K.E. Au, M. Humayun, Limited macular translocation: current concepts, Ophthalmology clinics of North America 15(4) (2002) 425-436.
[128] C.M. Eandi, F. Giansanti, G. Virgili, Macular translocation for neovascular age-related macular degeneration, Cochrane Database of Systematic Reviews (4) (2008).
[129] K.A. Eong, Initial experience of macular translocation in Singapore-One-year results, ANNALS-ACADEMY OF MEDICINE SINGAPORE 33(5) (2004) 641-648.
[130] E. Salero, T.A. Blenkinsop, B. Corneo, A. Harris, D. Rabin, J.H. Stern, S. Temple, Adult human RPE can be activated into a multipotent stem cell that produces mesenchymal derivatives, Cell stem cell 10(1) (2012) 88-95.
[131] Z. Liu, B.H. Parikh, Q.S.W. Tan, D.S.L. Wong, K.H. Ong, W. Yu, I. Seah, G.E. Holder, W. Hunziker, G.S. Tan, Surgical Transplantation of Human RPE Stem Cell-Derived RPE Monolayers into Non-Human Primates with Immunosuppression, Stem Cell Reports (2021).
[132] J. Assawachananont, M. Mandai, S. Okamoto, C. Yamada, M. Eiraku, S. Yonemura, Y. Sasai, M. Takahashi, Transplantation of embryonic and induced pluripotent stem cell-derived 3D retinal sheets into retinal degenerative mice, Stem cell reports 2(5) (2014) 662-674.

[133] H. Shirai, M. Mandai, K. Matsushita, A. Kuwahara, S. Yonemura, T. Nakano, J. Assawachananont, T. Kimura, K. Saito, H. Terasaki, Transplantation of human embryonic stem cell-derived retinal tissue in two primate models of retinal degeneration, Proceedings of the National Academy of Sciences 113(1) (2016) E81-E90.
[134] M. Mandai, M. Fujii, T. Hashiguchi, G.A. Sunagawa, S.-i. Ito, J. Sun, J. Kaneko, J. Sho, C. Yamada, M. Takahashi, iPSC-derived retina transplants improve vision in rd1 end-stage retinal-degeneration mice, Stem cell reports 8(1) (2017) 69-83.
[135] A.-J. Carr, A. Vugler, J. Lawrence, L.L. Chen, A. Ahmado, F.K. Chen, M.a. Semo, C. Gias, L. da Cruz, H.D. Moore, Molecular characterization and functional analysis of phagocytosis by human embryonic stem cell-derived RPE cells using a novel human retinal assay, Molecular vision 15 (2009) 283.
[136] D.E. Buchholz, S.T. Hikita, T.J. Rowland, A.M. Friedrich, C.R. Hinman, L.V. Johnson, D.O. Clegg, Derivation of functional retinal pigmented epithelium from induced pluripotent stem cells, Stem cells 27(10) (2009) 2427-2434.
[137] S. Okamoto, M. Takahashi, Induction of retinal pigment epithelial cells from monkey iPS cells, Investigative ophthalmology & visual science 52(12) (2011) 8785-8790.
[138] Y. Li, Y.-T. Tsai, C.-W. Hsu, D. Erol, J. Yang, W.-H. Wu, R.J. Davis, D. Egli, S.H. Tsang, Long-term safety and efficacy of human-induced pluripotent stem cell (iPS) grafts in a preclinical model of retinitis pigmentosa, Molecular medicine 18(9) (2012) 1312-1319.
[139] R.E. MacLaren, R. Pearson, A. MacNeil, R. Douglas, T. Salt, M. Akimoto, A. Swaroop, J. Sowden, R. Ali, Retinal repair by transplantation of photoreceptor precursors, Nature 444(7116) (2006) 203-207.
[140] J. Luo, P. Baranov, S. Patel, H. Ouyang, J. Quach, F. Wu, A. Qiu, H. Luo, C. Hicks, J. Zeng, Human retinal progenitor cell transplantation preserves vision, Journal of biological chemistry 289(10) (2014) 6362-6371.
[141] R.D. Lund, P. Adamson, Y. Sauvé, D.J. Keegan, S.V. Girman, S. Wang, H. Winton, N. Kanuga, A.S. Kwan, L. Beauchène, Subretinal transplantation of genetically modified human cell lines attenuates loss of visual function in dystrophic rats, Proceedings of the National Academy of Sciences 98(17) (2001) 9942-9947.
[142] R.D. Lund, S. Wang, B. Lu, S. Girman, T. Holmes, Y. Sauvé, D.J. Messina, I.R. Harris, A.J. Kihm, A.M. Harmon, Cells isolated from umbilical cord tissue rescue photoreceptors and visual functions in a rodent model of retinal disease, Stem cells 25(3) (2007) 602-611.
[143] B. Mead, A. Logan, M. Berry, W. Leadbeater, B.A. Scheven, Paracrine-mediated neuroprotection and neuritogenesis of axotomised retinal ganglion cells by human dental pulp stem cells: comparison with human bone marrow and adipose-derived mesenchymal stem cells, PloS one 9(10) (2014) e109305.
[144] P.A. Sieving, R.C. Caruso, W. Tao, H.R. Coleman, D.J. Thompson, K.R. Fullmer, R.A. Bush, Ciliary neurotrophic factor (CNTF) for human retinal degeneration: phase I trial of CNTF delivered by encapsulated cell intraocular implants, Proceedings of the National Academy of Sciences 103(10) (2006) 3896-3901.
[145] K. Kauper, C. McGovern, S. Sherman, P. Heatherton, R. Rapoza, P. Stabila, B. Dean, A. Lee, S. Borges, B. Bouchard, Two-year intraocular delivery of ciliary neurotrophic factor by encapsulated cell technology implants in patients with chronic retinal degenerative diseases, Investigative ophthalmology & visual science 53(12) (2012) 7484-7491.
[146] E.Y. Chew, T.E. Clemons, T. Peto, F.B. Sallo, A. Ingerman, W. Tao, L. Singerman, S.D. Schwartz, N.S. Peachey, A.C. Bird, Ciliary neurotrophic factor for macular telangiectasia type 2: results from a phase 1 safety trial, American journal of ophthalmology 159(4) (2015) 659-666. e1.
[147] Y. Shen, Stem cell therapies for retinal diseases: from bench to bedside, Journal of Molecular Medicine (2020) 1-22.
[148] M.S. Singh, S.S. Park, T.A. Albini, M.V. Canto-Soler, H. Klassen, R.E. MacLaren, M. Takahashi, A. Nagiel, S.D. Schwartz, K. Bharti, Retinal stem cell transplantation: balancing safety and potential, Progress in retinal and eye research 75 (2020) 100779.

[149] S.D. Schwartz, G. Tan, H. Hosseini, A. Nagiel, Subretinal transplantation of embryonic stem cell–derived retinal pigment epithelium for the treatment of macular degeneration: an assessment at 4 years, Investigative ophthalmology & visual science 57(5) (2016) ORSFc1-ORSFc9.
[150] M. Mandai, A. Watanabe, Y. Kurimoto, Y. Hirami, C. Morinaga, T. Daimon, M. Fujihara, H. Akimaru, N. Sakai, Y. Shibata, Autologous induced stem-cell–derived retinal cells for macular degeneration, New England Journal of Medicine 376(11) (2017) 1038-1046.
[151] L. da Cruz, K. Fynes, O. Georgiadis, J. Kerby, Y.H. Luo, A. Ahmado, A. Vernon, J.T. Daniels, B. Nommiste, S.M. Hasan, Phase 1 clinical study of an embryonic stem cell–derived retinal pigment epithelium patch in age-related macular degeneration, Nature Biotechnology 36(4) (2018) 328.
[152] J.S. Baldassarre, A. Joseph, M. Keane, J.S. Heier, Subretinal delivery of cells via the suprachoroidal space: Janssen trial, Cellular Therapies for Retinal Disease, Springer2017, pp. 95-104.
[153] A.C. Ho, T.S. Chang, M. Samuel, P. Williamson, R.F. Willenbucher, T. Malone, Experience with a subretinal cell-based therapy in patients with geographic atrophy secondary to age-related macular degeneration, American journal of ophthalmology 179 (2017) 67-80.
[154] R. Spencer, S. Fisher, G.P. Lewis, T. Malone, Epiretinal membrane in a subject after transvitreal delivery of palucorcel (CNTO 2476), Clinical Ophthalmology (Auckland, NZ) 11 (2017) 1797.
[155] J.S. Heier, A.C. Ho, M.A. Samuel, T. Chang, C.D. Riemann, J.W. Kitchens, J.S. Slakter, Y.I. Leiderman, R. Spencer, G.A. Williams, Safety and efficacy of subretinally administered palucorcel for geographic atrophy of age-related macular degeneration: phase 2b study, Ophthalmology Retina 4(4) (2020) 384-393.
[156] N. Lassota, J.F. Kiilgaard, J.U. Prause, M. la Cour, Correlation between clinical and histological features in a pig model of choroidal neovascularization, Graefe's Archive for Clinical and Experimental Ophthalmology 244(3) (2006) 394-398.
[157] J.F. Kiilgaard, J.U. Prause, M. Prause, E. Scherfig, M.H. Nissen, M. la Cour, Subretinal posterior pole injury induces selective proliferation of RPE cells in the periphery in in vivo studies in pigs, Investigative ophthalmology & visual science 48(1) (2007) 355-360.
[158] J.F. Kiilgaard, E. Scherfig, J.U. Prause, M. la Cour, Transplantation of amniotic membrane to the subretinal space in pigs, Stem cells international 2012 (2012).
[159] H. Akrami, Z.-S. Soheili, M. Sadeghizadeh, K. Khalooghi, H. Ahmadieh, M.R. Kanavi, S. Samiei, J. Pakravesh, Evaluation of RPE65, CRALBP, VEGF, CD68, and tyrosinase gene expression in human retinal pigment epithelial cells cultured on amniotic membrane, Biochemical genetics 49(5-6) (2011) 313-322.
[160] E.F. Moreira, H. Cai, T.H. Tezel, M.A. Fields, L.V. Del Priore, Reengineering human Bruch's membrane increases rod outer segment phagocytosis by human retinal pigment epithelium, Translational vision science & technology 4(5) (2015) 10-10.
[161] T.H. Tezel, L.V. Del Priore, H.J. Kaplan, Reengineering of aged Bruch's membrane to enhance retinal pigment epithelium repopulation, Investigative ophthalmology & visual science 45(9) (2004) 3337-3348.
[162] R.F. Mullins, M.N. Johnson, E.A. Faidley, J.M. Skeie, J. Huang, Choriocapillaris vascular dropout related to density of drusen in human eyes with early age-related macular degeneration, Investigative ophthalmology & visual science 52(3) (2011) 1606-1612.
[163] H. Skottman, J. Muranen, H. Lähdekorpi, E. Pajula, K. Mäkelä, L. Koivusalo, A. Koistinen, H. Uusitalo, K. Kaarniranta, K. Juuti-Uusitalo, Contacting co-culture of human retinal microvascular endothelial cells alters barrier function of human embryonic stem cell derived retinal pigment epithelial cells, Experimental cell research 359(1) (2017) 101-111.
[164] I.K. Sugino, Q. Sun, C. Springer, N. Cheewatrakoolpong, T. Liu, H. Li, M.A. Zarbin, Two Bioactive Molecular Weight Fractions of a Conditioned Medium Enhance RPE Cell Survival on Age-Related Macular Degeneration and Aged Bruch's Membrane, Translational vision science & technology 5(1) (2016) 8-8.
[165] J. Kundu, A. Michaelson, K. Talbot, P. Baranov, M.J. Young, R.L. Carrier, Decellularized retinal matrix: natural platforms for human retinal progenitor cell culture, Acta biomaterialia 31 (2016) 61-70.

[166] S. Suzuki, A.M. Shadforth, S. McLenachan, D. Zhang, S.-C. Chen, J. Walshe, G.E. Lidgerwood, A. Pébay, T.V. Chirila, F.K. Chen, Optimization of silk fibroin membranes for retinal implantation, Materials Science and Engineering: C 105 (2019) 110131.
[167] A.M. Shadforth, K.A. George, A.S. Kwan, T.V. Chirila, D.G. Harkin, The cultivation of human retinal pigment epithelial cells on Bombyx mori silk fibroin, Biomaterials 33(16) (2012) 4110-4117.
[168] A. Shadforth, S. Suzuki, R. Alzonne, G.A. Edwards, N.A. Richardson, T.V. Chirila, D.G. Harkin, Incorporation of human recombinant tropoelastin into silk fibroin membranes with the view to repairing Bruch's membrane, Journal of functional biomaterials 6(3) (2015) 946-962.
[169] D. Zhang, N. Ni, J. Chen, Q. Yao, B. Shen, Y. Zhang, M. Zhu, Z. Wang, J. Ruan, J. Wang, Electrospun SF/PLCL nanofibrous membrane: a potential scaffold for retinal progenitor cell proliferation and differentiation, Scientific reports 5(1) (2015) 1-14.
[170] S. Goncalves, I.P. Rodrigues, J. Padrão, J.P. Silva, V. Sencadas, S. Lanceros-Mendez, H. Girão, F.M. Gama, F. Dourado, L.R. Rodrigues, Acetylated bacterial cellulose coated with urinary bladder matrix as a substrate for retinal pigment epithelium, Colloids and Surfaces B: Biointerfaces 139 (2016) 1-9.
[171] S. Goncalves, J. Padrao, I.P. Rodrigues, J.o.P. Silva, V. Sencadas, S. Lanceros-Mendez, H. Girao, F. Dourado, L.R. Rodrigues, Bacterial cellulose as a support for the growth of retinal pigment epithelium, Biomacromolecules 16(4) (2015) 1341-1351.
[172] J.K. Gandhi, F. Mano, R. Iezzi Jr, S.A. LoBue, B.H. Holman, M.P. Fautsch, T.W. Olsen, J.S. Pulido, A.D. Marmorstein, Fibrin hydrogels are safe, degradable scaffolds for sub-retinal implantation, PloS one 15(1) (2020) e0227641.
[173] T.I. Harris, C.A. Paterson, F. Farjood, I.D. Wadsworth, L. Caldwell, R.V. Lewis, J.A. Jones, E. Vargis, Utilizing recombinant spider silk proteins to develop a synthetic bruch's membrane for modeling the retinal pigment epithelium, ACS Biomaterials Science & Engineering 5(8) (2019) 4023-4036.
[174] J.-Y. Lai, Y.-T. Li, Evaluation of cross-linked gelatin membranes as delivery carriers for retinal sheets, Materials Science and Engineering: C 30(5) (2010) 677-685.
[175] M. Phelan, K. Kruczek, J. Wilson, M. Brooks, C. Drinnan, F. Regent, J. Gerstenhaber, A. Swaroop, P. Lelkes, T. Li, Soy protein nanofiber scaffolds for uniform maturation of hiPSC-derived retinal pigment epithelium, Tissue engineering. Part C, Methods (2020).
[176] C. White, T. DiStefano, R. Olabisi, The influence of substrate modulus on retinal pigment epithelial cells, Journal of biomedical materials research part a 105(5) (2017) 1260-1266.
[177] P.H. Warnke, M. Alamein, S. Skabo, S. Stephens, R. Bourke, P. Heiner, Q. Liu, Primordium of an artificial Bruch's membrane made of nanofibers for engineering of retinal pigment epithelium cell monolayers, Acta biomaterialia 9(12) (2013) 9414-9422.
[178] M. Tomita, E. Lavik, H. Klassen, T. Zahir, R. Langer, M.J. Young, Biodegradable polymer composite grafts promote the survival and differentiation of retinal progenitor cells, Stem cells 23(10) (2005) 1579-1588.
[179] K.E. Kador, R.B. Montero, P. Venugopalan, J. Hertz, A.N. Zindell, D.A. Valenzuela, M.S. Uddin, E.B. Lavik, K.J. Muller, F.M. Andreopoulos, Tissue engineering the retinal ganglion cell nerve fiber layer, Biomaterials 34(17) (2013) 4242-4250.
[180] K.E. Kador, H.S. Alsehli, A.N. Zindell, L.W. Lau, F.M. Andreopoulos, B.D. Watson, J.L. Goldberg, Retinal ganglion cell polarization using immobilized guidance cues on a tissue-engineered scaffold, Acta biomaterialia 10(12) (2014) 4939-4946.
[181] K. Li, X. Zhong, S. Yang, Z. Luo, K. Li, Y. Liu, S. Cai, H. Gu, S. Lu, H. Zhang, HiPSC-derived retinal ganglion cells grow dendritic arbors and functional axons on a tissue-engineered scaffold, Acta Biomaterialia 54 (2017) 117-127.
[182] L. Krishna, S. Nilawar, M. Ponnalagu, M. Subramani, C. Jayadev, R. Shetty, K. Chatterjee, D. Das, Fiber Diameter Differentially Regulates Function of Retinal Pigment and Corneal Epithelial Cells on Nanofibrous Tissue Scaffolds, ACS Applied Bio Materials 3(2) (2020) 823-837.

[183] D.J. Moore, G.M. Clover, The effect of age on the macromolecular permeability of human Bruch's membrane, Investigative ophthalmology & visual science 42(12) (2001) 2970-2975.
[184] A. Hussain, C. Starita, A. Hodgetts, J. Marshall, Macromolecular diffusion characteristics of ageing human Bruch's membrane: implications for age-related macular degeneration (AMD), Experimental eye research 90(6) (2010) 703-710.
[185] B. Lu, D. Zhu, D. Hinton, M.S. Humayun, Y.-C. Tai, Mesh-supported submicron parylene-C membranes for culturing retinal pigment epithelial cells, Biomedical microdevices 14(4) (2012) 659-667.
[186] B. Diniz, P. Thomas, B. Thomas, R. Ribeiro, Y. Hu, R. Brant, A. Ahuja, D. Zhu, L. Liu, M. Koss, Subretinal implantation of retinal pigment epithelial cells derived from human embryonic stem cells: improved survival when implanted as a monolayer, Investigative ophthalmology & visual science 54(7) (2013) 5087-5096.
[187] B.B. Thomas, D. Zhu, L. Zhang, P.B. Thomas, Y. Hu, H. Nazari, F. Stefanini, P. Falabella, D.O. Clegg, D.R. Hinton, Survival and functionality of hESC-derived retinal pigment epithelium cells cultured as a monolayer on polymer substrates transplanted in RCS rats, Investigative ophthalmology & visual science 57(6) (2016) 2877-2887.
[188] M.J. Koss, P. Falabella, F.R. Stefanini, M. Pfister, B.B. Thomas, A.H. Kashani, R. Brant, D. Zhu, D.O. Clegg, D.R. Hinton, Subretinal implantation of a monolayer of human embryonic stem cell-derived retinal pigment epithelium: a feasibility and safety study in Yucatan minipigs, Graefe's Archive for Clinical and Experimental Ophthalmology 254(8) (2016) 1553-1565.
[189] A.H. Kashani, J.S. Lebkowski, F.M. Rahhal, R.L. Avery, H. Salehi-Had, W. Dang, C.-M. Lin, D. Mitra, D. Zhu, B.B. Thomas, A bioengineered retinal pigment epithelial monolayer for advanced, dry age-related macular degeneration, Science Translational Medicine 10(435) (2018).
[190] M.T. Calejo, T. Ilmarinen, H. Jongprasitkul, H. Skottman, M. Kellomäki, Honeycomb porous films as permeable scaffold materials for human embryonic stem cell-derived retinal pigment epithelium, Journal of Biomedical Materials Research Part A 104(7) (2016) 1646-1656.
[191] D.J. Mooney, H. Vandenburgh, Cell delivery mechanisms for tissue repair, Cell stem cell 2(3) (2008) 205-213.
[192] D. Gupta, C.H. Tator, M.S. Shoichet, Fast-gelling injectable blend of hyaluronan and methylcellulose for intrathecal, localized delivery to the injured spinal cord, Biomaterials 27(11) (2006) 2370-2379.
[193] B.G. Ballios, M.J. Cooke, D. van der Kooy, M.S. Shoichet, A hydrogel-based stem cell delivery system to treat retinal degenerative diseases, Biomaterials 31(9) (2010) 2555-2564.
[194] B.G. Ballios, M.J. Cooke, L. Donaldson, B.L. Coles, C.M. Morshead, D. van der Kooy, M.S. Shoichet, A hyaluronan-based injectable hydrogel improves the survival and integration of stem cell progeny following transplantation, Stem cell reports 4(6) (2015) 1031-1045.
[195] N. Mitrousis, S. Hacibekiroglu, M.T. Ho, Y. Sauvé, A. Nagy, D. van der Kooy, M.S. Shoichet, Hydrogel-mediated co-transplantation of retinal pigmented epithelium and photoreceptors restores vision in an animal model of advanced retinal degeneration, Biomaterials 257 (2020) 120233.
[196] J. Parker, N. Mitrousis, M.S. Shoichet, Hydrogel for simultaneous tunable growth factor delivery and enhanced viability of encapsulated cells in vitro, Biomacromolecules 17(2) (2016) 476-484.
[197] N. Mitrousis, R.Y. Tam, A.E. Baker, D. van der Kooy, M.S. Shoichet, Hyaluronic Acid-Based Hydrogels Enable Rod Photoreceptor Survival and Maturation In Vitro through Activation of the mTOR Pathway, Advanced Functional Materials 26(12) (2016) 1975-1985.
[198] L.J. Smith, S.M. Taimoory, R.Y. Tam, A.E. Baker, N. Binth Mohammad, J.F. Trant, M.S. Shoichet, Diels–Alder click-cross-linked hydrogels with increased reactivity enable 3D cell encapsulation, Biomacromolecules 19(3) (2018) 926-935.
[199] N.C. Hunt, L.M. Grover, Cell encapsulation using biopolymer gels for regenerative medicine, Biotechnology letters 32(6) (2010) 733-742.

[200] N. Hunt, A.M. Smith, U. Gbureck, R. Shelton, L. Grover, Encapsulation of fibroblasts causes accelerated alginate hydrogel degradation, Acta biomaterialia 6(9) (2010) 3649-3656.
[201] T.E. Eurell, D.R. Brown, P.A. Gerding, R.E. Hamor, Alginate as a new biomaterial for the growth of porcine retinal pigment epithelium, Veterinary ophthalmology 6(3) (2003) 237-243.
[202] J. Wikström, M. Elomaa, H. Syväjärvi, J. Kuokkanen, M. Yliperttula, P. Honkakoski, A. Urtti, Alginate-based microencapsulation of retinal pigment epithelial cell line for cell therapy, Biomaterials 29(7) (2008) 869-876.
[203] N.C. Hunt, D. Hallam, A. Karimi, C.B. Mellough, J. Chen, D.H. Steel, M. Lako, 3D culture of human pluripotent stem cells in RGD-alginate hydrogel improves retinal tissue development, Acta biomaterialia 49 (2017) 329-343.
[204] J.H. Park, E.Y. Shin, M.E. Shin, M.J. Choi, C. Carlomagno, J.E. Song, G. Khang, Enhanced retinal pigment epithelium (RPE) regeneration using curcumin/alginate hydrogels: In vitro evaluation, International journal of biological macromolecules 117 (2018) 546-552.
[205] E.Y. Shin, J.H. Park, M.E. Shin, J.E. Song, M. Thangavelu, C. Carlomagno, A. Motta, C. Migliaresi, G. Khang, Injectable taurine-loaded alginate hydrogels for retinal pigment epithelium (RPE) regeneration, Materials Science and Engineering: C 103 (2019) 109787.
[206] Y. Liu, R. Wang, T.I. Zarembinski, N. Doty, C. Jiang, C. Regatieri, X. Zhang, M.J. Young, The application of hyaluronic acid hydrogels to retinal progenitor cell transplantation, Tissue engineering Part A 19(1-2) (2013) 135-142.
[207] F. Jiang, Z. Tang, Y. Zhang, Y. Ju, H. Gao, N. Sun, F. Liu, P. Gu, W. Zhang, Enhanced proliferation and differentiation of retinal progenitor cells through a self-healing injectable hydrogel, Biomaterials science 7(6) (2019) 2335-2347.
[208] J. Park, P. Baranov, A. Aydin, H. Abdelgawad, D. Singh, W. Niu, M. Kurisawa, M. Spector, M.J. Young, In Situ Cross-linking Hydrogel as a Vehicle for Retinal Progenitor Cell Transplantation, Cell transplantation 28(5) (2019) 596-606.
[209] S.D. Fitzpatrick, M. Jafar Mazumder, F. Lasowski, L.E. Fitzpatrick, H. Sheardown, PNIPAAm-grafted-collagen as an injectable, in situ gelling, bioactive cell delivery scaffold, Biomacromolecules 11(9) (2010) 2261-2267.
[210] M.J. Mazumder, S.D. Fitzpatrick, B. Muirhead, H. Sheardown, Cell-adhesive thermogelling PNIPAAm/hyaluronic acid cell delivery hydrogels for potential application as minimally invasive retinal therapeutics, Journal of biomedical materials research Part A 100(7) (2012) 1877-1887.
[211] S.D. Fitzpatrick, M.J. Mazumder, B. Muirhead, H. Sheardown, Development of injectable, resorbable drug-releasing copolymer scaffolds for minimally invasive sustained ophthalmic therapeutics, Acta biomaterialia 8(7) (2012) 2517-2528.
[212] S.D. Fitzpatrick, Minimally invasive copolymers for posterior segment ocular therapeutics, 2012.
[213] H. Sheardown, S. Fitzpatrick, M.J. Mazumder, Biodegradable polymer system, United States, 2014.
[214] S. Fitzpatrick, M.A.J. Mazumder, B. Muirhead, D. Baek, X. Zhao, H. Wang, L. Fitzpatrick, S. Boyd, H. Sheardown, Optically transparent thermally gelling drug delivery scaffold for minimally invasive delivery to the posterior segment of the eye, Journal of Biomedical Materials Research Part A (submitted) (2020).
[215] H. Uludag, B. Norrie, N. Kousinioris, T. Gao, Engineering temperature-sensitive poly (N-isopropylacrylamide) polymers as carriers of therapeutic proteins, Biotechnology and bioengineering 73(6) (2001) 510-521.
[216] S. Ohya, H. Sonoda, Y. Nakayama, T. Matsuda, The potential of poly (N-isopropylacrylamide)(PNIPAM)-grafted hyaluronan and PNIPAM-grafted gelatin in the control of post-surgical tissue adhesions, Biomaterials 26(6) (2005) 655-659.
[217] H. Tan, C.M. Ramirez, N. Miljkovic, H. Li, J.P. Rubin, K.G. Marra, Thermosensitive injectable hyaluronic acid hydrogel for adipose tissue engineering, Biomaterials 30(36) (2009) 6844-6853.

[218] Z. Cui, B.H. Lee, B.L. Vernon, New hydrolysis-dependent thermosensitive polymer for an injectable degradable system, Biomacromolecules 8(4) (2007) 1280-1286.
[219] Z. Cui, B.H. Lee, C. Pauken, B.L. Vernon, Manipulating degradation time in a N-isopropylacrylamide-based co-polymer with hydrolysis-dependent LCST, Journal of Biomaterials Science, Polymer Edition 21(6-7) (2010) 913-926.
[220] Y.M. Chen, Z.Q. Liu, Z.H. Feng, F. Xu, J.K. Liu, Adhesive protein-free synthetic hydrogels for retinal pigment epithelium cell culture with low ROS level, Journal of Biomedical Materials Research Part A 102(7) (2014) 2258-2267.
[221] Y. Tian, M.R. Zonca Jr, J. Imbrogno, A.M. Unser, L. Sfakis, S. Temple, G. Belfort, Y. Xie, Polarized, cobblestone, human retinal pigment epithelial cell maturation on a synthetic PEG matrix, ACS Biomaterials Science & Engineering 3(6) (2017) 890-902.
[222] I.W. Hamley, Small bioactive peptides for biomaterials design and therapeutics, Chemical reviews 117(24) (2017) 14015-14041.
[223] E.S. Place, N.D. Evans, M.M. Stevens, Complexity in biomaterials for tissue engineering, Nature materials 8(6) (2009) 457-470.
[224] D. Sengupta, S.C. Heilshorn, Protein-engineered biomaterials: highly tunable tissue engineering scaffolds, Tissue Engineering Part B: Reviews 16(3) (2010) 285-293.
[225] R.L. DiMarco, S.C. Heilshorn, Multifunctional materials through modular protein engineering, Advanced Materials 24(29) (2012) 3923-3940.
[226] E. Ruoslahti, M.D. Pierschbacher, Arg-Gly-Asp: a versatile cell recognition signal, Cell 44(4) (1986) 517-518.
[227] E. Ruoslahti, M.D. Pierschbacher, New perspectives in cell adhesion: RGD and integrins, Science 238(4826) (1987) 491-497.
[228] R.O. Hynes, Integrins: versatility, modulation, and signaling in cell adhesion, Cell 69(1) (1992) 11-25.
[229] J. Samanen, F. Ali, T. Romoff, R. Calvo, E. Sorenson, J. Vasko, B. Storer, D. Berry, D. Bennett, M. Strohsacker, Development of a small RGD peptide fibrinogen receptor antagonist with potent antiaggregatory activity in vitro, Journal of medicinal chemistry 34(10) (1991) 3114-3125.
[230] L. Alig, A. Edenhofer, P. Hadvary, M. Huerzeler, D. Knopp, M. Mueller, B. Steiner, A. Trzeciak, T. Weller, Low molecular weight, non-peptide fibrinogen receptor antagonists, Journal of medicinal chemistry 35(23) (1992) 4393-4407.
[231] J. Graf, Y. Iwamoto, M. Sasaki, G.R. Martin, H.K. Kleinman, F.A. Robey, Y. Yamada, Identification of an amino acid sequence in laminin mediating cell attachment, chemotaxis, and receptor binding, Cell 48(6) (1987) 989-996.
[232] M. Sasaki, Y. Yamada, The laminin B2 chain has a multidomain structure homologous to the B1 chain, Journal of Biological Chemistry 262(35) (1987) 17111-17117.
[233] P. Simon-Assmann, G. Orend, E. Mammadova-Bach, C. Spenlé, O. Lefebvre, Role of laminins in physiological and pathological angiogenesis, International journal of developmental biology 55(4-5) (2011) 455-465.
[234] H.R. Coleman, C.-C. Chan, F.L. Ferris III, E.Y. Chew, Age-related macular degeneration, The Lancet 372(9652) (2008) 1835-1845.
[235] J. Chhablani, Central Serous Chorioretinopathy, Academic Press2019.
[236] P. Mitchell, G. Liew, B. Gopinath, T.Y. Wong, Age-related macular degeneration, The Lancet 392(10153) (2018) 1147-1159.
[237] A.-S. Mertgen, V.T. Trossmann, A.G. Guex, K. Maniura-Weber, T. Scheibel, M. Rottmar, Multifunctional biomaterials: combining material modification strategies for engineering of cell-contacting surfaces, ACS applied materials & interfaces 12(19) (2020) 21342-21367.
[238] G.T. Hermanson, Bioconjugate techniques, Academic press2013.

[239] O.D. Krishna, K.L. Kiick, Protein-and peptide-modified synthetic polymeric biomaterials, Peptide Science: Original Research on Biomolecules 94(1) (2010) 32-48.
[240] J. Wang, X. Li, Preparation and characterization of interpenetrating polymer network silicone hydrogels with high oxygen permeability, Journal of applied polymer science 116(5) (2010) 2749-2757.
[241] T. Nakagawa, S. Nagashima, A. Higuchi, Synthesis and gas transport properties of new copolymer membranes with trimethylsilyl groups, Desalination 90(1-3) (1993) 183-192.
[242] N.-P.-D. Tran, M.-C. Yang, Synthesis and characterization of soft contact lens based on the combination of silicone nanoparticles with hydrophobic and hydrophilic monomers, Journal of Polymer Research 26(6) (2019) 1-10.
[243] M. Sobiech, P. Luliński, Imprinted Polymeric Gels for Pharmaceutical and Biomedical Purposes, Polymer Gels, Springer2018, pp. 153-183.
[244] M. Pantoja, F. Velasco, D. Broekema, J. Abenojar, J.d. Real, The Influence of pH on the Hydrolysis Process of γ-Methacryloxypropyltrimethoxysilane, Analyzed by FT-IR, and the Silanization of Electrogalvanized Steel, Journal of adhesion science and technology 24(6) (2010) 1131-1143.
[245] T. Hooshmand, R. van Noort, A. Keshvad, Storage effect of a pre-activated silane on the resin to ceramic bond, Dental Materials 20(7) (2004) 635-642.
[246] M.-C. Brochier Salon, M.N. Belgacem, Hydrolysis-condensation kinetics of different silane coupling agents, Phosphorus, Sulfur, and Silicon 186(2) (2011) 240-254.
[247] F. Osterholtz, E. Pohl, Kinetics of the hydrolysis and condensation of organofunctional alkoxysilanes: a review, Journal of Adhesion Science and Technology 6(1) (1992) 127-149.
[248] M.L. Bender, Mechanisms of catalysis of nucleophilic reactions of carboxylic acid derivatives, Chemical Reviews 60(1) (1960) 53-113.
[249] R. Gómez-Bombarelli, E. Calle, J. Casado, Mechanisms of lactone hydrolysis in acidic conditions, The Journal of organic chemistry 78(14) (2013) 6880-6889.
[250] V. Castelletto, R.J. Gouveia, C.J. Connon, I.W. Hamley, Self-assembly and bioactivity of a polymer/peptide conjugate containing the RGD cell adhesion motif and PEG, European polymer journal 49(10) (2013) 2961-2967.
[251] M.O. Guler, L. Hsu, S. Soukasene, D.A. Harrington, J.F. Hulvat, S.I. Stupp, Presentation of RGDS epitopes on self-assembled nanofibers of branched peptide amphiphiles, Biomacromolecules 7(6) (2006) 1855-1863.
[252] X. Hu, M. Liao, H. Gong, L. Zhang, H. Cox, T.A. Waigh, J.R. Lu, Recent advances in short peptide self-assembly: from rational design to novel applications, Current Opinion in Colloid & Interface Science 45 (2020) 1-13.
[253] N. Uchida, T. Muraoka, Current Progress in Cross-Linked Peptide Self-Assemblies, International Journal of Molecular Sciences 21(20) (2020) 7577.
[254] J.M. Anderson, A. Andukuri, D.J. Lim, H.-W. Jun, Modulating the gelation properties of self-assembling peptide amphiphiles, ACS nano 3(11) (2009) 3447-3454.
[255] Y. Hong, R.L. Legge, S. Zhang, P. Chen, Effect of amino acid sequence and pH on nanofiber formation of self-assembling peptides EAK16-II and EAK16-IV, Biomacromolecules 4(5) (2003) 1433-1442.
[256] S. Zhang, Fabrication of novel biomaterials through molecular self-assembly, Nature biotechnology 21(10) (2003) 1171-1178.
[257] W.M. Saltzman, Biomedical engineering: bridging medicine and technology, Cambridge University Press2009.
[258] B. Li, M.E. Thompson, Phase transition in amphiphilic poly (N-isopropylacrylamide): controlled gelation, Physical Chemistry Chemical Physics 20(19) (2018) 13623-13631.
[259] N. Bayat, Y. Zhang, P. Falabella, R. Menefee, J.J. Whalen, M.S. Humayun, M.E. Thompson, A reversible thermoresponsive sealant for temporary closure of ocular trauma, Science translational medicine 9(419) (2017).

[260] T. Wang, L. Jin, Y. Song, J. Li, Y. Gao, S. Shi, Rheological study on the thermoinduced gelation behavior of poly (N-isopropylacrylamide-co-acrylic acid) microgel suspensions, Journal of Applied Polymer Science 134(35) (2017) 45259.
[261] M.T. Cook, P. Haddow, S.B. Kirton, W.J. McAuley, Polymers exhibiting lower critical solution temperatures as a route to thermoreversible gelators for healthcare, Advanced Functional Materials 31(8) (2021) 2008123.
[262] R.L. Avery, B.M. Glaser, Inhibition of retinal pigment epithelial cell attachment by a synthetic peptide derived from the cell-binding domain of fibronectin, Archives of Ophthalmology 104(8) (1986) 1220-1222.
[263] P.A. Campochiaro, J.A. Jerdan, B.M. Glaser, Serum contains chemoattractants for human retinal pigment epithelial cells, Archives of ophthalmology 102(12) (1984) 1830-1833.
[264] P.A. Campochiaro, B.M. Glaser, Platelet-derived growth factor is chemotactic for human retinal pigment epithelial cells, Archives of Ophthalmology 103(4) (1985) 576-579.
[265] C.G. Miller, G. Budoff, J.L. Prenner, J.E. Schwarzbauer, Minireview: Fibronectin in retinal disease, Experimental Biology and Medicine 242(1) (2017) 1-7.
[266] W.-C. Wu, Y.-C. Chang, K.-Y. Wu, S.-Y. Chen, M.-C. Hsieh, M.-H. Wu, H.-J. Wu, W.-S. Wu, Y.-H. Kao, Pharmacological implications from the adhesion-induced signaling profiles in cultured human retinal pigment epithelial cells, The Kaohsiung journal of medical sciences 30(1) (2014) 1-11.
[267] H. Wang, Y. Van Patten, I.K. Sugino, M.A. Zarbin, Migration and proliferation of retinal pigment epithelium on extracellular matrix ligands, Journal of Rehabilitation Research & Development 43(6) (2006).
[268] R. Li, A. Maminishkis, G. Zahn, D. Vossmeyer, S.S. Miller, Integrin α5β1 mediates attachment, migration, and proliferation in human retinal pigment epithelium: relevance for proliferative retinal disease, Investigative ophthalmology & visual science 50(12) (2009) 5988-5996.
[269] S. Proulx, S.L. Guérin, C. Salesse, Effect of quiescence on integrin alpha5beta1 expression in human retinal pigment epithelium, Mol Vis 9 (2003) 473-481.